Building a Dual-Species Optical Dipole Trap for Ultracold Lithium-6 and Rubidium-85,87

by

Meng Gao

A THESIS SUBMITTED IN PARTIAL FULFILMENT OF
THE REQUIREMENTS FOR THE DEGREE OF

Honours Physics and Computer Science

in

The Faculty of Undergraduate Studies

(Physics)

The University Of British Columbia

(Vancouver)

April, 2008

Abstract

This thesis documents the design, construction, and measurements made in building of an optical dipole trap. The first chapter provides an introduction to atom traps and our motivationm to building a dipole trap. The second chapter provides theory and calculations relevant to the building of a dipole trap. The third chapter documents the construction process of the dipole trap. The fourth chapter introduces our experimental control system used to image the atoms in the trap. The fifth chapter discusses how to load atoms into the trap. The last chapter describes how to image the atoms in the trap and results from this project.

Table of Contents

Appendices

List of Tables

List of Figures

Acknowledgements

I would like to prominently thank Kirk and Bruce for giving me the opportunity to work in the QDG lab for so long. They were huge influences in my undergraduate education and choosing my career path in physics. They showed me that experiment is beautiful, dedication and hard work is rewarding, and the most important thing in a career is to enjoy what you do.

I would like to thank Janelle all her hard work on this project. She is often the first person I turn to in need of any kind of help, explanations, or simply why the MOT isn't loading.

I would like to thank everyone else who contributed to this project, David and Art for general helpful advice, Yifei for help on the imaging system, Keith and Ovi for work on the computer control system.

And last but not least, I would like to thank my parents for their endless loving support and pushing me to go as far as I can in whatever I choose to do in life.

A Note to the reader

1

This project is a sub-project of the photoassociation spectroscopy experiment in the QDG lab. I will only try to focus on my personal contributions in this document. Thus much of this thesis will have many references to past and future work in the lab which will only be explained briefly. I apologize if there appears to be gaps in the continuity for the non-expert in the field.

2

Even though the trap is built for both rubidium and lithium, most of the work in this thesis focuses on lithium because it is technically more difficult to trap and have several tighter constraints than rubidium.

3

The original plan of this project was to build a resonator trap, however due to technical issues and availability of time, we never attempted to implement the resonator. I decided that the calculations,designs,and measurements pertaining to the resonator will not be included. Also not included are the intensity and pointing spectrums measurements of the fiber laser as I felt these measurements needed to be repeated for proper analyses.

Chapter 1

Introduction

In the past ten to fifteen years, modern physics has witnessed an unprecedented growth of technology and theory in the field of cold atomic and optical physics. From the first development of the laser cooling technique to the realization of the Bose-Einstein Condensate (BEC), as the atomic samples became colder and denser, the application of storing these atoms naturally arose. Optical Dipole Traps[1] offer a simple and efficient storage mechanism that paved the road for new precision spectroscopy techniques, cooling methods, and applications in the simulation and development of the quantum computer.

1.1 Traps for neutral atoms

There exist several categories of traps for neutral atoms whose distinctions should be made clear.

1.1.1 Radiation Pressure Traps

These traps are based on the principles of inelastic scattering (radiation force) of photons by atoms. Here the atom gets a momentum kick by absorbing a photon and promotes an electron to an excited state. The electron then moves down to a lower state by spontaneously emitting another photon. Laser cooling and Magnto-Optic traps are all based on this principle. These traps are usually referred to as *dissipative* traps because the atom's internal states are constantly being changed in order to maintain the trapping force. Cooling by radiation pressure is also fundamentally limited by the recoil energy of the atom. Typically for alkali atoms,the lower bound for temperatures in a radiation pressure trap is a few microkelvins.

1.1.2 Magnetic Traps

Magnetic traps are based on the principle of the zeeman energy shifts of atomic levels by an external magnetic field. Gradients of magnetic fields are applied so that a cloud of atoms can experience spatially dependent zeeman shifts, leading to bound potentials. Magnetic traps are considered *conservative* potentials because the internal energy of the atoms are conserved when the atom interacts with the magnetic field. Several orders of magnitude lower temperatures have been achieved in magnetic traps than radiation pressure traps. The magnitude of the magnetic potential depends on the magnetic dipole moments of the atomic orbitals and the strength of external magnetic field.

---

[1]commonly referred to as *optical traps* or *dipole traps* or *optical tweezers*

Figure 1.1: Photoassociation[13]
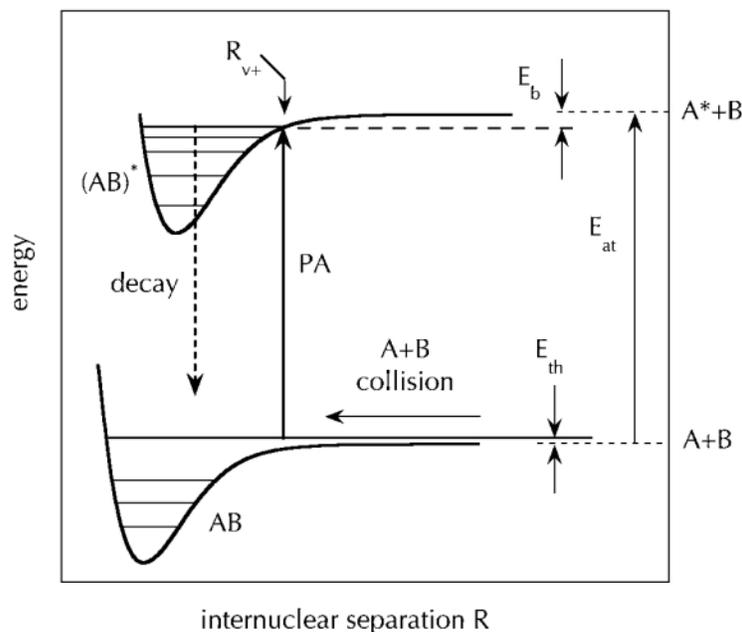
1.1.3 Optical Traps

Optical traps are based on the elastic scattering (Rayleigh scattering) of photons by atoms. Optical traps are also considered conservative potentials because the internal energy is conserved in elastic scattering. Equivalent, optical traps are based on the stark shift of the atomic energy levels by static or time-varying electric fields. An intensity gradient will introduce a spatially dependent stark shift and a bound potential for the atoms. Similar types of sub-recoil cooling techniques can be applied in optical traps as well as magnetic traps. However, it is easier to achieve high binding potentials for optical traps than magnetic traps. Typically to achieve the same potential created by a focused laser beam in a magnetic trap, the gradient of the magnetic field required is enormous (explained later). High intensity gradients will also produce high atomic densities in the trap. These are part of the reasons why we will be using an optical trap for our experiment.

1.2 Photoassociation

While the field of ultracold atoms has recently reached maturity, the field of ultracold molecules is still in infancy. In the QDG lab, our research is devoted to the formation and studies of ultracold molecules. Since molecules tend to have large numbers of internal states, it is difficult or nearly impossible to laser cool them. While other techniques exist such as buffer gas cooling[4], we will use a technique called *photoassociation* that will be able to achieve much lower temperatures. When two atoms ,A and B, collide and absorb a photon, γ, tuned to a molecular resonance, they can be promoted to molecular excited states. Such a state can then decay back to two free atoms or a molecular bound state. This is illustrated clearly from [Fig 1.1] borrowed from [13].

Figure 1.2: a Magneto-Optical Trap[20]
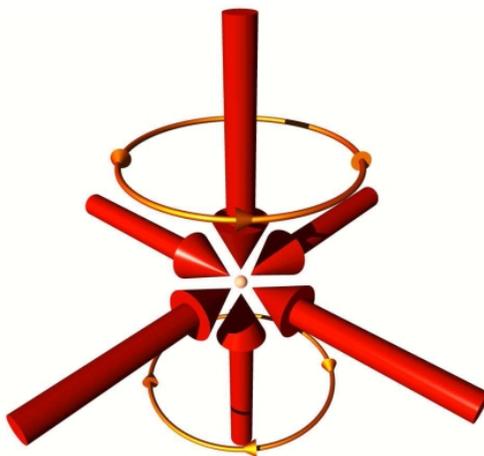
In our lab, we wish to realize by photoassociation and study the dipole-dipole interactions of the lithium-rubidium molecule. We want to do this in the optical trap as opposed to the MOT because we can achieve higher densities and lower temperatures to increase the collision rates[13]. Also it allows for more versatile spectrascopy techniques such as measuring photoassociative collisions by trap loss.

Our collaboraters David Jones, Arthur Mills, and Yifei Chen will be building a narrow linewidth, fiber-comb locked, tunable Ti-Sapphire laser to tune to the molecular resoances. This optical trap will provide the atomic sample and density needed to observe photoassociation.

1.3   Laser Cooling and the MOT

The Magneto-Optical Trap (MOT)[Fig 1.2] is our starting point for this project. We will transfer the atoms from the MOT to the optical trap. The theory and operation of the MOT is thoroughly documented in contemporary phyical literature[15] and I will but give a brief summary of the details relevant to this project.

The MOT is composed of 6 counterpropagating beams producing an optical molasses at the intersection. A pair of magnetic field coils in the *Anti-Helmholtz* configuration is used to produce an inhomogenous magnetic field whose field is approximately 0 at the center and increases radially outwards This (magically) gives the atoms both a velocity-depedent and a spatially-dependent force towards the center of the trap in all directions.

Due to the hyperfine splitting of the ground state into two (degenerate in the absence of external magnetic fields) of states in the atom we wish to cool, it is typically required to have 2 lasers beams of slightly different frequency, one called the *pump*, and the other called the *repump* to keep the electron cycling in the atomic levels and not fall into a state where the laser can no

Figure 1.3: Level Diagrams Courtesy of Yeifei
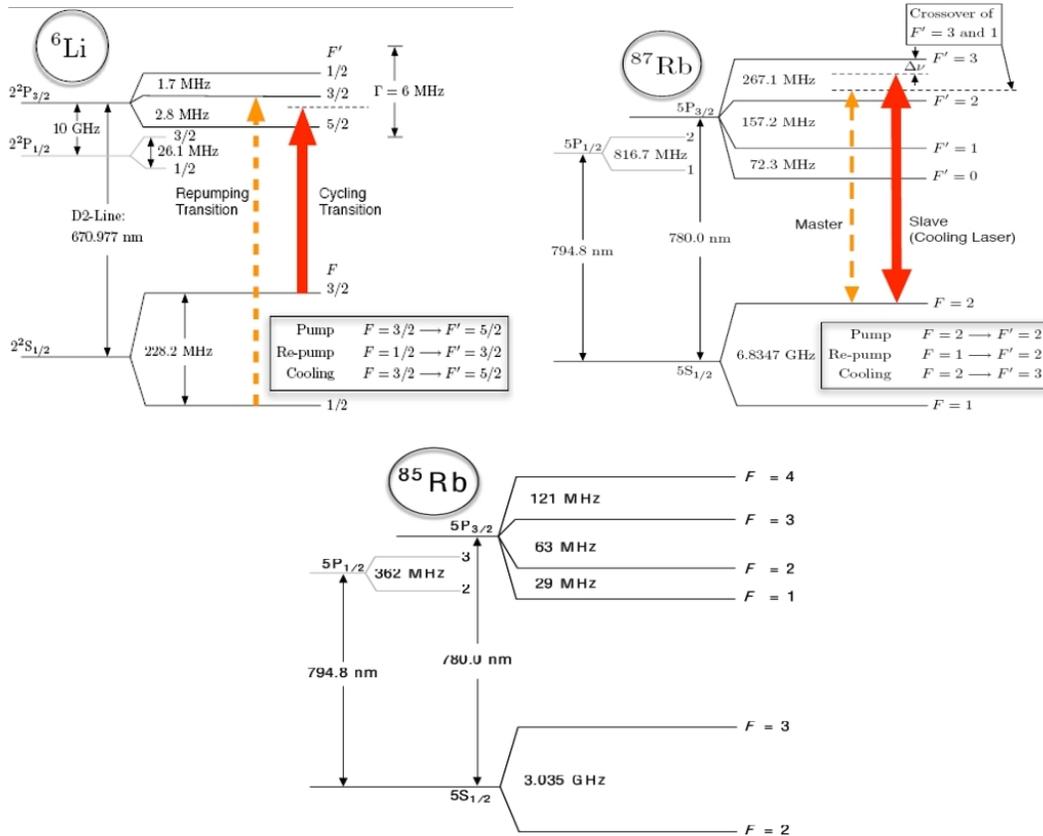
longer interact with it.

1.4   the Atoms

We have 3 species of atoms in trapped in MOTs, Li6, Rb85 and Rb87. I will be mostly discussing Li6 throughout this document. Li6 has 2 hyperfine ground states with a splitting of 228Mhz. The trapping potential we will be concerned with is the energy shift of these 2 states due to the stark effect.

1.4.1   Dipole Matrix Elements

The Dipole Matrix Elements are the transition probabilities for these levels and are needed to calculate the potentials in an optical trap. Some of these are calculated and tabulated using a mathematica notebook by Janelle.[Appendix J]

Chapter 2

Theory

The purpose of this section is to review formalism and calculate the potential of a dipole trap, scattering losses, and the expected number of trapped atoms.

2.1 Overview

There are several typical ways of describing light-matter interactions and the optical dipole force: classical, semi-classical, and quantum mechanical. Both the classical and semi-classical descriptions are enough to treat the topic of dipole trapping with the appropiate assumptions so we will not discuss the full quantum theory[9] of light-matter interactins here. This classical description assumes the electron of the trapped atom is tied to the atom by a spring and the light is a wave that exerts a force on the electron. The semi-classical method treats the interactions of light as a wave with the energy levels of the atom.

2.1.1 Assumptions

Electric Dipole Approximation

When the inter atomic distances are small compared to the wavelength of the light, $\lambda \gg d$, we can assume that all electric dipoles in question are point dipoles and the intensity of the light does not vary over the dipole.

Far-Far Detuning

Since our trapping light is $1064nm$, we will be focusing on the *"far-far" detuning* regime. In many literature [15][17][18], *far detuning* refers to the regime where the detuning, the difference between the laser frequency and the transition in question, $\omega_0 - \omega$, is much greater than the Rabi frequency [Eqn 2.16] but not much less than $2\omega_0$ such that the Rotating-Wave Approximation(RWA) [Eqn 2.18] breaks down. This is typically referring to a few nanometers to tens of nanonmeters detuning. However, we will be talking about hundreds of nanometers detuning and the RWA begins to break down. We call this regime *"far-far" detuning*.

2.1.2 Pitfalls

Saturation

The classical model fails to predict the effects of saturation (when the atoms in the excited state is a significant fraction of the total atom number). However if we are talking about far detuning, the scattering rate due to absorption is very small and saturation is not relevant here.

Figure 2.1: The Lorentz Model of Atom-Light Interactions
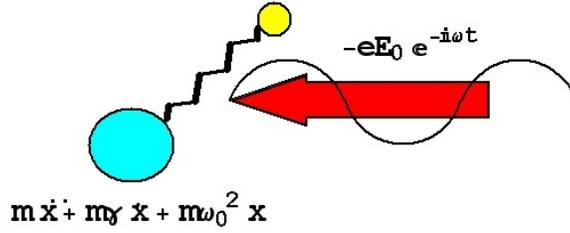
Light Shifts

The classical model will correctly predict the dipole potential of a 2-level atom corresponding to the potential due to light shift in semi-classical and quantum theory. However, it cannot go beyond this to predict such things as light shifts for different levels in multi-level structures and or even the sign of the light shift for ground and excited states in a 2-level atom.

Spontaneous Emission

Neither the classical nor semi-classical theory is able to treat spontaneous emission. Thus many of the derivations that require terms tied to spontaneous emission such as damping in the oscillator model will be taken for granted.

2.2 The Lorentz Model

The Lorentz Model is a classical theory of light matter interactions. We assume that the electron is attached to the nucleus on a spring and oscillates with some frequency ω_0 [Fig 2.1]. Then we will assume that the light is an oscillating driving electric field that induces polarization on the atom.[20]

The full equation of motion is given by:

$$m\ddot{x} + m\gamma\dot{x} + m\omega_0^2 x = -\hat{\varepsilon}eE_0e^{i\omega t} \tag{2.1}$$

where x represents the relative coordinate of the electron to the nucleus and γ is the damping coefficient that is introduced ad hoc in the classical theory to keep absorption from being infinite at resonance. This can be verified in the quantum theory and corresponds to the decay of oscillator motion or light intensity due to spontaneous emission.

if we assume that the solution to [Eqn 2.1] is of the form

$$x(t) = -\hat{\varepsilon}x_0e^{-i\omega t} \tag{2.2}$$

then x_0 can be solved:

$$x_0 = \frac{eE_0}{m}\frac{1}{\omega^2 - \omega_0^2 + i\gamma\omega} \tag{2.3}$$

6

if we define the dipole moment of our atom as:

$$\mathbf{p} = \alpha(\omega)E_0\hat{\varepsilon} \tag{2.4}$$

then the complex polarizability α becomes:

$$\alpha = \frac{e^2}{m}\frac{1}{\omega^2 - \omega_0^2 + i\gamma\omega} \tag{2.5}$$

Classical theory cannot determine γ nor the fact that γ has a frequency dependence. Quantum mechanics shows that:

$$\gamma = \frac{\omega_0^3}{3\pi\epsilon_0\hbar c^3}|D_{mn}|^2 \tag{2.6}$$

where $D_{mn} = \langle m|\,\mu\,|n\rangle$ is the dipole matrix element between the m and n state of the atom. If we are talking about a 2 level atom, then m and n will be referring to the ground and excited states.

2.3   The Dipole Potential

The classical potential energy of a dipole is given by:

$$U_{dip}(\mathbf{r}) = -\mathbf{p}\cdot\mathbf{E} \tag{2.7}$$

This is the result of the fact that when a point dipole is placed in a uniform electric field, its energy is minimized when anti-aligned with the direction of the field. Again, we are inherently making the electric dipole approximation. If we have an oscillating electric field, we can find the energy by time-averaging over the frequency of oscillation:

$$U_{dip}(\mathbf{r}) = -\frac{1}{2}\langle\mathbf{p}\cdot\mathbf{E}\rangle = -\frac{1}{2\epsilon_0 c}Re(\alpha)I(\mathbf{r}) \tag{2.8}$$

where is $\frac{1}{2}$ comes from the fact that the dipole moment is induced, not permanent. [17]

The dipole force then is simply the gradient of the potential.

$$\mathbf{F}_{dip}(\mathbf{r}) = -\bigtriangledown U_{dip}(\mathbf{r}) = -\frac{1}{2\epsilon_0 c}Re(\alpha)\bigtriangledown I(\mathbf{r}) \tag{2.9}$$

[Eqn 2.9] is a simple yet fundamental result stating that *whenever there is a gradient in light intensity, there is a dipole force on the atom.*

If we take the classical expression for polarizability [Eqn 2.5] with the quantum mechanical expression for the damping term [Eqn 2.6] and substitute into the dipole potential [Eqn 2.8], we recover a useful expression for the dipole potential for a 2 level atom[17]:

$$U_{dip}(\mathbf{r}) = -\frac{3\pi c^2}{2\omega_0^3}\left(\frac{\gamma}{\omega_0 - \omega} + \frac{\gamma}{\omega_0 + \omega}\right)I(\mathbf{r}) \tag{2.10}$$

Since [Eqn 2.10] is derived from the classical polarizability, it does not take into account any saturation effects. But this is perfectly fine in our case of large tuning.

For comparision in the next section, we can goto the extreme case where we are so far detuned that $\omega \simeq 0$ and [Eqn 2.10] reduces to:

$$U_{dip}(\mathbf{r}) = -\frac{3\pi c^2 \gamma}{\omega_0^4} I(\mathbf{r}) \tag{2.11}$$

This expression, as we will see next, is equivalent to the potential an atom in a near-dc electric field.

2.4 Light Shifts

In the semi-classical model of light-matter interactions, we quantized the energy levels of the atom but treat the fields as classical waves. [16] This allows us to look at the dipole potential in a different perspective, namely the shift of the energy levels of the atom by light.

2.4.1 AC Stark Shift

We begin with a simple model of a two-level atom in a light field. We assume that the Hamliltonian of our system is the sum Hamiltonian of the atom and an external time-dependent and spatially varying potential.

$$H = H_0 + V_{ext}(\mathbf{r}, t) \tag{2.12}$$

It can be shown [15] that, to first order, the interaction of the electronic structure of the atom with light can be expressed in terms an oscillatory potential. We assume that the electric field is uniform across the atom so that E only depends on the center of mass coordinate $\mathbf{R}$. $\mathbf{r}$ is the relative electron-nucleus distance. [Eqn 2.13] is again expressing the *electric dipole approximation.*

$$V_{ext}(\mathbf{r}, \mathbf{R}, t) = -e\mathbf{r} \cdot \mathbf{E}(\mathbf{R}, t) \tag{2.13}$$

$$\mathbf{E}(\mathbf{R}, t) = E_0 \cos(\mathbf{k} \cdot \mathbf{R} - \omega t)\hat{\varepsilon} \tag{2.14}$$

The time-dependent Schrödinger equations for a 2-level atom is given by

$$i\hbar \dot{a}_1(t) = E_1 a_1(t) + V_{12} a_2(t) \tag{2.15a}$$

$$i\hbar \dot{a}_2(t) = E_2 a_2(t) + V_{21} a_1(t) \tag{2.15b}$$

Where subscript 1 denotes the ground state and 2 denotes the excited state. E_1 and E_2 are the eigenenergies and a_1 and a_2 are the probability amplitudes. V_{nm} are the dipole matrix elements. We have also ignored the diagonal dipole matrix elements because dipole transitions forbid them.

Now we define the natural oscillation frequency ω and Rabi frequency χ

$$\omega_{21} = \frac{E_2 - E_1}{\hbar} \tag{2.16a}$$

$$\chi_{21} = e(\mathbf{r}_{21} \cdot \hat{\epsilon})\frac{E_0}{\hbar} \tag{2.16b}$$

$$\chi_{12} = e(\mathbf{r}_{12} \cdot \hat{\epsilon})\frac{E_0}{\hbar} \tag{2.16c}$$

[Eqns 2.15] becomes

$$i\dot{a}_1 = -\frac{1}{2}(\chi_{12}e^{-i\omega t} + \chi_{21}^*e^{-i\omega t})a_2 \tag{2.17a}$$

$$i\dot{a}_2 = \omega_{21}a_2 - \frac{1}{2}(\chi_{21}e^{-i\omega t} + \chi_{12}^*e^{-i\omega t})a_1 \tag{2.17b}$$

From here these equations can only be solved exactly if we make the Rotating Wave Approximation (RWA) [Eqn 2.18]. The solutions are illustrated. [Fig 2.2]

$$\omega_0 - \omega \ll \omega_0 + \omega \tag{2.18}$$

But the RWA, as mentioned previously, is not a good approximation for our case of "far-far" detuning [Chapter 2.1.1]. Nonetheless, the algebraic solution is very elegant and clearly demonstrates the shifting of the energy levels so I will leave it in the appendix [Appendix A] to avoid confusion. A more appropriate solution is to use time-dependent perturbation theory and calculate the energy shifts. Without going through the derivation, I will reference the result[22][14][3][11]:

$$\Delta E_{1,2} = \mp \frac{|\langle 1| \mu |2\rangle|^2 |E_0|^2}{4\hbar} \left(\frac{1}{\omega_{21} - \omega} + \frac{1}{\omega_{21} + \omega}\right) \tag{2.19}$$

The sign of [Eqn 2.19] is important because it implies that the ground state is shifted down in the presence of an external field while the excited state is shifted up, a feature not predicted by classiacal theory.[Fig 2.2]

Replacing $|E_0|^2$ by $I/2\epsilon_0 c$ shows that this agrees with the classical dipole potential 2.10.

2.4.2 DC Stark Shift

In the case that the laser frequency ω is so far below ω_0, we can approximate the oscillating electric by a near static one. [22] This is the case with CO2 laser dipole traps where $\lambda = 10.6\mu m$.[14] Now we can find the shift of the energy levels by *time-independent perturbation theory* of an atom in a static electric field.[2]

$$V_{ext}(\mathbf{r}) = -\mu \cdot \mathbf{E} = -e\mathbf{r} \cdot \mathbf{E} \tag{2.20}$$

To the shift in energy to first-order perturbation for some state m is:

---

[2]Note that we still need a local field minimum or maximum to have a trapping potential. But static electric fields potentials must satisfy laplace's equations and therefore cannot have a local maxima or minima except at boundaries. We can dismiss this problem because we are not really using static fields but simply borrowing their solutions.

$$\Delta E_m^{(1)} = \langle \psi_m | V_{ext} | \psi_m \rangle = -e\mathbf{E} \cdot \langle \psi_m | \mathbf{r} | \psi_m \rangle \tag{2.21}$$

but by symmetry, this is always zero.

Thus we proceed to look at perturbation to second order:

$$\Delta E_m^{(2)} = \sum_{m \neq n} \frac{|\langle n | V_{ext} | m \rangle|^2}{E_m - E_n} \tag{2.22}$$

Turning to the 2-level atom, we look at the ground and excited state energies. In the 'dressed state' picture[17], the total energy of an atom in the ground state in a light field is equal to the energy of the light field, $E_1 = n\hbar\omega$, where n is the number of photons. The atom can absorb 1 photon to move into the excited state with energy $E_2 = \hbar\omega_0 + (n-1)\hbar\omega = -\hbar\Delta + n\hbar\omega$ and $E_1 - E_2 = \hbar\Delta$ where again $\Delta = \omega_0 - \omega$. Thus for the 2-level atom, the 2nd order shift is:

$$\Delta E_{1,2}^{(2)} = \pm \frac{|\langle 1 | \mu | 2 \rangle|^2}{\hbar\Delta} |E|^2 \tag{2.23}$$

The sign of [Eqn **??**] again is important because it implies that the ground state is shifted down in the presence of an external field while the excited state is shifted up.[Fig 2.2]

Now we can assume that our "DC" field is really a slowly oscillating ac field. Note that square of the time average of an AC field $E_0^{AC} e^{i\omega t}$ is $|E_0^{AC}|^2/2$ where as the square of the field amplitude of a DC field E_0^{DC} is simply $|E_0^{DC}|^2$ we must take into account an extra factor of 2 to make our fields comparable:

$$2|E^{DC}|^{(2)} = \frac{I}{2\epsilon_0 c} \tag{2.24}$$

and then use [Eqn 2.6] to express the dipole matrix elements in terms of γ to check our classical result again

$$\Delta E_{e,g}^2 = \pm \frac{3\pi c^2}{\omega_0^3} \frac{\gamma}{\hbar\Delta} I \tag{2.25}$$

Now if let ω goto 0 for extremly large red detuning, we get the same expression as the classical potential for a near DC field [Eqn 2.11].

2.4.3 Multi-Level Atom Light Shift

If we now consider a more realistic model where an atom has multiple atomic energy levels, then we need to modify our results and [Eqn 2.23] from the above sections. Fortunately, this modification is a simple one, we just need to take into the contributions to the energy shift from all other levels. This follows from 2nd order perturbation theory.

[Eqn 2.19] changes to:

$$\Delta E_n = \Sigma_{m \neq n} |\langle n | \mu | m \rangle|^2 \frac{|E_0|^2}{4\hbar} \left(\frac{1}{\omega_{nm} - \omega} + \frac{1}{\omega_{nm} + \omega} \right) \tag{2.26}$$

[Eqn 2.23] changes to:

Figure 2.2: The AC and DC Stark Shifts for the 2-level atom.[6] (a) is the AC stark shift for detuning below resonance (b) is the AC stark shift for detuning above resonace (c) is the DC stark shift
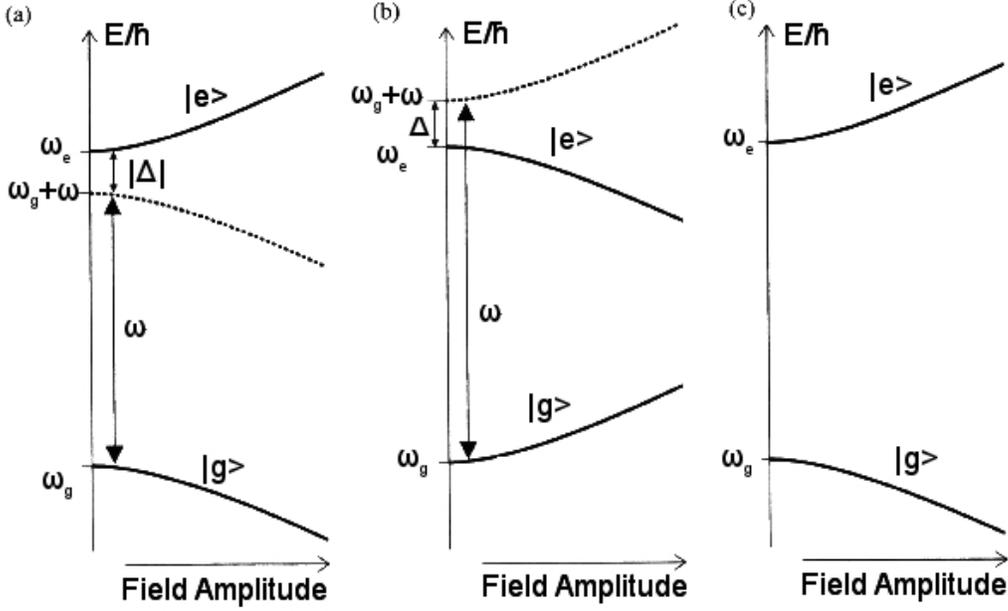
$$\Delta E_n^{(2)} = \Sigma_{m \neq n} \frac{|\langle n| \mu |m\rangle|^2}{\hbar \Delta} |E|^2 \tag{2.27}$$

2.5 Scattering Rate

All of the theory of dipole potential and force is the result of elastic scattering of light on atoms. This is known as rayleigh scattering. However, the atom can also inelastically absorb an photon from the light field and spontaneously re-emit it. When this happens, the atom will get a momentum kick as well as gain some kinetic energy and can leave the trap. In classical terms, the absorption process is related to the imaginary part of the complex polarizability α [Eqn 2.5]:

$$P_{abs} = \langle \dot{\mathbf{p}} \cdot \mathbf{E} \rangle = \frac{\omega}{\epsilon_0 c} Im(\alpha) I \tag{2.28}$$

The rate at which photons are being absorbed (and re-emitted) is:

$$\Gamma(\mathbf{r}) = \frac{P_{abs}}{\hbar \omega} = \frac{1}{\hbar \epsilon_0 c} Im(\alpha) I(\mathbf{r}) \tag{2.29}$$

again assuming far tuning and neglecting saturation effects, we use the classical polarizability α and the quantum γ [Eqn 2.6], we can derive a useful expression for the scattering rate:

$$\Gamma(\mathbf{r}) = \frac{3\pi c^2}{2\hbar \omega_0^3} \left(\frac{\omega}{\omega_0} \right)^3 \left(\frac{\gamma}{\omega_0 - \omega} + \frac{\gamma}{\omega_0 + \omega} \right)^2 I(\mathbf{r}) \tag{2.30}$$

11

Figure 2.3: The gaussian beam profile[20]
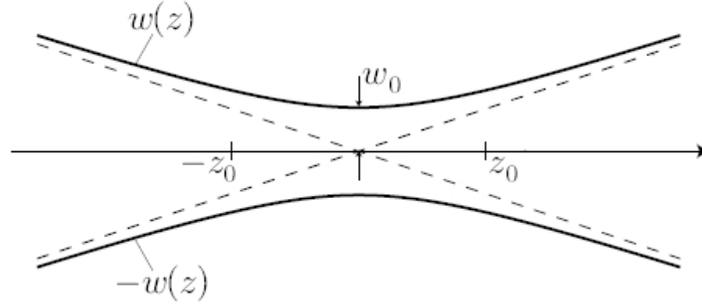
This number is generally very small for large detunings as the denominator goes as $\frac{1}{\Delta^2}$. This is the one of the main reasons why atoms can have long lifetimes in a far detuned dipole trap.

2.6   Gaussian Beam Traps

If we use a laser beam with a gaussian profile and tightly focus it [Fig 2.3], the gradient of intensity is huge at the center and can give rise to large dipole potentials according to [Eqn 2.10].The intensity profile of a gaussian beam is given by:

$$I(r, z) = I_0 e^{\left(- \frac{2r^2}{w^2(z)} \right)} \tag{2.31}$$

where $w(z)$, the *beam width*, and z_0 the *rayleigh range* is given by:

$$w(z) = w_0 \sqrt{1 + \left(\frac{z}{z_0} \right)^2} \tag{2.32a}$$

$$z_0 = \frac{\pi w_0^2}{\lambda} \tag{2.32b}$$

I_0 can be expressed in terms of the beam power

$$P_0 = \frac{I_0}{2} \pi w_0^2 \tag{2.33}$$

and the intensity can be rewritten as:

$$I(r, z) = \frac{2P_0}{\pi w^2(z)} e^{-\frac{2r^2}{w^2(z)}} \tag{2.34}$$

Since z_0 varies with the square of w_0, the confinement in axial direction of the beam is typically much smaller than radial confinement and the potential surface resembles the shape of a peanut in 3 dimensions.

If the kinetic energies of the atoms are small compared to the height of the potential well $U_0 = |U(r = 0, z = 0)|$ or *trap depth* such that they are sitting near the bottom of the well, we can approximate the form of the potential by the harmonic oscillator potential:

Figure 2.4: An intensity isosurface for a gaussian beam trap in 3D
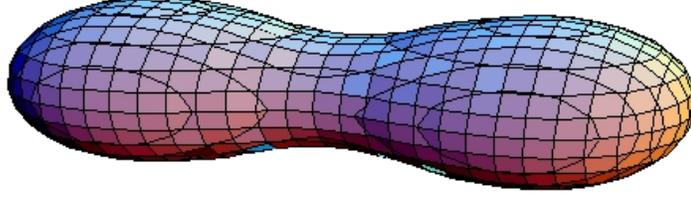
$$U(r, z) \simeq -U_0 \left[1 - 2 \left(\frac{r}{w_0} \right)^2 - \left(\frac{z}{z_0} \right)^2 \right] \qquad (2.35)$$

where U_0 is given by [Eqn 2.10] and [Eqn 2.34] and setting $r = 0, z = 0$

$$U_0 = -\frac{3\pi c^2}{2\omega_0^3} \left(\frac{\gamma}{\omega_0 - \omega} + \frac{\gamma}{\omega_0 + \omega} \right) \frac{2P}{\pi w_0^2} \qquad (2.36)$$

For harmonic potentials, we can define frequencies of oscillation for the radial and axial directions:

$$w_r = \sqrt{\frac{4U_0}{mw_0^2}} \qquad (2.37a)$$

$$w_z = \sqrt{\frac{2U_0}{mz_0^2}} \qquad (2.37b)$$

[Eqn 2.37] are called the *trapping frequencies*.

To achieve better radial confinement, we can create a standing wave trap by reflecting the gaussian beam back onto itself. This trap has the potential of the form:

$$U(r, z)_{sw} \simeq -2U_0 \cos^2 (kz) \left[1 - 2 \left(\frac{r}{w_0} \right)^2 - \left(\frac{z}{z_0} \right)^2 \right] \qquad (2.38)$$

The standing wave potential gains naturally gains a factor of 2 in depth U_0, and an additional factor of 2 from the fact the intensity is doubled from the beam passing over the same spot twice. Effectively, this is 4 times the potential depth of a single pass beam and achieves much better radial confinement by forming antinodes with periodicity $\lambda/2$. This is also called an *optical lattice* [Fig 2.5].

2.7 Trap Numbers

Here we will look at a simple model given by O'Hara[14] for predicting the number of trapped atoms in a dipole trap. This model looks at the number of atoms in a gas in a dipole potential and in thermal equilibrium with their motions described by Hamiltonian dynamics.

Figure 2.5: A potential isosurface for a standing wave trap in 3D
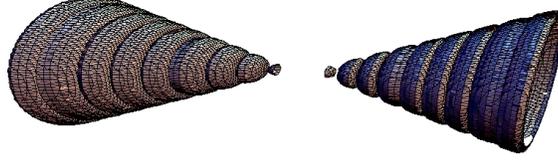
We assume that initially our atom cloud has density and temperature given by n_{MOT} and T_{MOT}, the parameters of our MOT.

The single particle Hamiltonian is

$$H(\mathbf{x}, \mathbf{p}) = \frac{p^2}{2m} + U(\mathbf{x}) \tag{2.39}$$

where $U(\mathbf{x})$ is the dipole potential [Eqn 2.10].Then the phase-space distribution in equilibrium is given by

$$W(\mathbf{x}, \mathbf{p}) = \frac{n_{MOT}}{(2\pi m k_B T_{MOT})^{\frac{3}{2}}} exp\left[-\frac{H(\mathbf{x}, \mathbf{p})}{k_B T_{MOT}}\right] \tag{2.40}$$

$W(\mathbf{x}, \mathbf{p})$ is normalized such that the spatial density $\to n_{MOT}$ for $x, y, z \gg w_0, z_0$. This assumes that the MOT is much greater in all dimensions than the trap and the fraction of atoms in the MOT is much greater than the number of atoms in the trap.

At the center of the trap, the density is enhanced

$$n(0) = n_{MOT} exp\left[\frac{U_0}{k_B T_{MOT}}\right] \tag{2.41}$$

The total number of trapped atoms is the integral over phase space where the kinetic energy is less than the potential energy.

$$N_T = \int_{U-E<0} d^3x d^3p W(\mathbf{x}, \mathbf{p}) \tag{2.42}$$

This integral can be simplified and then computed numerically

$$N_T = N_0 \mathcal{F}\left[\frac{U_0}{k_B T_{MOT}}\right] = n_{MOT} V_{trap} \mathcal{F}\left[\frac{U_0}{k_B T_{MOT}}\right] \tag{2.43}$$

where N_0 represents the number of atoms at the MOT density that fall in the trapping volume $V_{trap} = \pi^{3/2} w_0^2 z^0$. The trapping factor $\mathcal{F}(q)$, $q = \frac{U_0}{k_B T_{MOT}}$ is given

$$\mathcal{F}(q) = \frac{q^{3/2}}{2} \int_0^1 dx x^2 g(x) e^{q(1-x)} \tag{2.44}$$

where

$$g(x) = \frac{\beta^{3/2}(1-x)^{1/2}}{x^2} \frac{16}{\pi} \int_0^1 du u^2 \sqrt{e^{\beta(1-u^2)} - 1} \tag{2.45a}$$

14

$$\beta = -ln(1-x) \tag{2.45b}$$

[Eqn 2.43] shows that in this model, the number of trapped atoms is proportional to the trapping volume V_{trap} and to some function of the potential $\mathcal{F}(U_0)$. This tells us that we can enhance the trapping number in several ways:

- increase the light intensity

- decrease the MOT temperature

- increase the MOT density

The trap number also has a more subtle dependance on the width the beam. The trapping volume has a w^4 dependance while the function $\mathcal{F}$ increases rapidly with the potential, which has a $1/w^2$ dependance. This is intuitive: increasing w makes the trap deep but skinny, decreasing the w makes the trap shallow but large. Thus the parameter w can be, at least in this model, optimized to maximum trap number.

Note that this model will break down if the number of atoms trapped approaches a significant fraction of the number of atoms in the MOT or if any factor of the trap significantly affects the equilibrium density of the MOT.

2.8   Calculations for Lithium

For our 20W Fiber Laser at 1064nm, we have about 11W of power arriving at the cell. This power is focused down to a spot size of approximately 50μm. In a double pass configuration, the effective power is multiplied by 4 to form a standing wave potential.[Eqn 2.38] In this way, the axial trapping frequency will need to be revised as the atoms sit in a periodic lattice. Given a MOT temperature of $300\mu K$ and MOT density of $10^{16} atoms/m^3$ and the dipole matrix elements for the D1 and D2 lines [Appendix J], we calculate [Appendix D] the following parameters:

Table 2.1: Calculated Trapping Parameters for Li6

Standing wave potential Depth for $F = 3/2$ Ground State (mk)	1.23089
Standing wave potential Depth for $F = 1/2$ Ground State (mk)	1.2309
Radial trapping frequency (kHz) for $F = 3/2$ Ground State	52079.3
Scattering rate (photons/s/atom)	0.397818
Expected atom number from simple model	$1.94 * 10^6$

Chapter 3

Construction

In this chapter I will describe the construction, design, and measurements made towards building the optical dipole trap.

3.1 The Fiber Laser

In this section, I will introduce our trapping laser and discuss the measurements and calibrations done on it before setting it up for the dipole trap.

3.1.1 Choice of Laser

There are many choice of lasers for building a far detuned optical trap. We have choosen to use a IPG Photonics YAG fiber laser with the following notable specifications:

- 20W CW Intensity

- 100KHz linewidth

- 1064nm

In this section, I will discuss the reasons why we are using this laser for the optical trap.

For each type of laser, there are many factors to consider such as the power, bandwidth, and wavelength. Fo example, there are traps made from 300mW titanium sapphire lasers detuned only a few nanometers from the laser cooling atomic resonances.[18] There are traps made from

Figure 3.1: The IPG Photonics Fiber Laser Amplifier

10.6μm 40Watt CO2 lasers which are detuned by more than an order of magnituide in wavelength. We want a laser that is tailored to our experimental needs. Namely, we require low losses and narrow bandwidth for photoassociative spectroscopy, high power for trap depth and density. [14]

Wavelength

Since the probability for absorption is inversly proportional to the square of the detuning from resonance, after a few nanometers detuned, trap losses due to scattering become negligible compared to other collisional loss mechanisms such as photoassociative collisions and hyperfine-changing collisions.[18] However, when far enough detuned ($10\mu m$), even these losses are reduced significantly and 1/e trap lifetimes of 300 seconds have been observed.[12] We considered purchasing a CO2 laser but later decided that 1064nm would give us sufficient trap lifetimes while the fiber laser is more compact and easier to work with.

Power and Bandwidth

The calculation in [Chapter 2.8] shows that if we can retain 10W of optical power at the atoms, a retroreflection would provide us with 44W of standing wave intensity leading to a trap depth of 1.2mK (for 50μm waist), while a resonant amplification of 10 times would allow a 100W circulating intensity and a trap depth of 3mK. Only having a narrow bandwidth laser would allow us resonant amplication in a cavity. This because if we were to amplify a beam with linewidth broad compared to the linewidth of the resonant cavity, most of the power in the unmatched modes would be rejected.

3.1.2 Collimation

The fiber laser needed to be collimated before anything else can be setup. The usual method is to propagate the beam unobstructed over a long distance (compared to distance in the experiment over which the beam need to stay collimated) and minimize the spot size. However, since the fiber laser is invisible and can only be seen by IR viewers and IR cards, it is fairly difficult to judge the size of the beam by eye. So We developed a computer program with Labview and C that grabs images of beams in real time, automatically fits gaussian curves and displays the width of the beam along with other information. This allowed us to image the beam either on the camera or a screen and adjust the collimation screw to minimize the beam size over a long distance. When viewing the beam on a screen, it is very hard to avoid speckle on the image unless the surface is extremely smooth. Thus we used a small mechanical motor to drive a rotating cardboard and use that as the screen. This effectively averages the effects from speckle and produces a much cleaner image. These techniques also proved to be useful later.

3.1.3 Mirror Damage

We found that using the fiber laser with silver coated mirrors can incur irreversible damage on the mirrors. The reason we considered using silver mirrors is because they have > 97% (Eg: Thorlabs protected silver mirrors) reflectivities at infrared wavelengths and are cheaper than dielectric mirrors. However, they tend to absorb the light that is not reflected and heat up very quickly. We observed two major effects of the fiber laser on the silver mirrors. The first effect is

Figure 3.2: Damage of the silver mirror incurred by the fiber laser

the temporary heating of the coating surface which causes a thermal lensing effect that expands the beam. The higher the power of the laser, the more the beam expanded upon reflection. The second effect is permanent damage on the mirror when the intensity exceeds the damage thresholds of the silver coatings which are typically $0.5J/cm^2$ (Thorlabs Silver). The laser tends to burn a hole [Figure 3.2] on the coating and then diffracts around it to produce airy rings so it becomes very clear when this happens. In the end, we decided to avoid using metal mirrors and bought high powered dielectric mirrors for the trap.

3.1.4   Laser Spectrum

In order for trapping to work, we need to make sure that the laser is running in single mode near 1064nm as specified. The first scan [Figure 3.3] shows the lineshape of the laser near the lasing wavelength. Note, the laser is specified to have a 20kHz linewidth and our OSA (Optical Spectrum Analyzer) can only resolve 0.05nm. Thus if there were narrow multi-mode operations, this OSA sweep would not detect it. A fabry-perot is needed to precisely determine the linewidth and the single mode operation. The second scan [Figure 3.4] sweeps across 1300nm to make sure that there the entire spectrum is 'clean' (10nm resolution).

3.1.5   Mounting

The fiber laser light is coupled out from the housing, through a 1m fiber and passes through a 60dB optic isolator. Unfortunately there was no mounting equipment supplied by the manufacture so we had to build our own. The mounting assembly uses a cylindrical clamp to hold the isolator in place and the clamp fits into an arch-type structure that directs the beam vertically down onto the table where it can be caught by a mirror placed under the arch. The CAD drawings are included[Appendix C].

3.2   Trap Design

In this section, I will discuss the considerations that went into the design of the trap and choosing the trap optics. It is important to note that the design of the trap revolved around the fact that we wanted to achieve 1mK trap depth for lithium and at least 10^5 lithium atoms in our trap for
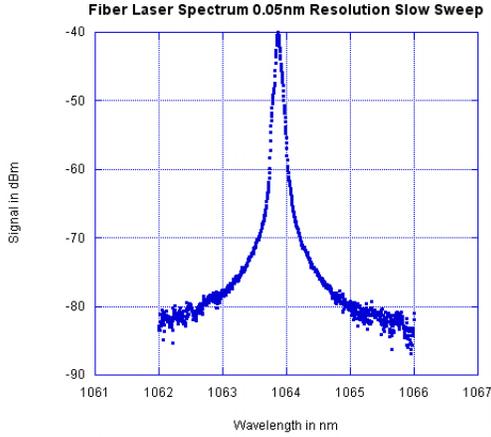
Figure 3.3: Narrow Spectrum Sweep
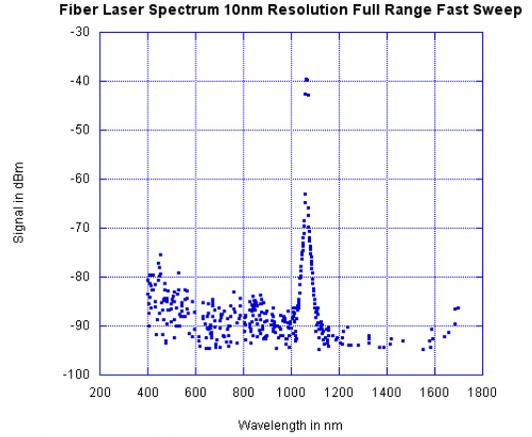
Figure 3.4: Broad Spectrum Sweep

photoassociation spectroscopy. For the same trap parameters, rubidium would give higher trap depth (1.7 mK) and more atoms so this is not our limiting factor. Other considerations include the ability to tune the trap depth over 4 orders of magnitude in dynamic range[11] for evaporative cooling and having fast shuttering mechanisms for quickly switch on/off the trap.

3.2.1 Lenses

In order to achieve the desired 1mK trap depth we need to either have high optical power or a small beam waist. We choose to use a standing wave power of 44W and 50μm beam waist. This has been calculated [Chapter 2.8] to give us a 1.2mK trap depth, and in theory, greater than the amount of trapped atoms needed. To achieve tigh focusing, we bought two 300mm Achromatic Doublet lenses from Thorlabs (**AC254-300-B**) with a AR (Anti-Reflection) coating in the IR range. These lens are made from a pair of convex and concave lens to correct for both spherical and chromatic abberation. Their main feature is the parabolic focusing curve [Fig 3.7] that allows light of 2 different wavelengths to come to a focus at the same spot. We planned to have the photoassociation light (800nm) propagate colinear with the trap and also come to a focus on the atoms. This achromat allow us to focus both beams within 150μm of each other, which is much shorter than the axial trap dimension (7mm).

3.2.2 Mirrors

To create the standing wave trap, we purchased two 1064nm 1/2inch 250mm ($R > 99.9\%$) spherical mirrors (**Layertech Art. 100708**) from Layertech. We only need one for the current setup but originally planned to build a resonator with these two mirrors. These mirrors also have high transmission at 808nm to allow our photoassociation light to pass through cleanly.

For flat mirrors, we purchased three high energy ND:YAG mirrors with CW damage threshold of 500kW$/cm^2$ (**NewFocus 5104**) and two Thorlab Broadband Near-IR dielectric mirrors with

Figure 3.5: Mounting Assembly the for Fiber Laser Output Isolator
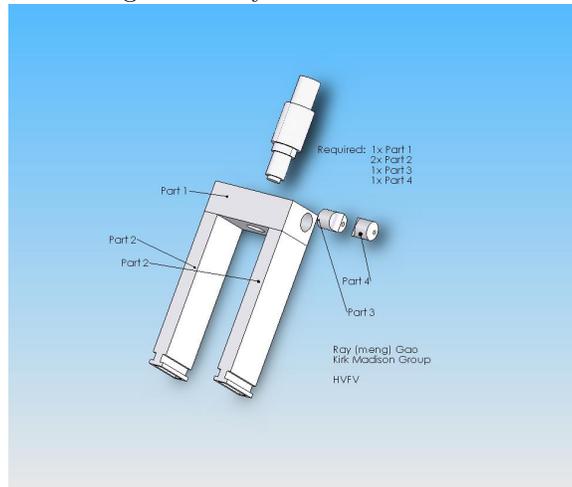
Figure 3.6: Double Pass Standing Wave Trap
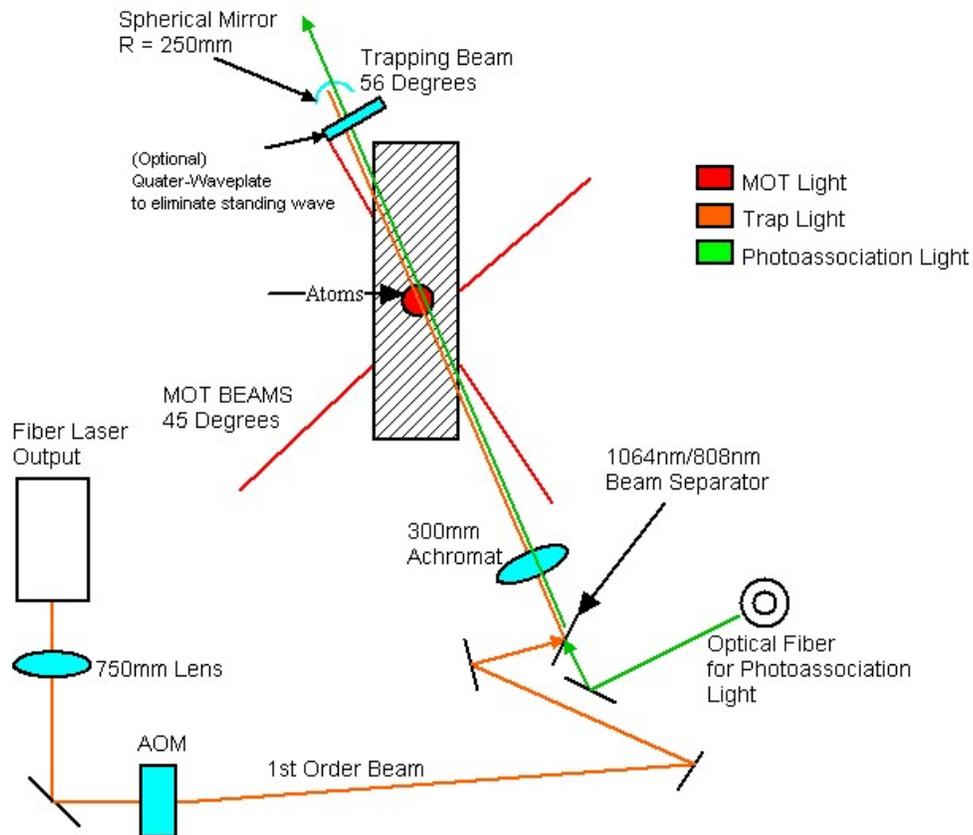
Figure 3.7: The chromatic focusing properties of the Thorlabs AC254-300B
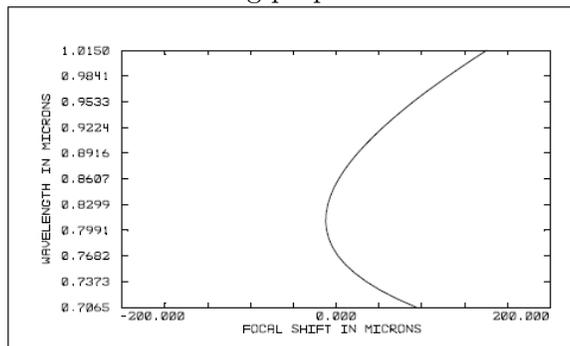
CW damage threshold of 2kW/cm^3 (**Thorlab BB1-E03**). We also have several high energy ND:YAG dielectric mirrors extracted from an old Coherent Antares laser.

3.2.3 Other

To couple in the photoassociation light so that it is colinear with the trap light, we purchased a 45 degrees 1064nm/808nm beam separator from Laytertech (**Layertech Art. 104738**). This special optic reflects 1064nm and transmits 808nm light at 45 degrees.[Fig 3.6]

We have also purchased two 1064nm $\lambda/2$ waveplates (**CASIX WPZ1315-L/2-1064**) and one $\lambda/4$ (**CASIX WPZ1315-L/4-1064**)waveplate from CASIX optics. Although, not put to use yet, the $\lambda/2$ waveplate,in conjunction with a polarzing beam splitter allow us to manually control the intensity of the beam while the $\lambda/4$ waveplate will give us the option of using a double-pass running wave trap.

3.2.4 AOM

We used an AOM (Acousto-Optic Modulator) for both shuttering and controlling the intensity of the trap beam. There are plenty of references[20] on how an AOM works so I will not explain it in detail here. We did not have any AOM available except for an old unspecified one and a modelocking AOM from a Coherent Antares laser. (Although now we have recently purchased a new high power 1064nm AR coated AOM for the trap) Thus we needed to characterize these AOMs to see if one was usable. There are three properties that are relevant to us, resonance frequency, static power loss, and 1st order diffraction efficiency.

Resonance Frequency

The AOM's internal RF circuit is designed with some specific resonance frequency. When RF is coupled into the circuit near resonance, the impedance will drop and so will the reflected power. Thus to find the resonance, we couple in a variable RF source through a RF power divider and into the AOM.[Fig 3.9] The reflected power can be measured at the other output of the power divider.

We coupled in a 30dB signal and swept it from 15-150MHz with a computer program.[Appendix F] The results are shown. [Fig 3.10][Fig 3.11] The "old" AOM shows a clear resonance at ap-

Figure 3.8: The 'old' AOM
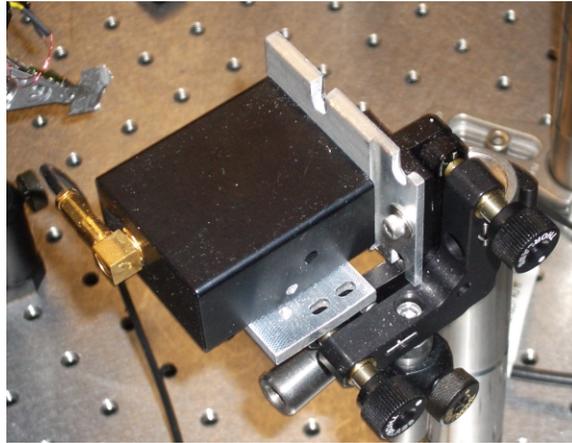
Figure 3.9: Setup for measuring AOM resonances. When the input frequency is swept through a resonance of the AOM, the measured reflected power drops.
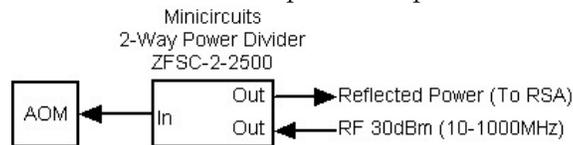
proximately 78MHz while the Antares AOM does not. Thus we decided to employ the "old" AOM.

Static Insertion Loss

We measured the "old" AOM has a static insertion loss of 12% at 1064nm. Thus 12% of the input power is immediately lost due to reflection (and hopefully not absorption).

1st Order Diffraction Efficiency vs Input Optical Power

We maximized the diffraction to the 1st order at low power and then measured the efficiency as a function of optical power. We want to know this because we want to know if the AOM crystal is being heated by the beam and possibily producing thermal lensing effects. The efficiency here is defined as the ratio of the power in the first order beam to the power in the AOM when no RF is driving it.

AOM Driver

The AOM driver is the device used to produce the RF signal to drive the AOM. We used the *Intraaction* 60Mhz 3W deflector driver (Model DE-603H6).
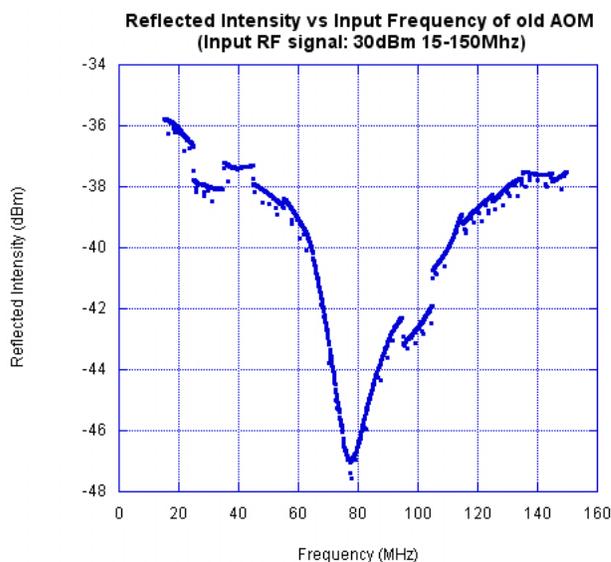
Figure 3.10: Old AOM Resonance Curve
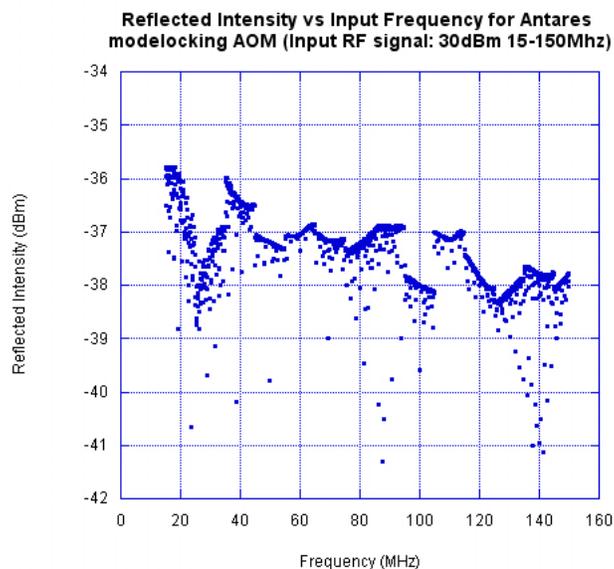
Figure 3.11: Antares AOM Resonance Curve

3.2.5 Beam Dumps

Due the relatively high power of the fiber laser, most of the unwanted/rejected light will need to be captured by beam dumps. Beam dumps can be purchased commercially but we decided to build our own due to simplicity and cost.

Design

A beam dump essentially just absorbs the light in a material and dissipate it as heat. Depending on the material of the beam dump, each time the beam is incident on it, it will absorb some light and reflect the rest (We don't want transmission so we usually choose opague materials). Thus to maximimze absorption, we designed the geometry in such a way that the beam is reflected as many times as possible inside the beam dump. Typical geometries include a block of stacked razor blades and cones. We decided to use torus geometry adopted from Florian Schreck[19]. The idea was to bend a copper tube into a torus with a large radius of curvature so that the incident beam is reflected near grazing incidence and so will each subsequent reflection. The beam will travel around on the inside of the torus and hopefully be almost completely absorbed by the time it reflects back out.

Building the Beam Dump

Even though copper is rather malleable, it is difficult to bend a 3/4" hollow copper pipe without denting or breaking it. A common way is to anneal copper. Pure copper begins to anneal(recrystalize) at 250 Celsius but actually need to be heated to much higher temperatures so it becomes really soft. Also, inpure copper and copper alloys tend to have much higher recrstal-

Table 3.1: AOM Diffraction Efficiency vs Optical Power

Optical Power(W)	Diffraction Efficiency (%)
0.5	0.69
1	0.66
2	0.67
3	0.68
4	0.7
5	0.7
10	0.7
15	0.7
20	0.71
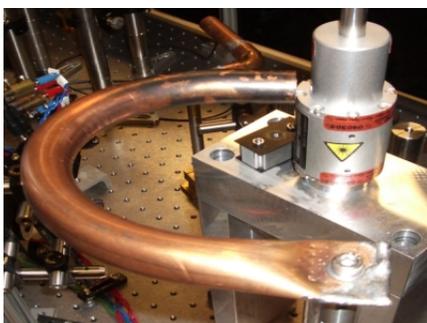
Figure 3.12: A torus shaped beam dump

Figure 3.13: A simpler beam dump

ization temperatures. Another way is to use a metal pipe bender. However, this requires the inside of the pipe to be filled with some support material so that the copper pipe will not break while being bent. This can be done by inserting a spring or sand into the pipe. With the spring, any large angle bends will cause the spring to become lodged against the inner surface of the pipe and almost impossible to remove. With sand, care must be taken to seal the ends of the tube so it will not flow out when being bent. In the end, we made a few large copper torus with the metal bender[Fig 3.12]. We then found that a simpler design that also works. This is by simply soldering two smaller straight copper pipe sections onto a copper elbow and then clamping one of the ends. This design is gives less reflection surfaces than the torus but is more compact and simpler to build[Fig 3.13].

3.2.6 Final Design

[Fig 3.14] Shows the current a flat cartoon layout of the current optics setup that we use for the dipole trap. The first lens is required to focus the beam through the AOM because the crystal has a very small clear aperature. [Fig 3.15] shows this layout on the optics table.

3.3 Trap Focusing Properties

To verify that our trap can work, we measured the beam focusing properties of the achromat lense and the 250mm spherical mirror.

Figure 3.14: Distance layout and corresponding beam waists at each optic
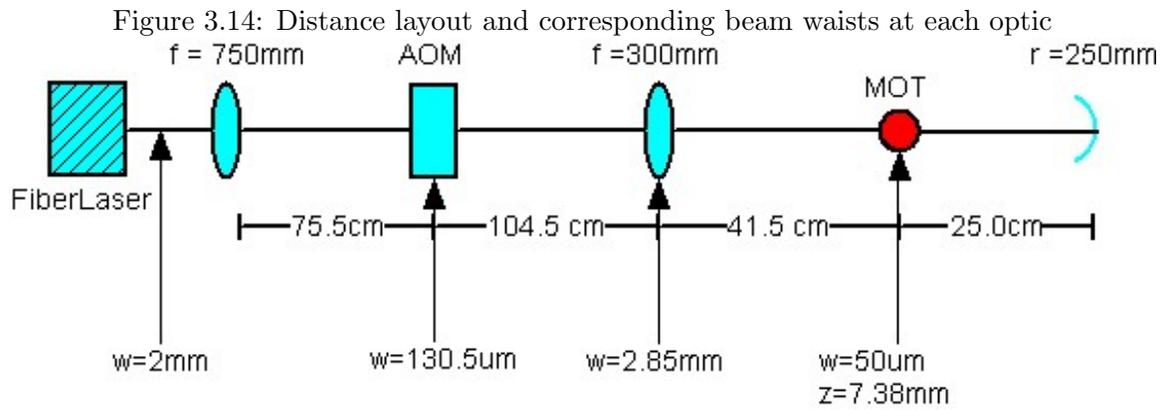
Figure 3.15: Dipole Trap in real life

Figure 3.16: Setup for measuring the minimum focus of our trap
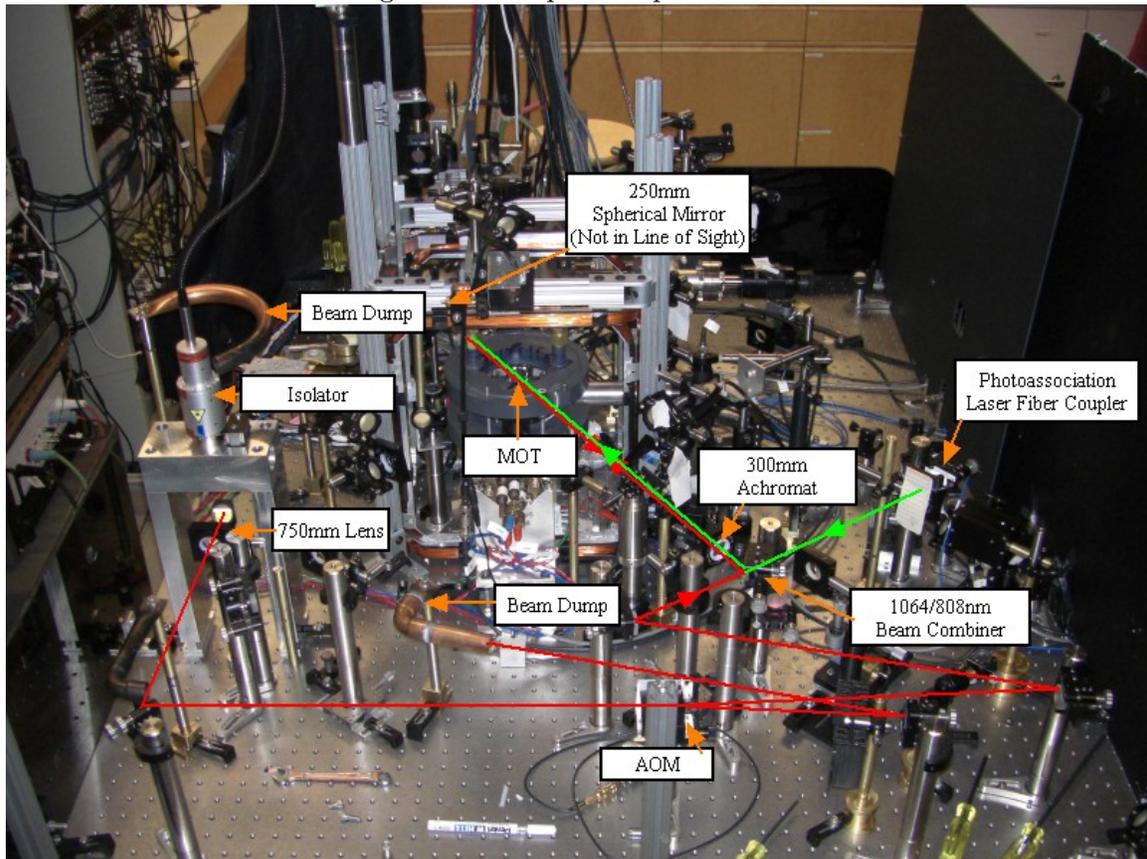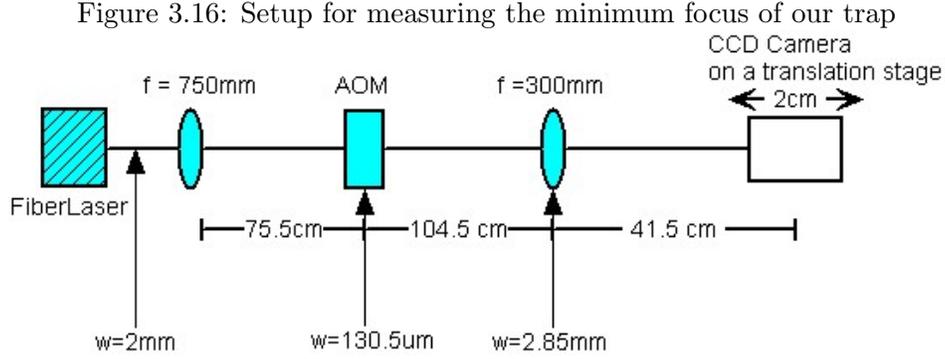
Figure 3.17: Plot of the minimum focus our trap beam
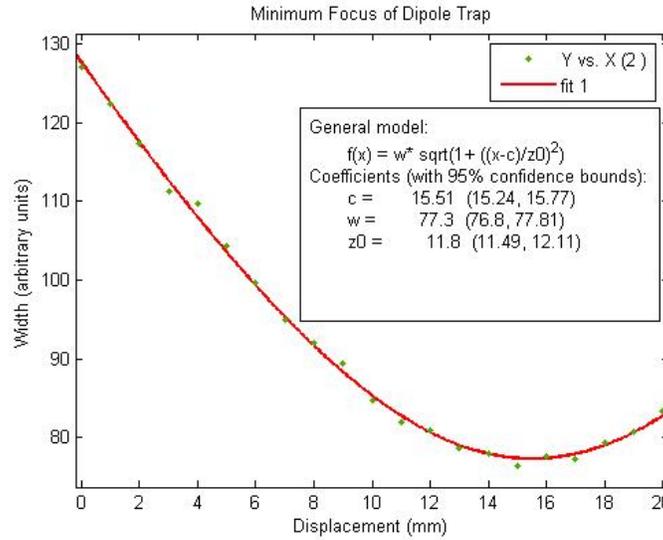
3.3.1   Minimum Focus

The minimum spot size for for focusing a beam through a lens is easily found by propagating a gaussian beam through a lens and requiring the radius of curvature to approach ∞ and using the approximation that the focal distance d is approximately equal to f, the focal length[20].

$$w_{min} = \frac{\lambda f}{\pi w_{in}} \tag{3.1}$$

In practice, lenses are not parabolic and exhibit abberations that limit this minimum focus. The Melles-Griot catalog recommends multiplying [Eqn 3.1] by 4/3 as a rule of thumb for accounting for abberations. We proceeded to measure the minimum focus by use exactly the same setup as [Fig 3.14] but except with a piece of glass instead of the cell. Qe placed a CCD camera on a translation stage and recorded the width of beam with a computer program as the camera was translated through the focus.[Fig 3.16]

[Fig 3.17] is the result in one dimension and shows $z_0 = 11.8 \pm 0.31cm$ which corresponds to a beam waist of $w_0 = 63.2 \pm 1.7\mu m$. Since our beam impinging on the 300mm lens is not

Figure 3.18: A Melles-Griot explanation of astigmatism [23]
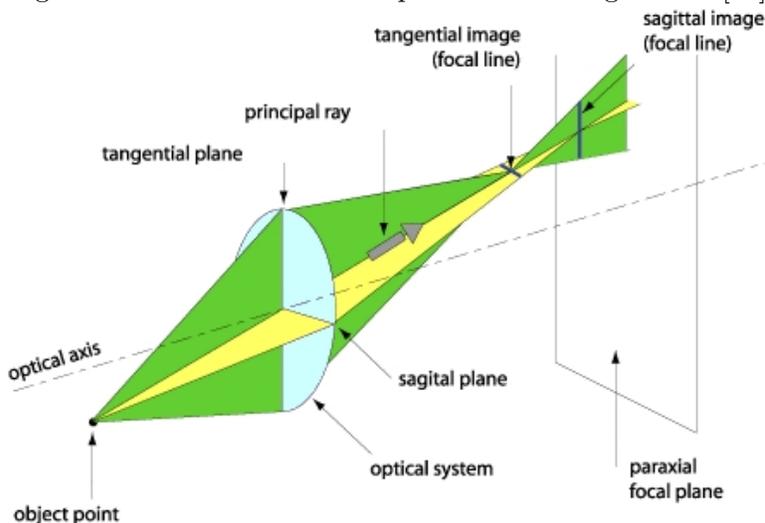
collimated, we also wanted to know how sensitive the beam waist was to the radial alignment of the 300mm achromat (knowing that we have set it to approximately the right location to begin with). This is important because we want to how sensitive would the radial alignment of this lens affect trapping and because we have no way to finding out precisely how far away this lens is from the atoms. So we repeated this measurement but translated the 300mm upto 1mm displaced from its current position (on a translation stage) and recorded how the waist changes. We found that over this distance, the rayleigh range only varied about 1%, which is acceptable.

3.3.2   Astigmatism

Another important feature of the trap geometry is astigmatism. A beam is astigmatic if its focusing distance is different along the tangential and sagittal planes. [Fig 3.18]This can be caused by off-axis focusing by a lens or more generally defects in optics. The AOM is known to introduce astigmatism in beams. We are interested in knowing the amount of astigmatism of the beam focus at the trap because if the distance betweeen the tangential focus and the sagittal focus is greater than $\sqrt{2}$ times the waist (rayleigh length) in either direction, then our trap will have significantly shallower depth at the center. Then we would require astigmatism compensation optics. We did a similar beam focus measurement as before but in a longer axial range and in 2 dimensions. We did this by translating a camera on a rail over 10-15cm and taking images at even intervals. Then we reflected the beam off the spherical mirror measured the focus of the reflected beam. We did this by moving the rail so that it was slightly misaligned off the beam axis so that it wouldn't block the forward beam. Results show that there was very little astigmatism as the beam aspect ratio at the waist was approximately 1:1.

In addition, we need to check that the retro-reflected beam comes to a focus at nearly the same spot as the forward beam. Results showed that at 41.5cm, the forward beam focus and reflected beam waist was displaced by approximately 1cm. Thus we moved the back mirror by an amount such that the foci of both beams overlapped.

Figure 3.19: Contours rotated to show the ellipticity (unintended) of our beam as it passes through the focus(1 pixel $\approx 6\mu$m)
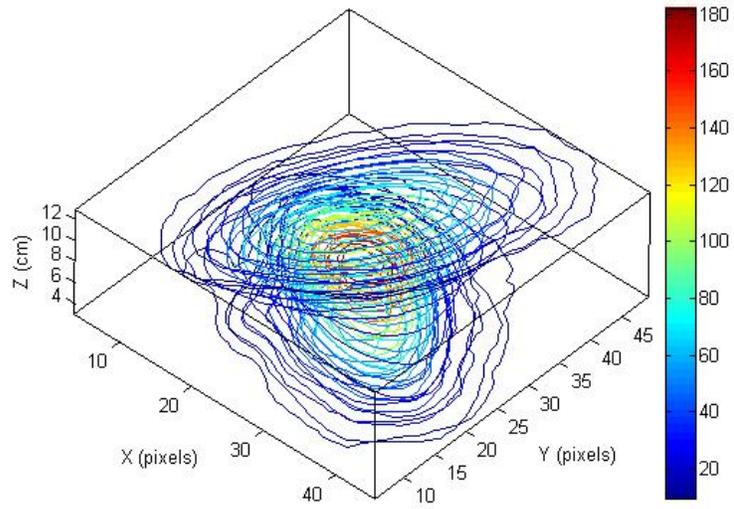
Figure 3.20: Contours of the trap beam near focus (1 pixel $\backsimeq 6\mu m$)
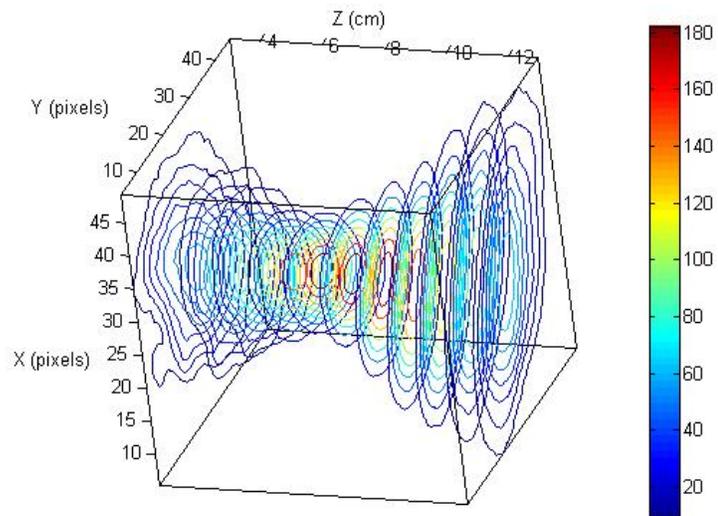
Chapter 4

Experimental Control Overview

In order to load and image the trapped atoms, we need precise timing controls. This is done by our QDG computer control system (derived from the UT Austin Control System[21]). Here I will briefly outline how this system works so that it becomes clear how we are running our experiments. Details can be found here. [2]

4.1 Hardware

All our experiments require millisecond scale timing. We use a 20Mhz National Instruments Data Acquistion (DAQ) PCI card from a computer to issue commands to the system. This card is capable of sending 32-bit data words at 20Mhz. These 32-bit words drive a special 50 pin 'UT bus' [21] that control 3 classes of instruments: 50 Ohm Digital Output buffers, -10/+10V Analog output buffers, and 0-150Mhz DDS (Direct Digital Synthesizer). These 3 types of outputs are enough to run our entire system. The digital outputs are simply +5/0V TTL signals that are used to send triggers to cameras,shutters,and switches etc. The analog outputs are used to for voltage controlled drivers, such as the magnetic coil drivers and electro-optic drivers etc. The DDS are used to generate high frequency RF signals to control mostly our AOMs.

4.2 Software

The software suite for the control system was developed by Ovidiu Toader. The idea is that we write our experimental sequences, or 'Recipes', in the form of **Python** (a simple scripting language) code. Then a main server translates the python code to bytecode (32-bit binary instructions) to feed the National Instruments card. All of the experimental work in the subsequent chapters are written as Python recipes.

Figure 4.1: QDG Control System overview [2]
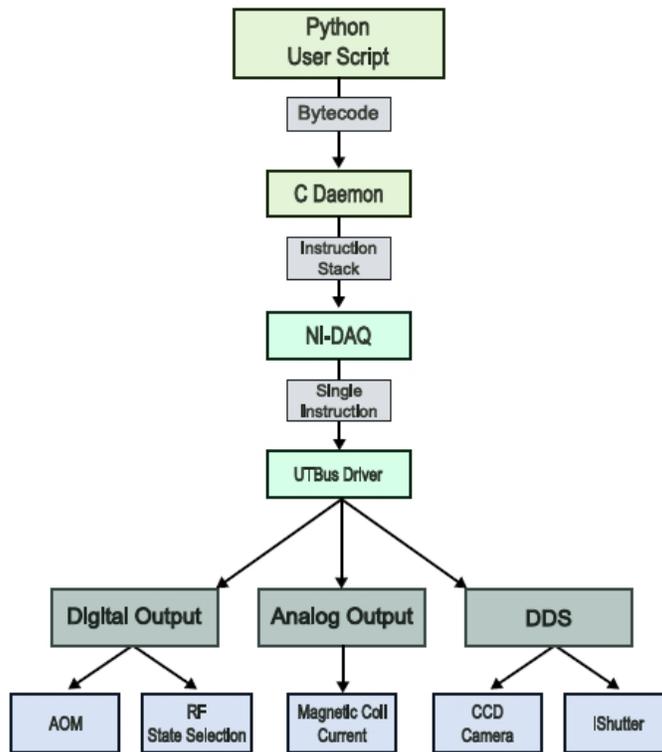
Chapter 5

Loading and Alignment

5.1 Loading

The optical trap can be loaded by simply overlapping the focus of the trapping beam with the MOT. Then if we turn the MOT off, we should be able to observe the trapped atoms in the optical trap. To improve loading, we need to improve the density of the MOT and minimize the MOT temperature as predicted in [Chapter 2.7]. To minimize the MOT temperature, we can employ cooling schemes such as polarization gradient cooling or raman sideband cooling [15]. However, this is for future work. It is much easier to increase the density by 'compressing' the MOT. We can do this by tuning the trapping lasers closer to resonance and increasing the magnetic field strength. Both of these processes will reduce the atom number in the MOT so there are optimizations that need to be worked out. It has been shown that certain timing schemes yield higher compression and better trap loading efficiency than others[11], but again this is future work.

In our setup we will perform a naive compression by detuning and increase the field 'instantaneously'. However, the center our magnetic field may not be the center of the trap, so the MOT is seen to move when we detune the lasers or increase the field strength. Thus we needed to find the 'optimal' static compression parameters, observe where the MOT moved to, and align the trapping beam to that location.

5.2 Alignment

To align the trap beam to the MOT, we use an alignment beam to 'guide' our trap beam to the MOT[Fig 5.2]. This is done by tuning the alignment beam on resonance and overlap the alignment beam with the MOT. This is easy to do because when the alignment beam is on top of the MOT, we can see the MOT completely disappear or reduce in intensity depending on the

Figure 5.1: Loading the Trap
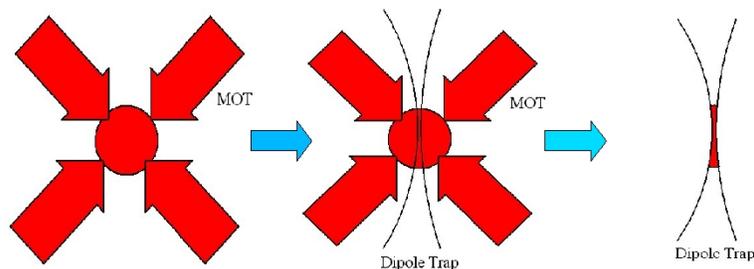
Figure 5.2: Aligning the Trap Beam to the MOT
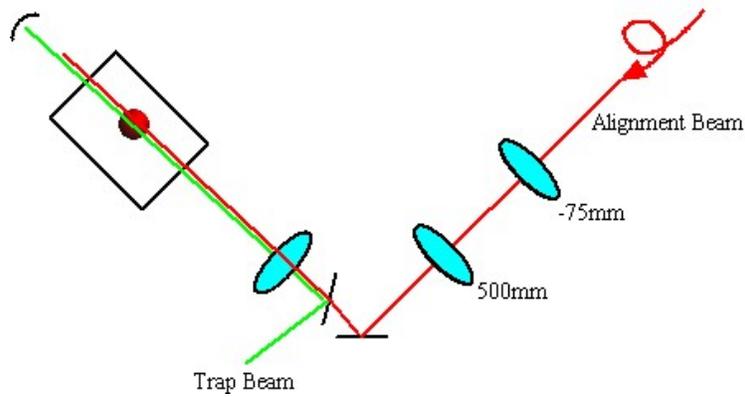
intensity of the alignment beam. The alignment beam is sent through the path of the trap optics so then all we need to do is make the trap beam collinear with the alignment beam. For the most accurate results, we need to make the alignment beam as narrow as possible with lenses and reduce the intensity such that we can clearly see it centered on the MOT.

Chapter 6

Imaging

In this chapter, I will discuss the techniques and results of imaging the trapped atoms. This chapter will be broken into two fundamentally different techniques that we have used, Florescence and Absorption Imaging.

6.1 Florescence Imaging

In florescence imaging, we are simply using resonant light to scatter light from the atoms and then collect the light with a camera. [Fig 6.1] For this, we used the *Pixelink PL-A741* 8-10 digital bit depth, digital readout noise of 2 counts RMS, CMOS camera. The camera objective we used was the *ZOOM 7000 Navitar*.

6.1.1 SNR

In both imaging systems, it is important to know the signal to noise ratio achievable by the system. This will limit the number of atoms we will be able to image. In florescence imaging, the signal, or number photons we can capture is intuitively given by

$$N_{photons} = N_{atoms}\gamma_p\eta_c T \tag{6.1}$$

where η_c is the collection efficiency given by the solid angle of the imaging aperature of radius r subtends when placed R distance away from the atom cloud. T is the exposure time, this is limited by the amount of light the atom can absorb before being accelerated out of the trap.

$$\eta = \frac{r^2}{4R^2} \tag{6.2}$$

and γ_p is photon scatter rate per atom near resonance (in RWA) given by[15]

Figure 6.1: Florescence Imaging
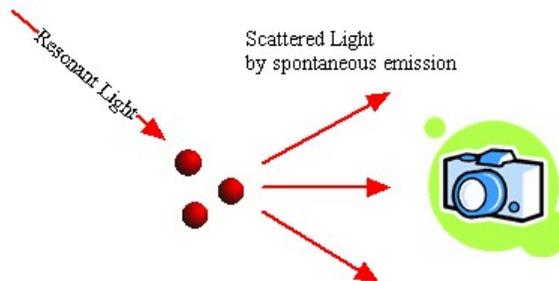
$$\gamma_p = \frac{s_0 \Gamma / 2}{1 + s_0 + (2\delta/\Gamma)^2} \tag{6.3a}$$

$$s_0 = \frac{I}{I_s at} \tag{6.3b}$$

where I is the intensity of the beam, $I_s at$ is the saturation intensity [Appendix J], delta is detuning from resonance, Γ is the natural linewidth of the transition [Appendix J].

On the camera, the total number of electrons collected is simply $N_{photon}\eta_q$ where η_q is the *quantum efficiency* of the CCD chip or CMOS sensor array. It is the ratio of the number electrons produced to the number of photons incident on the chip. This number is usually frequency dependent.

The total noise of the system σ per pixel is given by the quadrature sum of the electronic noise σ_e created in the readout and the photon noise in the background σ_{bg}. We assume that very little photons from the resonant beam directly scatters into the camera so that σ_{bg} is independent of intensity. Note in real life, background noise tend to dominate digital readout noise.

$$\sigma = \sqrt{\sigma_e^2 + \sigma_b g^2} \tag{6.4}$$

where

$$\sigma_{bg} \propto T \tag{6.5}$$

If we assume that we are not overfilling the quantum wells on the chip and each pixel is uncorrelated, then we can infer that the total noise is given by the pixel noise times the square root of the number of pixels we are imaging with.

$$\sigma_T = \sigma \sqrt{N_{pix}} \tag{6.6}$$

We can further assume that our imaging system has some magnification given by the camera objective M. Then the number of pixels that the trap appears on the camera is

$$N_{pix} = \frac{A_{Trap} M^2}{A_{pix}} \tag{6.7}$$

where A_{Trap} is the cross section area of the MOT and A_{pix} is the actual size of each pixel on the chip.

This gives us an expression for the signal to ratio of florescence imaging

$$SNR_{florescence} = \frac{N_{photons}\eta_q}{\sigma_T \sqrt{N_{pix}}} = \left[\frac{\eta_c \eta_q A_{pix} N_{atoms}}{A_{trap}}\right] \left[\frac{\gamma_p T}{M^2 \sigma_T}\right] \tag{6.8}$$

The first term on the right of the [Eqn 6.8] represents the parameters that cannot be or not easily be changed in our trap and imaging setup. The second term represents the parameters that we can vary to improve our SNR. It is obvious from this that we can increase SNR by demagnifying the image on the camera. The other parameters are not so obvious. Note that γ_p increases with intensity, but the higher the intensity, the faster the atoms leave the trap, which limits the exposure time T. Also σ_T is proportional to the square root of T. Thus for exposure times less than the time scales which atoms are accelerated out of the trap, the SNR approximately

Figure 6.2: Inelastic Scattering
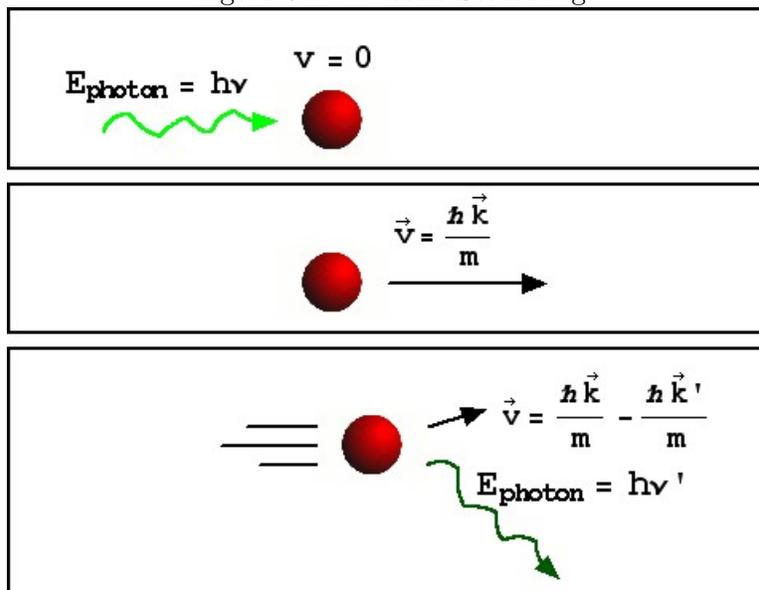
improves with the $\sqrt{T}$.

We can get an idea of how fast an atom is accelerated from absorption and spontaneous emission. When an atom absorbs a photon, it gets a momentum kick of $\hbar k$ in the direction of the photon and then another kick of hk' in a random direction due to spontaneous emission [Fig 6.2], where k' is the doppler shifted wavenumber of the moving atom after the atom absorbed the photon. We assume $k \approx k'$ for narrow atomic linewidths. Thus on average an atom gains an amount of energy $\hbar^2 k^2 / 2M$ per photon scattered. This is called the *recoil energy*. For lithium, this is 3.54μk for a resonace photon. With an optical trap depth 1.2mk, a lithium atom at rest on average can leave the trap after scattering $\sim$340 photons on resonace(not accounting the doppler shift). The Li6 ground state lifetime is approximately 26ns, which mean it takes approximately 9μs to scatter 340 photons (again not accounting the doppler shift). Magnetic traps (described below) have even smaller potentials and the atoms leave faster when scattering. This results in an important point, to significantly improve the number of photons we can collect, we need to introduce damping mechanisms. As we will see, for the optical trap, we will add an additional counterpropagating beam to slow down the atoms. And for the magnetic trap, we will examine it in the optical molasses.

6.1.2 Magnetic Trapping

Magnetic trapping allows us to test the signal to noise ratio of florescence imaging and to see if we are capable to seeing trapped atoms in the optical trap. The magnetic trap in our case is refering to the MOT with laser cooling beams switched off.

Figure 6.3: Florescence Imaging
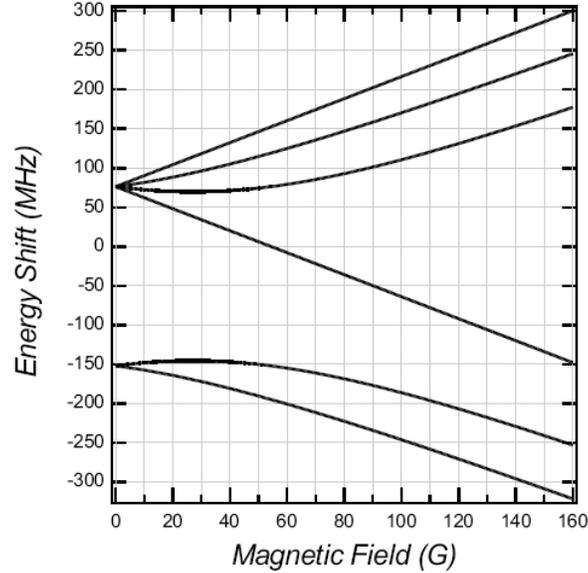
Theory

Magnetic trapping is based on confining potentials created by the zeeman shifts of hyperfine sublevels in the atom. The zeeman shift is a consequence of the interaction between the dipole moment of the orbital angular momentum of the electron and dipole moment of the spin of the electron[8]. For example, in the Li6 $2^2S_{1/2}$ ground state, the $F = 3/2$ state splits into 4 levels and the $F = 1/2$ ground state splits into 2 [Fig 6.3]. It is generally hard to achieve tight confining potentials in magnetic traps (compared to the optical trap) for several reasons. The zeeman shifts are widly different for different sub-levels and different field strengths. For example, in the $F = 1/2$ ground state splitting of Li6, the $m = +1/2$ state starts out as a binding potential, but when at approximately 27 gauss, the potential gradient rolls over to become an unbound potential and keeps decreasing towards the strong field zeeman effect regime. Also for this state, the potential is very low, < 1MHz/gauss. Our MOT coils have a magnetic field of 100 gauss/cm in one direction in the lab, which means this is < 100Mhz/cm. Compare this to the optical potential for the same state, we have 1.2 millikelvin, which corresponds to approximately 25Mhz/50μm which is is about 5GHz/cm.
The zeeman shift can be easily calculated[7] but it is not important to us for us to do so.

Trapping Scheme

Here I will describe how we carry out magnetic trapping experimentally with our control system[Chapter 4]. Instead of capturing single florescence images of the magnetric trap, we actually took a sequence of images of the atoms loading into the MOT from a residual background of atoms collected from the magnetic trap. We then compared this to the loading curve of a MOT

without this residual background to find the number of atoms in the magnetic trap.

The following [Table 6.1] gives, in words, a sample sequence that was used to load and image the magnetic trap. This corresponds to the code given in [Appendix I].

Table 6.1: Magnetic Trapping Scheme (Simplified)

1	Turn MOT on
2	Wait for MOT to load (60s)
3	Take an image
4	Compress MOT for 20ms
5	Turn MOT beams off
6	Wait a 'Hold Time'
7	Take a series of 110 images at 25ms intervals, 24ms exposure time
8	At the time of the 5th image, turn MOT beams on
9	At the time of the 40th image, turn MOT beams off and coils off
10	At the time of the 50th image, turn MOT beams and coils back on

In [Table 6.1], Step 4 is a compression stage where we detune our trapping lasers closer to resonance and increase the current of the coils to achieve a higher density MOT while sacrificing some atoms. Typically we detune the pump and repump beams 10-20MHz closer to resonance than the normal loading stage and we increase current by a few amps. Step 6 is a variable amount of time that we choose to hold the atoms in the magnetic trap. We have used this to measure magnetic trap lifetimes. In Steps 7-10, we take 2 loading curves, the first is one with atoms previously sitting in the magnetic trap, and the second is where there are no atoms in the trap. We simply compare the first curve to the second to find out how many atoms were in the magnetic trap.

Results

[Fig 6.4] and [Fig 6.5] shows the result of magnetric trapping sequence in [Table 6.1] and [Appendix I]. The first loading curve is higher than the second because there were atoms in the magnetric trap initially. A small linear section in the beginning of the second loading curve is artificial: we waited for a few ms to more clearly 'see' the base level.

We can use [Fig 6.5] to get an idea of how many atoms we have in the magnetic trap. Also note we cannot determine the number of atoms from [Fig 6.4]by comparing the counts from the bottom of the loading curve to the top where the MOT is fully loaded because there the camera is saturated.

According to a calibrated florescence measurement previously, 1 second in the loading curve corresponds to 10^6 atoms and for this measurement we had $2.8 * 10^7$ atoms in total in the MOT. On the loading curve[3] without residual atoms (bottom), we can infer that in approximately 15 images, the florescence increased by 5000 counts. We know that each image is taken at 25ms intervals so 15 images corresponds to 0.375s which corresponds to $0.375 * 10^6$ atoms. The number of atoms,which is the difference between the top loading curve and the bottom, then corresponds to 30000 counts which is $2.5 * 10^6$ atoms. Thus we are approximately 9% of atoms in this trial.

---

[3]Note we assume all these loading curves are in the very beginning stages of loading where the number of atoms increase linearly with time.
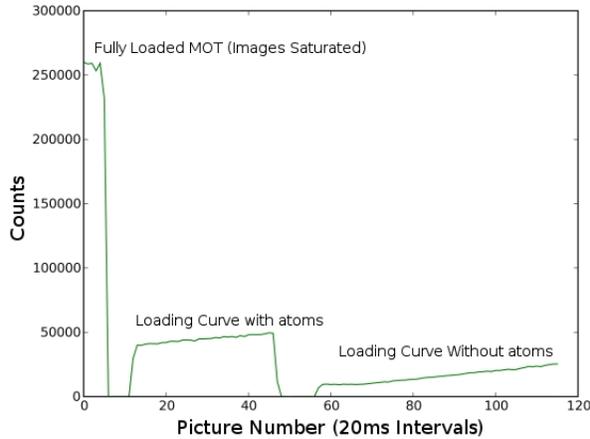
Figure 6.4: Magnetic Trapping Data taken (Jan 2 2008)
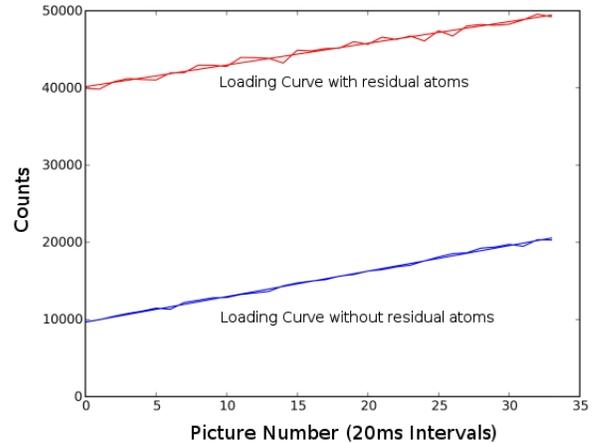
Figure 6.5: Magnetic Trapping Data Overlaid (Jan 2 2008)

Other trials have shown that we can load upto 20%. The absolute limit loading into the 2S ground state of Li6 is 50% because at least 3 out of 6 zeeman splittings are unbound [Fig 6.3].

Furthermore we can look at the SNR of this picture, the rms noise on top curve is approximately 1000 counts. This means that if we have less than $0.375/5 * 10^6 = 75000$ atoms, we would not be able to resolve it in this imaging system.

6.1.3   Attempts at Optical Trapping

We attempted to load the optical trap with a similar scheme as the magnetric trap. Instead of the keeping the magnetic field on during the hold time, we turn it off but keep the optical trap on instead. However, we did not see any evidence of optical trapping. In theory, we should be able to see the trapped atoms with florescence imaging but that may require optimization of many parameters and we cannot optimize if we have no signal to begin with. Thus we decided to switch to absorption imaging for two reasons: a) it will allow us to resolve few atoms, b)we will need it eventually to resolve spatial varations in the optical lattice.(Future work)

6.2   Absorption Imaging

In absorption imaging, we are not collecting light directly from the atoms. Instead, we image their shadows by directing a resonant beam through the cloud of atoms and into the camera[Fig 6.6]. For absorption imaging, we originally used the *Apogee Alta-U32* CCD camera for its high bit depth(16) and low readout noise(7 electrons/pixel)[10]. However, recently we have been using the Pixelink camera for its ability to take images in fast succession. The reasons will be discussed in this section.

Figure 6.6: Absorption Imaging
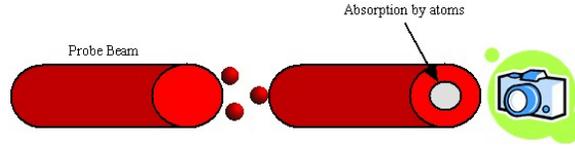
Figure 6.7: Absorption Signal and Noise
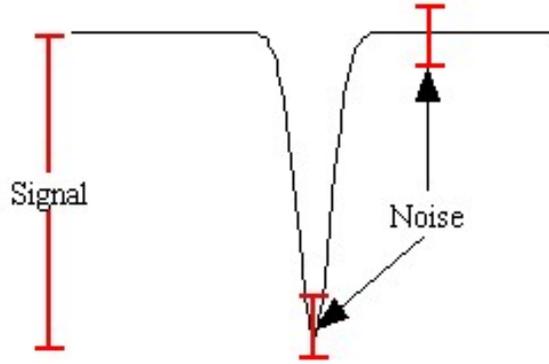
6.2.1 SNR

We can calculate the SNR for absorption imaging in a similar manner as florescence imaging. However, we need to define by what we mean by signal to noise here. The signal is the number of photons in the absorption beam minus the number of photons scattered out of the beam.

We also considered the number of photons scattered into the beam by the atoms, but we can show that this is a small fraction. The collection angle is given by [Eqn 6.2] $\eta_c = \frac{r^2}{4R^2}$. In our setup, $r = 12.7mm$ and $R = 1500mm$, giving $\eta_c = 0.18\%$, which is maximum percent of photons that can be scattered into the beam.

Since the signal is a difference of two quantities, the noise in our system is then quadrature sum of the noise on these two quantities[Fig 6.7].

Assuming that the atom cloud isn't optically dense to the absorption beam and the atom density has approximately constant value of integrated density along the axis of the beam ρ_{2D} with cross sectional area A so that the number of atoms is $N_{atoms} = \rho_{2D}A$, we can write down the number of photons scattered out of the beam as

$$N_{scatt} = (1 - \eta_c)N_{atom}\Gamma_p T \tag{6.9}$$

where Γ_p is again the single atom scattering rate given by [Eqn 6.3]. And again we require that T is not longer the amount of time needed to accelerate the atoms out of the trap. However we must also impose the condition that no pixel on the camera must be saturated. We will see later that this puts an additional constraint on T. [4]

Now the total number of photons incident in the beam incident on the camera (without the atoms) is

---

[4]We didn't impose this extra condition in florescence imaging because it only depends on the exposure time, and for imaging atoms in the trap, we most likely will encounter a shortage of photons and not the contrary.

$$N_{beam} = A\Phi T \tag{6.10}$$

where Φ is the photon flux, $\Phi = I/h\nu$

Thus our signal is

$$N_T = N_{beam} - (N_{beam} - N_{scatt}) = N_{scatt} \tag{6.11}$$

To get the signal in terms of the number electrons produced on the camera, we again multiply this quantity by the quantum efficiency for the camera in question η_q.

The noise in the system is the quadature sum of all the sources of noise, including the beam noise, readout noise, and background noise. The noise from the beam will most likely dominate the readout noise and the background noise. The beam noise can have 2 significant contributions, shot noise and intensity noise. The intensity noise can be controlled. And assuming that we do, then we can infer the most significant source of noise in the system is shot noise. The shot noise for a signal of N photons is given by $\sqrt{N}$ assuming each photon striking the detector is an uncorrelated event. Thus the shot noise in number of electrons is

$$\sigma_T = \sqrt{\eta_q(N_{beam} + (N_{beam} - N_{scatt}))} \tag{6.12}$$

we can put an upperbound on this

$$\sigma_T \leq \sqrt{2\eta_q N_{beam}} \tag{6.13}$$

Thus our SNR is

$$SNR_{abs} \leq \frac{\eta_q(1 - \eta_c)N_{atom}T\frac{\Gamma}{2}}{\sqrt{2\eta_q A \frac{I_{sat}}{h\nu}T}} \frac{\sqrt{s}}{1 + s} \tag{6.14}$$

now the function $\frac{\sqrt{s}}{1+s}$ is maximum when $s = I/I_{sat} = 1$ so we can choose to make our absorption beam exactly at saturation intensity[Appendix J] and reduce the expression for SNR to

$$SNR_{abs} \leq (1 - \eta_q)N_{atom}\Gamma\sqrt{\frac{\eta_q h\nu}{I_{sat}}}\sqrt{\frac{T}{A}} \tag{6.15}$$

Now we see that the only variables that are easily varied are T and A. A is limited by the dimensions of the trap. T, as described before, is limited by how fast the atom is knocked out of the trap. As described in the florescence imaging section, a lithium atom will leave the trap after a few μs on average and thus we need to improve the limit on T by introducing damping mechanisms. T is also limited by the fact that the pixels on the camera must not be saturated.

On a CCD chip, there is a specified amount of electrons each quantum well can hold before overflowing. This is called the *full well capacity*, C_f. When this happens, the camera response can become either highly nonlinear or saturated. Given the pixel size on a CCD is A_{pix}

$$\Phi A_{pix} T \eta_q \leq C_f \tag{6.16}$$

For the Apogee Alta Camera, it has a full well capacity of 55000 electrons, a quantum efficiency of 75% for lithium light, and a square pixel size of 6.8μm. If use saturation intensity for Li6 of 2.5mW/cm^2, we find that [Eqn 6.16] limits T to 18μs. We can increase this time if we magnify the image or if we reduce the intensity of the beam *after* it has passed the atom cloud so that we saturate the camera slower or a combination of both.

As an example, given these parameters and using $T = 10\mu s$, $A = 5mm^2$, and require that the SNR be at least 10:1, we can infer from [Eqn 6.15] that we need only 5000 atoms in the trap!

6.2.2 Apogee Camera

Where the Apogee Alta[10] camera gains in high dynamic range (16-bit) and low system noise (8electron/pixel) and large imaging area(2184 x 1472), it loses on speed. It is limited by a mechanical shutter that requires at least 10ms to open[5]. However it does have a special *kinetics mode* that will allow us to take several images in quick succession without shuttering [Fig 6.9]. This is done by dividing the camera's short dimension (1472) into N section of width W. The user would arrange to mask the N-1 section counting from the bottom and leaving 1 section at the top exposed. The camera then opens its shutter and expose the entire CCD for some time T and then physically shift all the electrons from the first section downwards on the chip by W. The camera can continously do this until the CCD chip runs out of room. The amount of time to shift each row on the CCD is specified to be $24\mu s$.[6]

In reality, we setup a knife edge in the imaging plane of the MOT as the optical mask. However, we never used it due to technical difficulties encountered while running kinetics mode. Hopefully we will implement this feature soon.

6.2.3 Apogee Server

To be able to integrate the Apogee camera with the computer control system, we needed to be able to program it through python. However, the camera vendor supplied us only with a proprietary driver that can be programmed using ActiveX. Thus we needed to write a wrapper program for the camera driver to give us more flexibility. This program was written in MSVC Studios 2008 to access the Active library. It is a TCP/IP server that receives text commands from a user, translates it, and send it to the Apogee device driver. The code is too long to include in this thesis but the reference to for commands is included in [Appendix E]. We were able to incorporate this server seamlessly with the computer control system.

Figure 6.8: The Apogee Alta U32 Camera

Figure 6.9: Kinetis Mode Function of the Apogee Alta
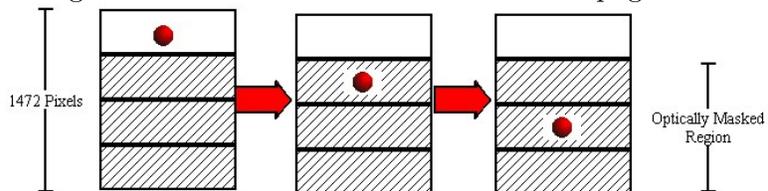
Figure 6.10: An image captured on a mini black and white camera suspended in on a rail during alignment of the imaging optics
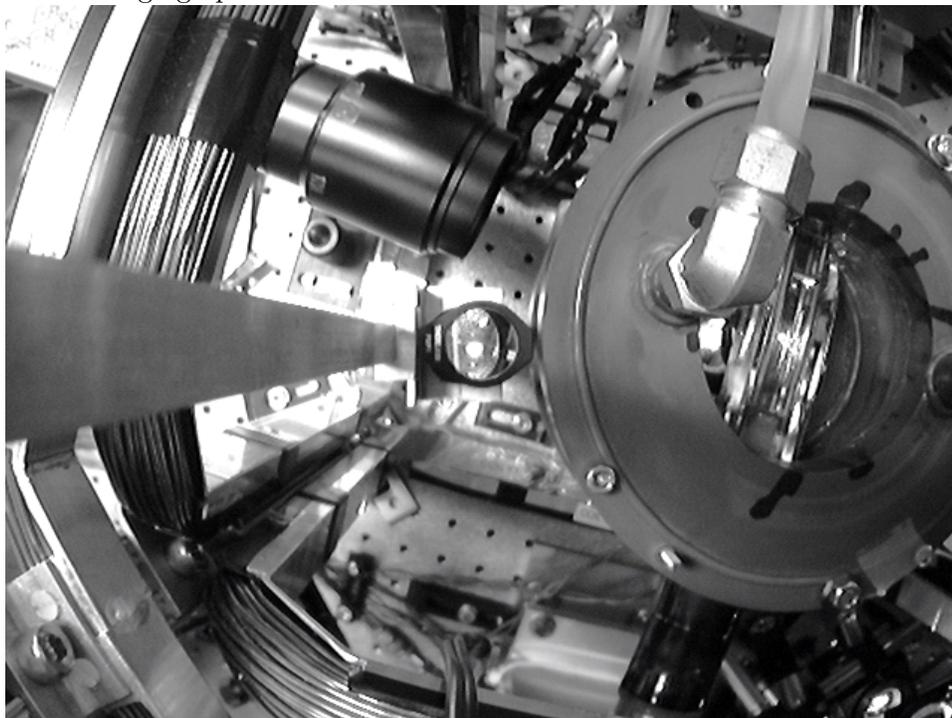
6.2.4   Imaging Setup

We used a 1:1 to imaging system with an objective lens mounted onto a CCD camera for this optical system. Since the incident beam will diffract around the MOT like a circular aperture, we want to ideally place our imaging system as close to the MOT as possible. However, this is impossible as we are mechanically limited by the vacuum cell and the opto-mechanics around it. However, we are able to place a mirror 13mm from the cell wall [Fig 6.13] and reflecting the absorption beam upwards from the table. This allowed us to use a pair of 150mm achromats to create a 1:1 imaging system [Fig 6.12]. The first achromat was naturally placed 2mm from the first mirror. The second one is placed 300mm away from the first. A second mirror redirects the beam towards the camera that sits on a suspended rail. The Apogee Camera is mounted on a 3-axis translation stage attached to a mini optics breadboard and bolted on the rail [Fig 6.11].

6.2.5   Imaging a cloud of atoms

After the optics are setup, we proceeded to take absorption images of the MOT. Similar to magnetic trapping, we needed an experimental procedure for optical trapping. There are two ways to carry out absorption imaging.

---

[5]A CMOS camera such as the Pixelink uses electronic, not mechanical, shutters and thus can operate much faster

[6]source: Gary McAnally, (Apogee Engineer) through email, this is untested upto now due to technical difficulties using the kinetic mode

Figure 6.11: Apogee Camera Mounting
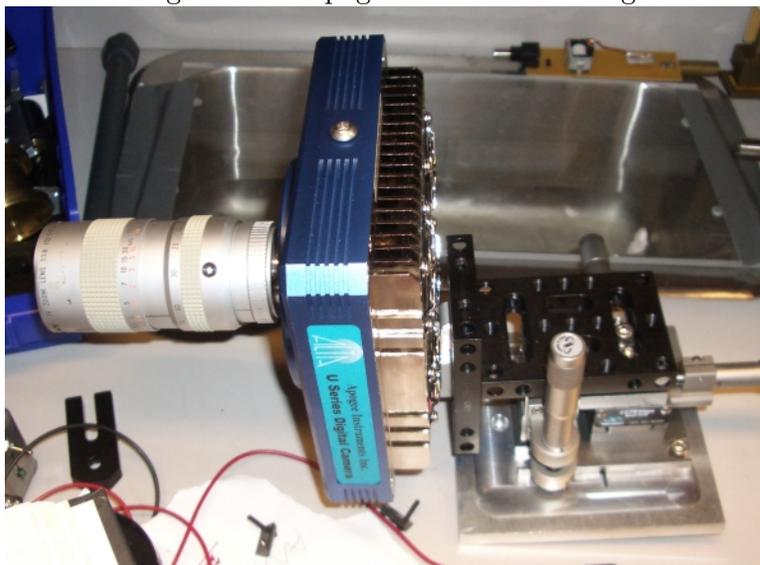
Figure 6.12: Absorption Imaging Layout
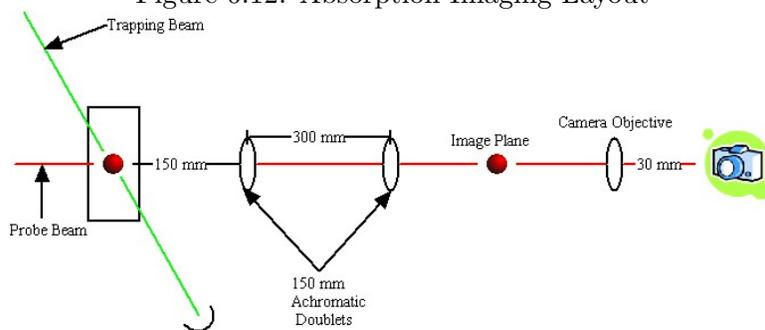
Figure 6.13: Absorption Imaging Optics - Mechanics
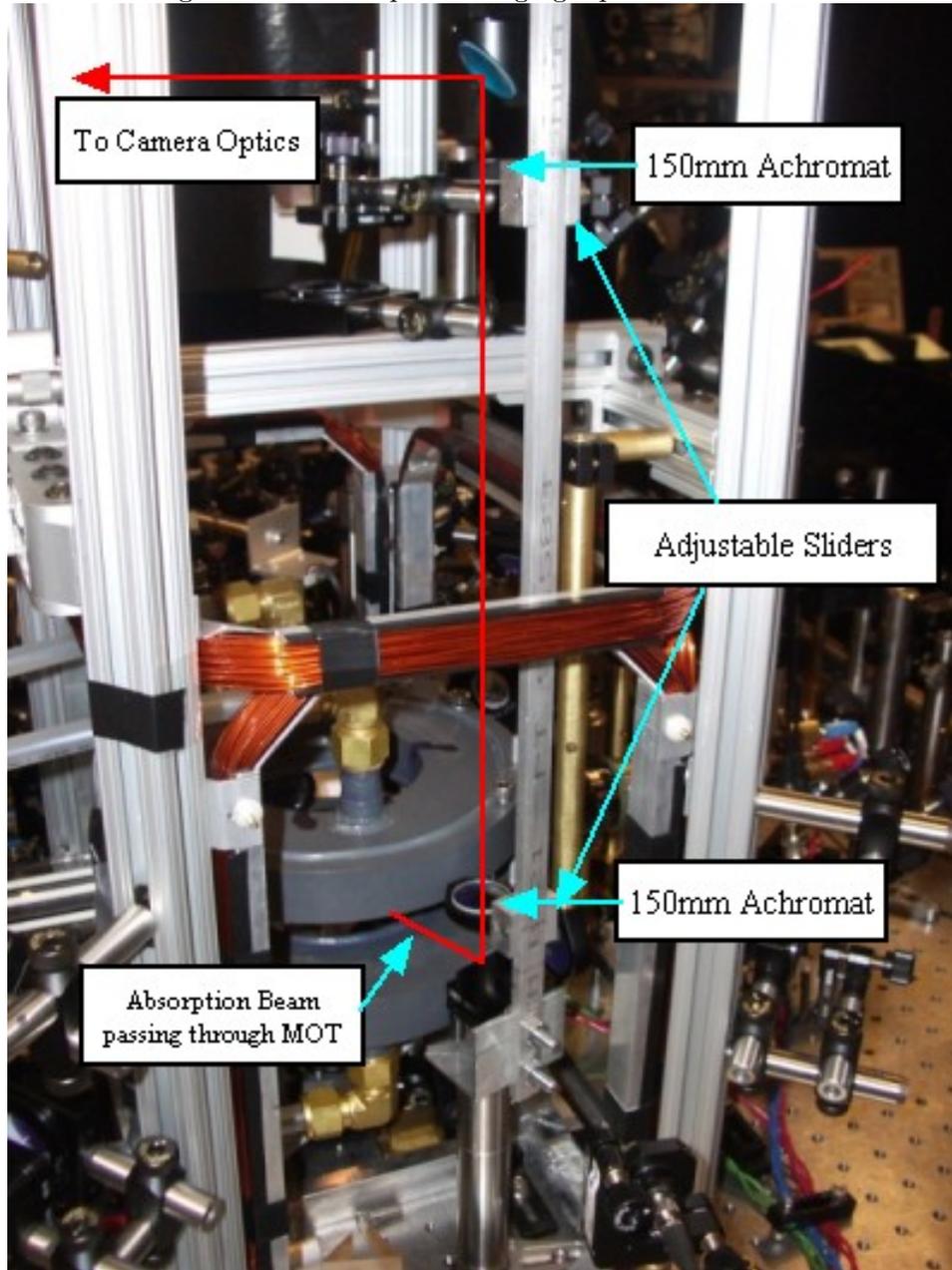
Figure 6.14: Absorption Imaging Beams
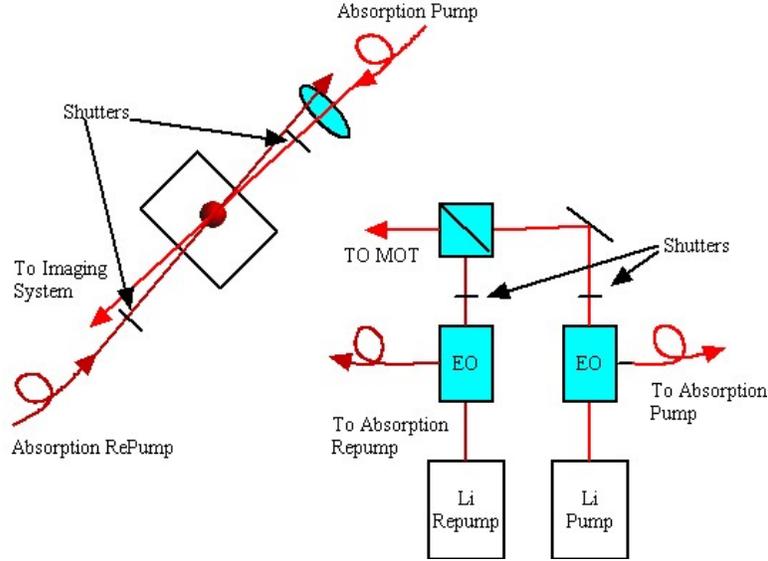
Method 1 - Counting photons

Take an image of the beam(I_{light}) with the atoms, and then an image of the beam without (I_{atoms}) the atoms. *Subtract I_{light} from I_{atoms}* to get the total number of photons absorbed by the camera. The will give us the number of atoms but no information about the density distribution. Method 2 will tell us that.

Method 2 - Counting optical density

Take an image of the beam(I_{light}) with the atoms, then an image without (I_{atoms}) the atoms, then take an image with no beam and no atoms (I_{dark}). The intensity of the beam decreases exponentially with the optical density as it passes through the atom cloud.

$$I(r) = I_0 e^{-OD(r)} \tag{6.17}$$

where $OD(r) = \int (n(r)\sigma_0 dz$, $n(z)$ is the atomic density and σ_0 is optical cross section.

then the optical density is given by

$$OD = ln\left(\frac{I_{light} - I_{dark}}{I_{atoms} - I_{dark}}\right) \tag{6.18}$$

if I is close to I_{sat}, then we need to account for saturation effects[5].

$$OD_{true} = OD_{observed} + (1 - e^{-OD_{observed}})(I/I_{sat}) \tag{6.19}$$

6.2.6 Imaging Procedure

Experimentally [Fig 6.14], we used 2 beams to carry out absorption: the pump beam to scatter photons, and the repump to drive the atoms back to the upper ground state so that they can rescatter. Also the repump is setup to be nearly counterpropagating with the pump beam to introduce a molasses effect to slow down the atoms. Both the pump and the repump are derived from the MOT pump and repump beams through EOMs (Electro-Optical Modulator)[7]. The EOMs are able to switch the power from the MOT beams to the absorption beams in $6\mu s$ with a 100 : 1 extinct ratio. This allows us to load the MOT into the dipole trap, and then turn off the MOT beams and image with the absorption beams.

[Table 6.2] gives a sample procedure for taking the absorption image of a MOT with a $100\mu s$ absorption pulse. Due the technical complexity of the shutter and camera shutter timings, more details will not be included here.

Table 6.2: Absorption Imaging of the MOT (Simplified)

1	Turn MOT on
2	Wait for MOT to load (60s)
3	Turn off pump and repump shutter
4	Detune pump and repump close to resonance
5	Turn on the pump and repump shutters
6	Expose Camera
7	Flash the absorption pump and repump beams for $100\mu s$
8	Turn off MOT coils
9	Expose Camera
10	Flash the absorption pump and repump beams for $100\mu s$

Steps 1-3 loads the MOT. In steps 3-5, the pump and repump shutters are turned off before detuning so that no resonant light is hitting the MOT before we start imaging. The order in which we turn on/off the pump and repump also matters. For example if we turn off the repump first then the pump, the atoms will be pumped to the lower ground state. Now during imaging, if we switch on the pump first followed by the repump, the atoms won't absorb until both beams are on so that we get less atoms being knocked out. Step 6 takes the image with the atoms, and step 9 takes the image without the atoms. The result is shown in [Fig 6.15]

---

[7]the EOM introduces a voltage dependent polarization to the incident beam

Figure 6.15: (left)Image with atoms,(center)Image without,(right)Difference Image
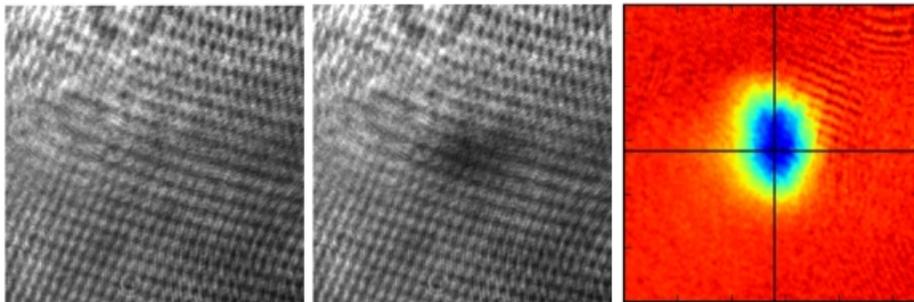
Chapter 7

Reconstruction

This chapter, and the next one, are written 4 months after the previous chapters and describe the working dipole trap in a different setup. Specifically, in this chapter, I will describe the work done in rebuilding the dipole trap. In the next chapter, I will describe the results of the working dipole trap.

7.1 Summary of Changes

In the previous setup, we were unable to observe trapping. We suspected this was due to the poor beam shape near the focus and also lack of SNR in the imaging system. The beam shape looked highly astigmatic near the focus. In absorption imaging system, we could see approximately 50% MOT absorption but a noise level of no better than 2%. To improve the beam quality, we carefully characterized the beam at after every optic and found/fixed many sources of astigmatism. Also we switched to a beam transport setup that focuses to 30μm instead of 50. To improve the imaging system, we switched back florescence detection with the Apogee Camera, which allowed us to see atomic clouds as small as a few thousand atoms, limited by technical shot to shot fluctuations of the MOT light.

7.2 New Design

The new design [Figure 7.1] [Appendix K] is similar to the old design except the first lens is replaced by a 500mm lens and the waist at the trap is now 30μm. Also we decided to use the 0th order beam from the AOM instead of the 1st order. This was because the 1st order beam is highly elliptical and is most dominant source of astigmastism. The disadvantage of using the 0th is that we cannot use the AOM as a shutter and also cannot evaporate the sample to very low temperatures.

7.2.1 New AOM

We bought a new IntraAction AOM [Figure 7.2] and driver to replace the old one described in [Chapter 3]. The AOM (MODEL ATD-1153DA6M) is AR coated for 1064nm and allows for watercooling. The frequency runs between 82 Mhz to 152Mhz. The manufacturer quoted the AOM to run at peak 1st order diffraction efficiency of 81.5% with a 4.27W incident rf power. However, the deflector driver supplied with the AOM (MODEL DE-1154M) is only capable of driving 4Watts (in specifications). Empirically, we found that the AOM and driver combination has a peak efficiency of 70% at 86Mhz with a incident beam width of 86μm. The efficiency could be improved by going to larger beam sizes. Additionally the efficiency does not peak at maximum

Figure 7.1: The new trap design
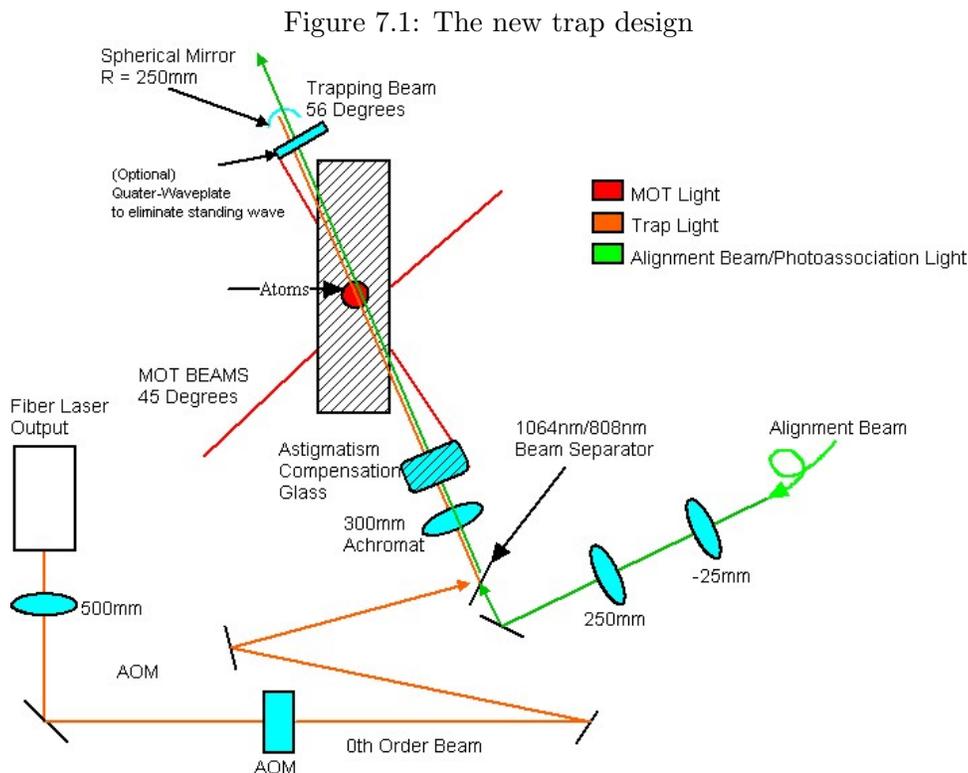
drive power supplied by the DE-1154M so using a more powerful rf source can also incrase the efficiency.

7.3 Beam Measurements

In order to improve the beam shape, we used a ccd camera to measure the beam widths after every optic. This section will include a collection of the most important plots and findings. The beam images were captured on a ccd mounted on a translation stage. Cross-sections of a few pixels wide are taken across the center of the beam in both the horizontal and vertical directions. Then these an average of the cross-sections are taken and fitted to gaussians to produce the final plots. There are also knife-edge measurements to confirm the validity of the camera measurements.

7.3.1 Cameras

There were 2 cameras used in these measurements. One is the **Supercircuits PC100XS** cheap security camera and the other is the **Sony ExwaveHAD (Model no. SSC-M383)**. I started using the PC100XS because it was small and maneuverable. However later I found that the Sony camera has much less electronic noise and therefore better at analyzing low intensity images. Both these cameras exhibited nonlinear response to light. That is the number of counts per pixel did not scale linearly with the input beam intensity. By measuring the input-response curve, we can calibrate the images taken with the camera to give the correct results. I did this study

Figure 7.2: The new IntraAction AOM
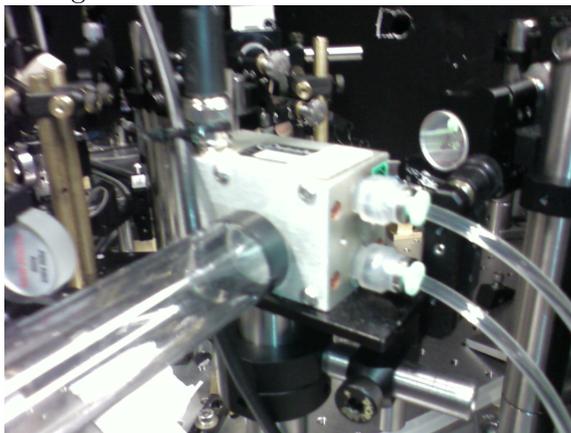
earlier for the Sony camera[Appendix G] but repeated [Figure 7.3] it with more data and for both cameras. All of the following plots are calibrated with this camera responsivity data.

7.3.2 Focusing Asymmetry

One outstanding issue that was common to almost all these plots was the fact that the beam width appears to have different gradients before and after the focus especially with the 300mm achromat. That is, the beam appears to focus faster before the focus (the side closer to the focusing lens) and slower after the lens. This is clearly seen for example in [Figure 7.4]. We believe this might be caused by the interference between reflections off the front and back surfaces of the lens or wedge in between the convex and concave lens of the achromat. Evidence for such interference pattern is seen [Figure 7.5]. The shape and degree of this interference tend to depend on how well the beam is aligned through the center of the lens. We did not further investigate this because all that matters to us is having a tight focus. However, sometimes the beam can be very asymmetric such that the rayleigh range of left of the focus is vastly different from the right of the focus. In such cases, the plots indicate which side (left or right) the curve was fitted to produce rayleigh range and waist measurements.

7.3.3 Astigmatism from the AOM

The most significant contribution to the beam astigmatism was the 1st order beam from the AOM being naturally ellipitical

compare the 1st order [Figure 7.6] beam focusing properties to the 0th order [Figure 7.7]

We eventually decided to go with the 0th order beam. However, this does not allow the intensity to be turned down below 30% and thus effective evaporation of the the sample. However, we decided that after the 0th order is setup, we can use the 1st order beam in a cross-beamed geometry for evaporation.

Figure 7.3: Inverse response curve used to calibrate images taken with the Sony camera
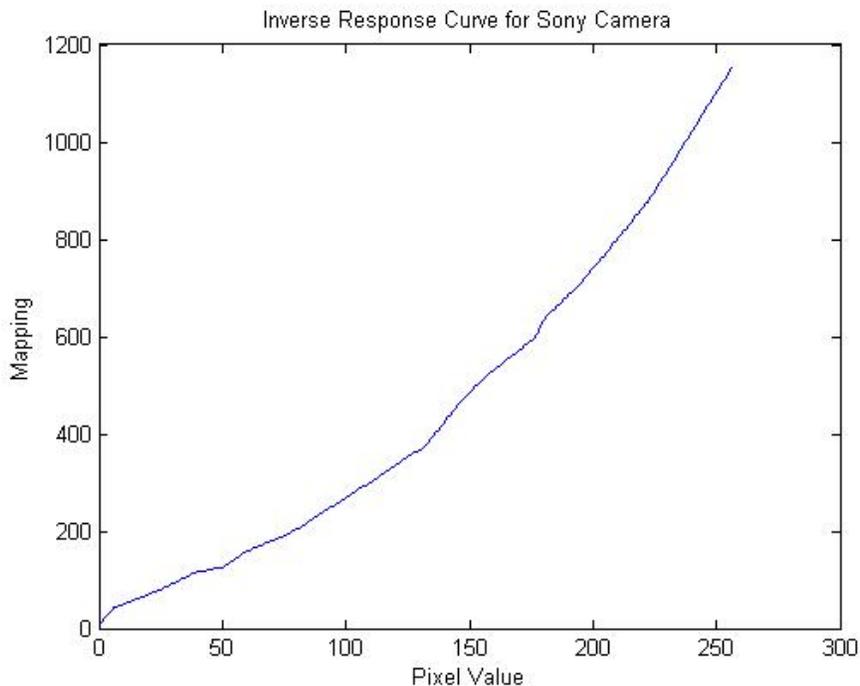
Figure 7.4: Focusing of the tweezer beam with a 500mm AR coated lens and the 300mm achromat, measured on the PC100XS camera
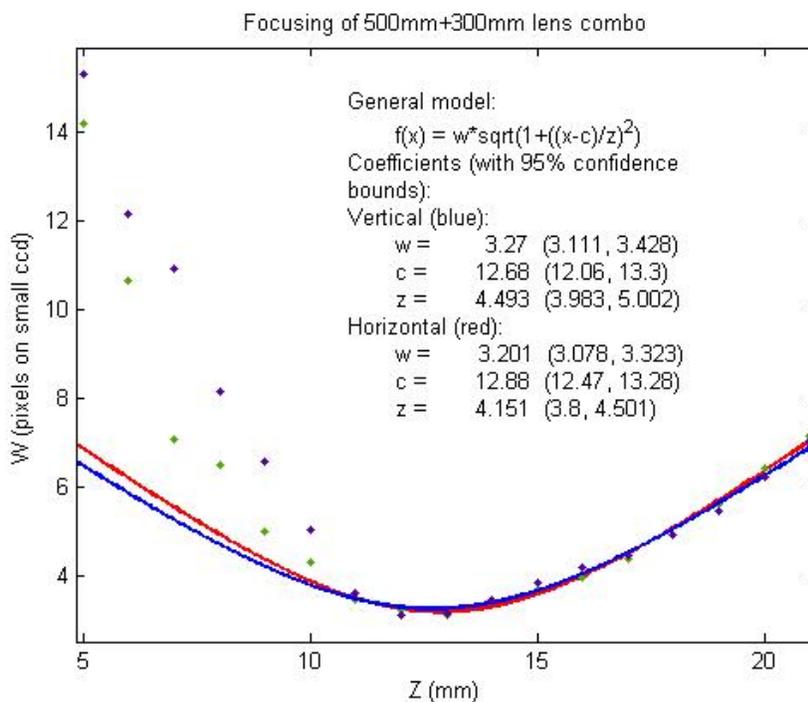
Figure 7.5: Interference patterns of the tweezer beam after the 300mm achromat and before the focus. The images show pictures of the beam before the focus (top left) to after the focus (bottom right). Each image is separated by 1mm in the longitudinal direction. The first few images show a 'hole' cut out near the center.
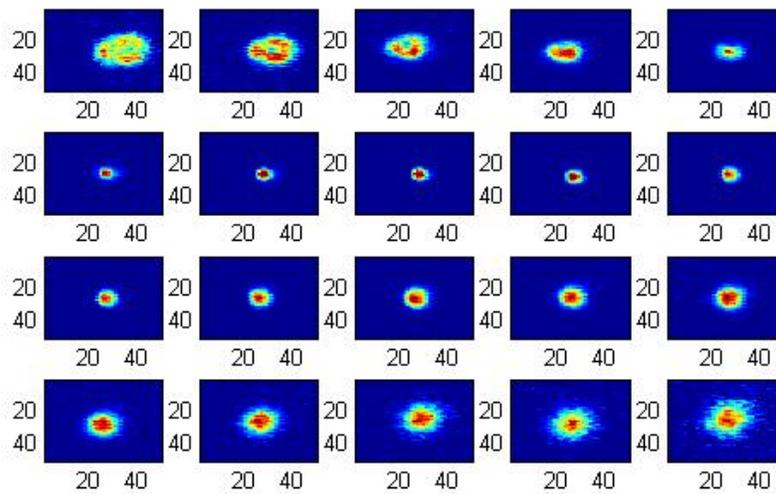
Figure 7.6: Focusing of the 1st order beam through 500mm+300mm achromat measured on PC100XS camera
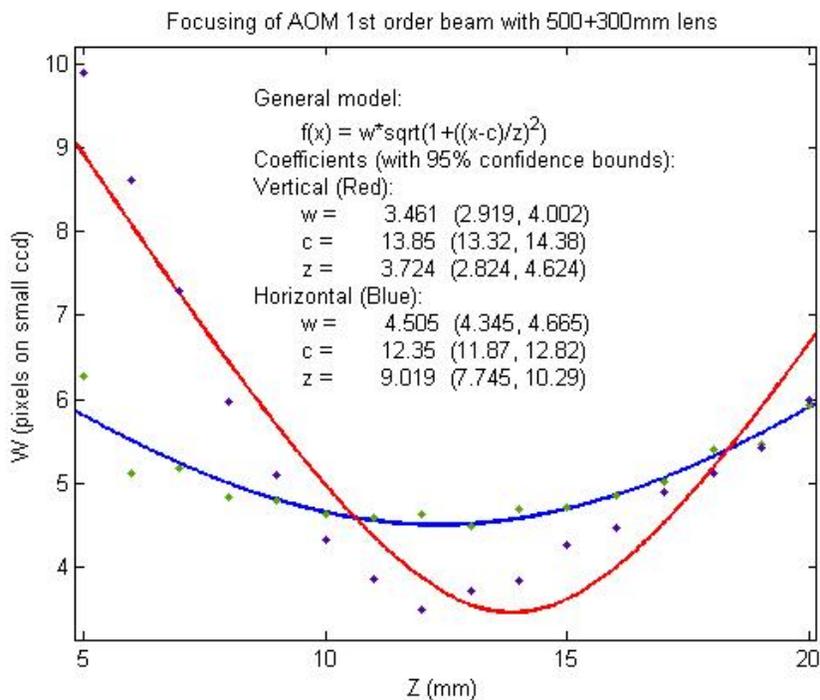
Figure 7.7: Focusing of the 0th order beam through 500mm+300mm achromat measured on PC100XS camera
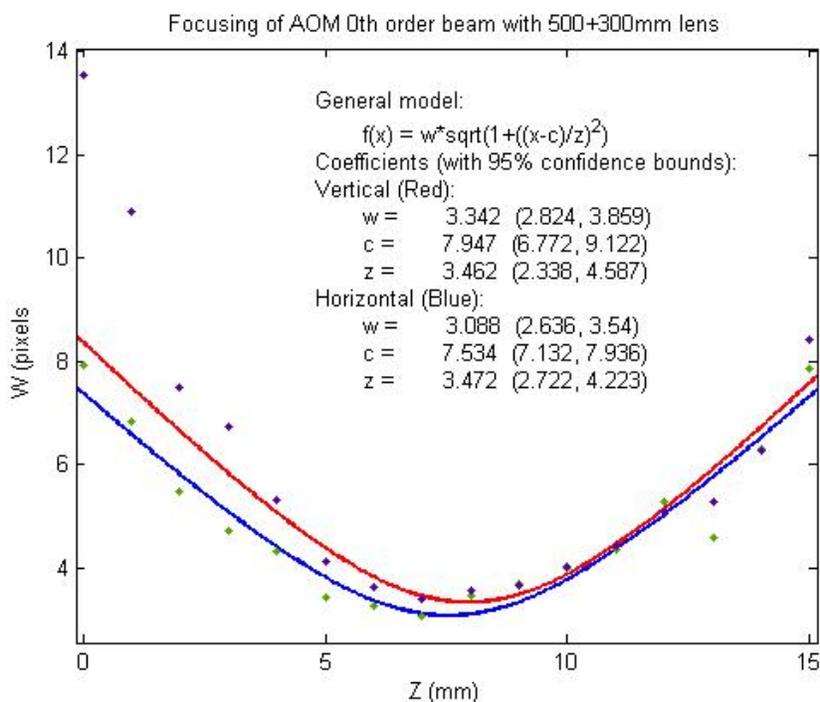
Figure 7.8: Focusing of the 0th order beam through 500mm+300mm achromat measured with knife-edge using error function fits
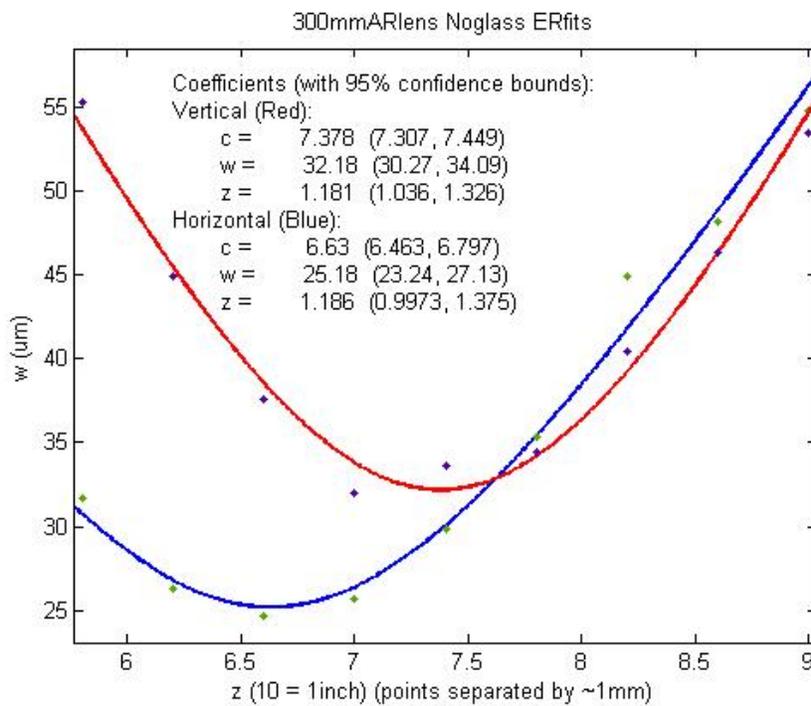
7.3.4 Comparison with KnifeEdge Measurements

To validate the ccd camera beam measurements, we took a set of 2D knife-edge measurements. We did this in two ways. The first is to use the 30-70 method. This is where we measure the locations of the beam in the x and y axial directions for which the the portion of the beam power is at 30% and 70% for each point in z longitudinal direction. Multiplying the displacements by 1.92 gives roughly the gaussian beam waist in both directions. A more accurate way is to take a set of points in the axial directions and fit them to an error function to determine the beam waist. The latter,being more precise, takes much longer so we only took one set of data.

[Figure 7.8] shows the beam focused by the achromat to 25μ and 32μ with the foci slightly offset by a few millimeters.

[Figure 7.9] shows the same beam measure on the Sony CCD camera.

7.3.5 Misalignment by pointing

In order to align the tweezer, we need to be able to adjust beam splitter in order to "point" the beam precisely to the location we want. This will inevitably cause the beam to pass through the achromat at non-perpendicular angles and cause astigmatism. However, if we keep the beam splitter close enough to the achromat, this effect should be small. We sitmulated this situation by "pointing" the beam on the ccd from one side of the camera to another (approximately 3.5mm) with the mirror. We measured the beam profiles on the extremes and compared it to the beam profile when it was aligned. See [Figures 7.10, 7.11, 7.12]. These figures show that no drastic

Figure 7.9: Focusing of the 0th order beam through 500mm+300mm achromat measured with Sony CCD and calibrated
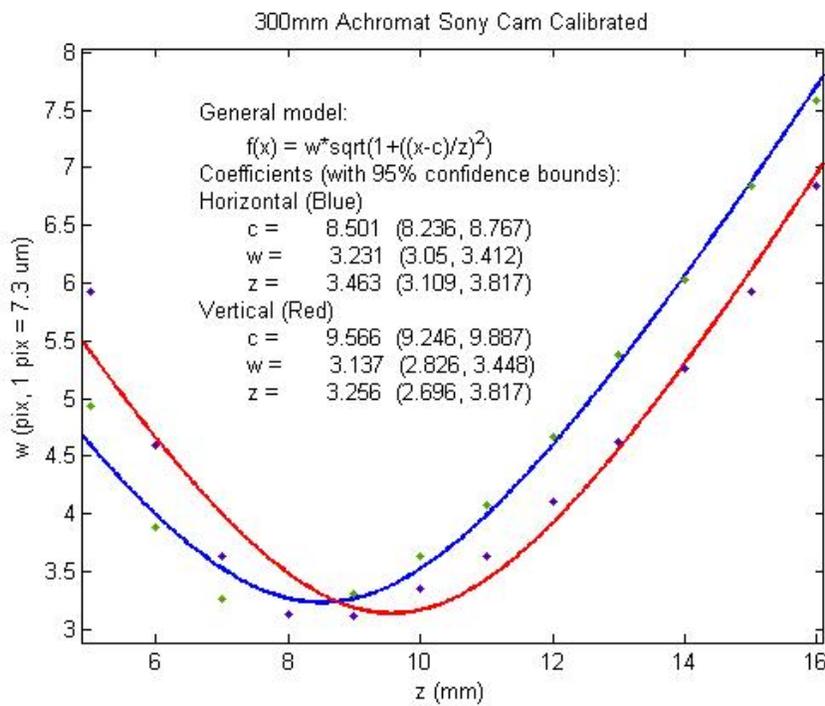
changes of the beam is observed.

7.3.6   Astigmatism by misaligning the achromat

As mentioned before, if the beam does not pass through the lens center or perpendicular to the lens plane, astigmatism is again introduced. For example, consider the effect of rotating the lens on the axis of a lens mounted on a rotational stage clockwise and counterclockwise by 1 degree. [Figures 7.13,7.14]

7.3.7   Astigmatism by focusing through glass

A non-collimated beam passing through a glass oriented at a non-perpendicular angle (wrt to the k-vector) will also cause astigmatism [Chapter 3.3.2]. To simulate this, we sent our beam through a piece of glass the same thickness as our vacuum cell walls [Fig 7.15]. The glass shifted the foci apart by almost 3mm. To compenstate for this, we set in place another piece of glass at a sagittal angle before the cell glass. The effect of the compenstation glass is seen in [Fig 7.16,7.17]

7.3.8   Working beam profile

[Figures 7.18,7.19] shows the profile of the trapping beam taken before the first working version of the dipole trap. The beam was asymetric across the focus so two fits were done on the same set of data.

Figure 7.10: The aligned beam in the center of the ccd
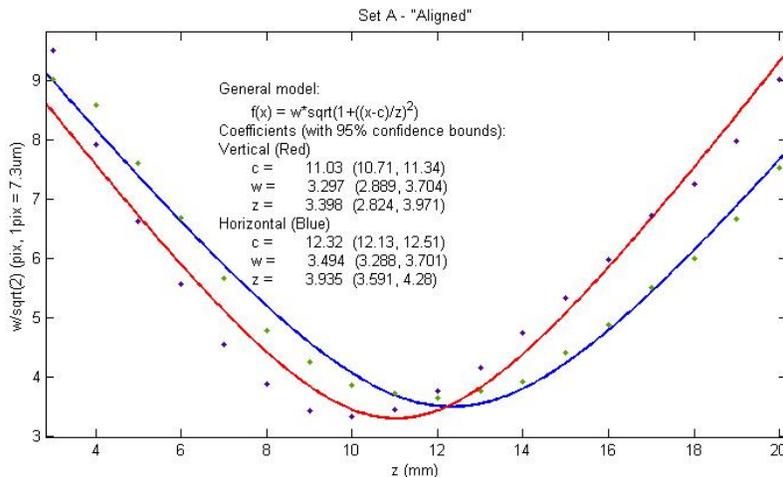
Figure 7.11: Misalignment of the beamsplitter so that the beam appears to one edge of the ccd
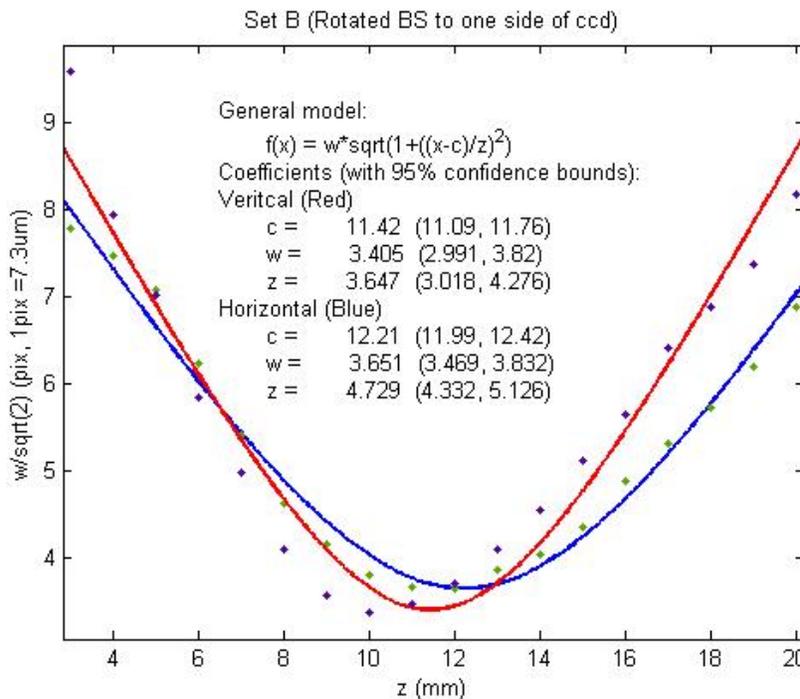
Figure 7.12: Misalignment of the beamsplitter so that the beam appears to other edge of the ccd
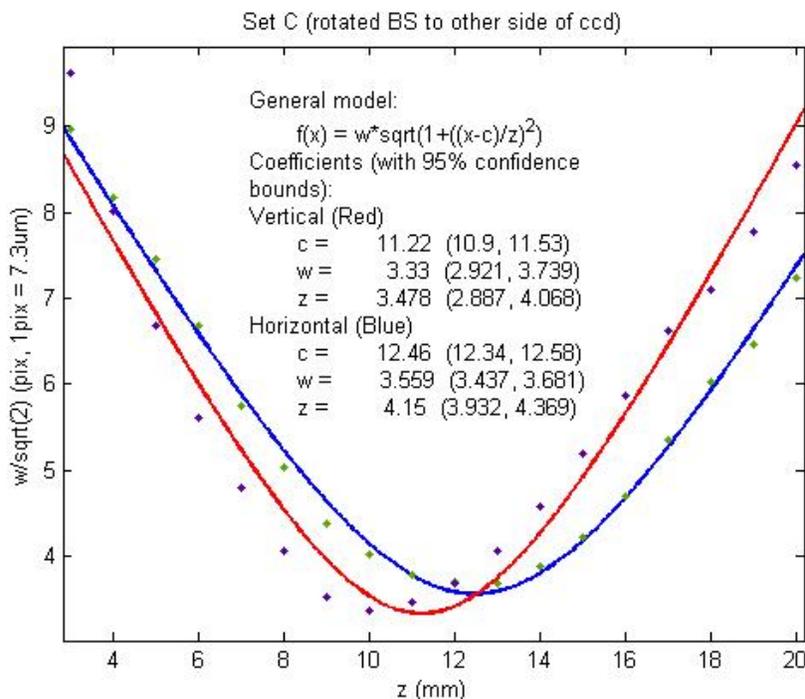
Figure 7.13: Misalignment of the 300mm achromat by 1 degree clockwise around the axis of the rotational stage
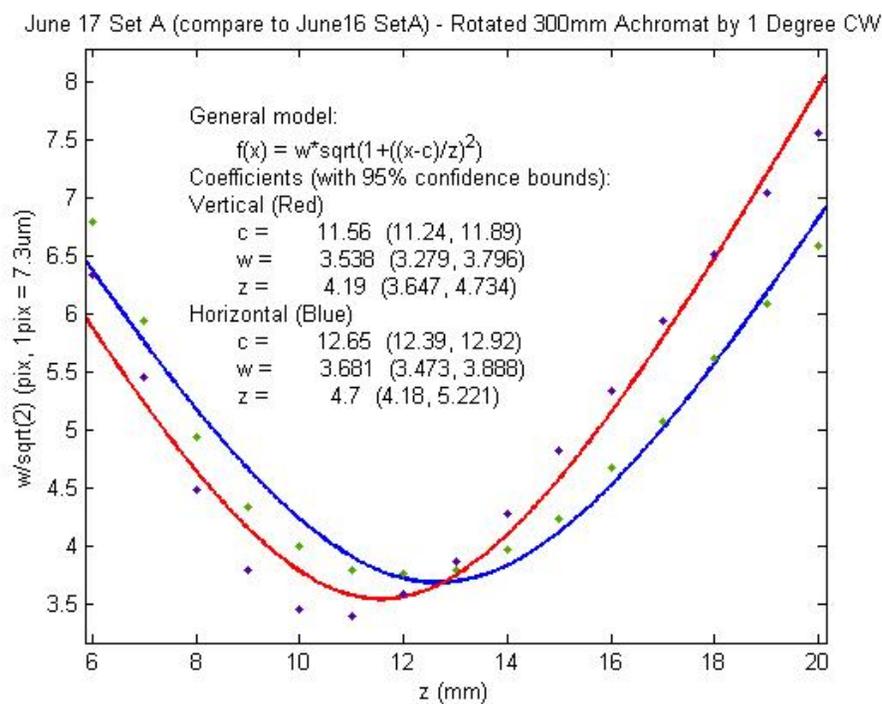
Figure 7.14: Misalignment of the 300mm achromat by 1 degree counterclockwise around the axis of the rotational stage
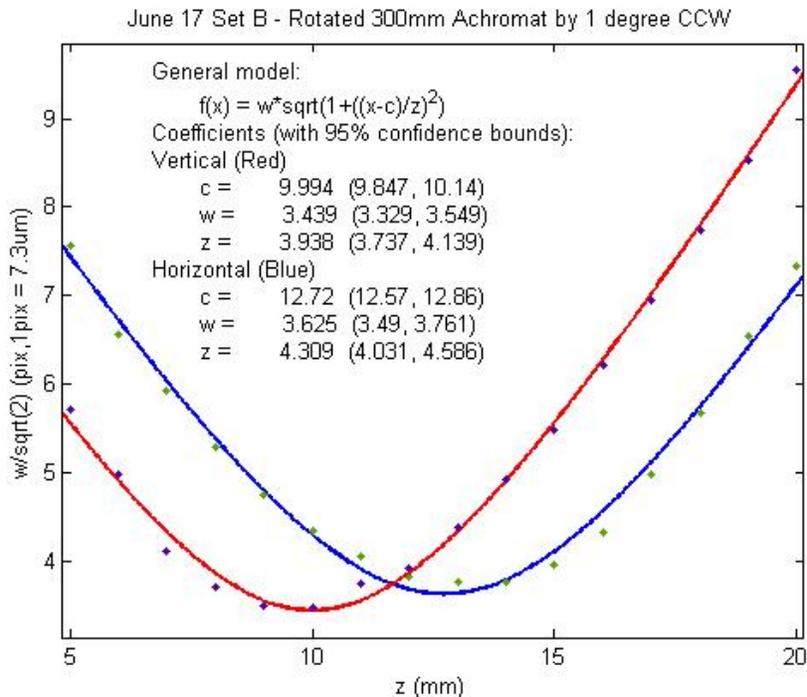
Figure 7.15: Astigmatism caused by introducing a piece glass at brewster angle in the tangential plane. Compare to [Fig 7.13] for beam shape without glass
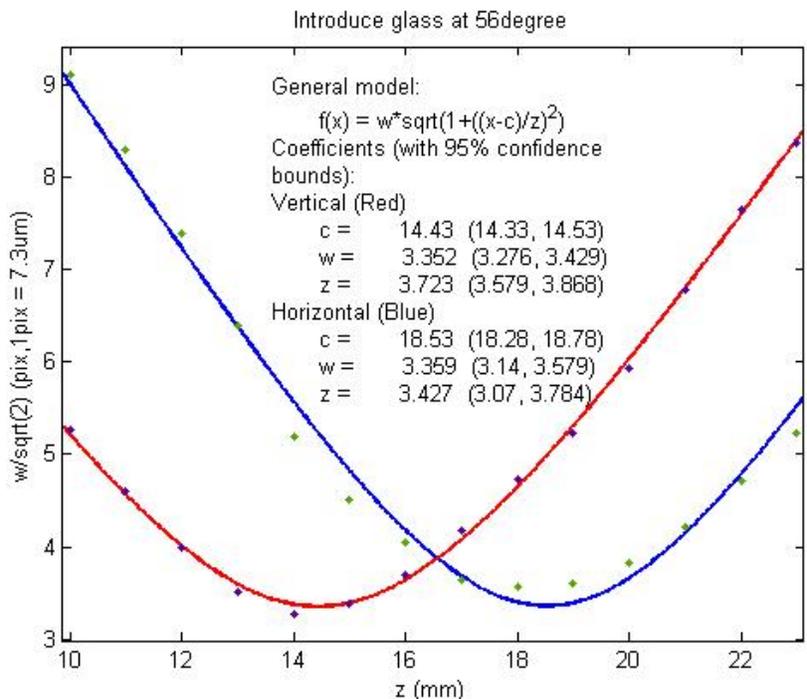
Figure 7.16: Adding a piece of compensation glass at a sagital angle to the beam's path
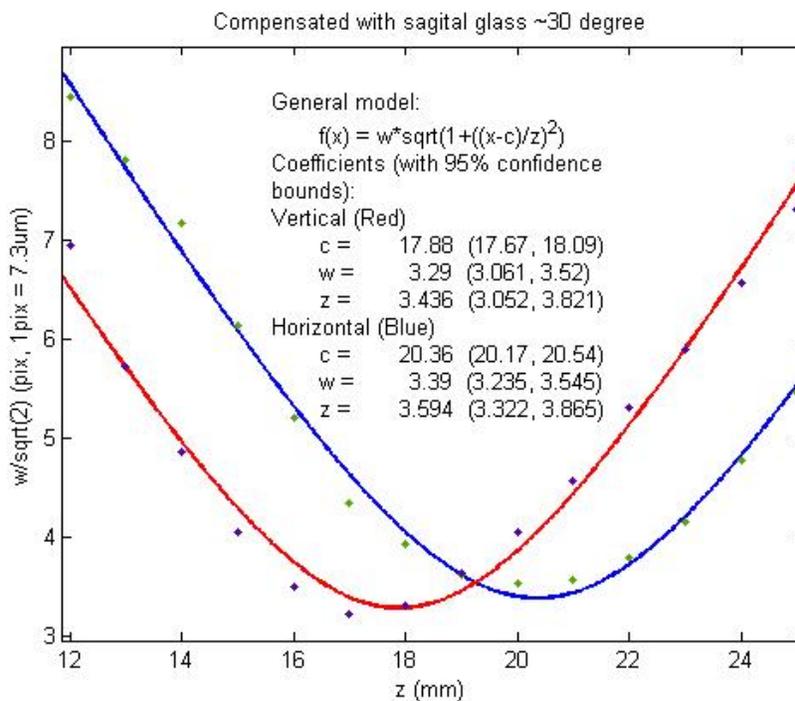
Figure 7.17: Rotating the compensation glass even more
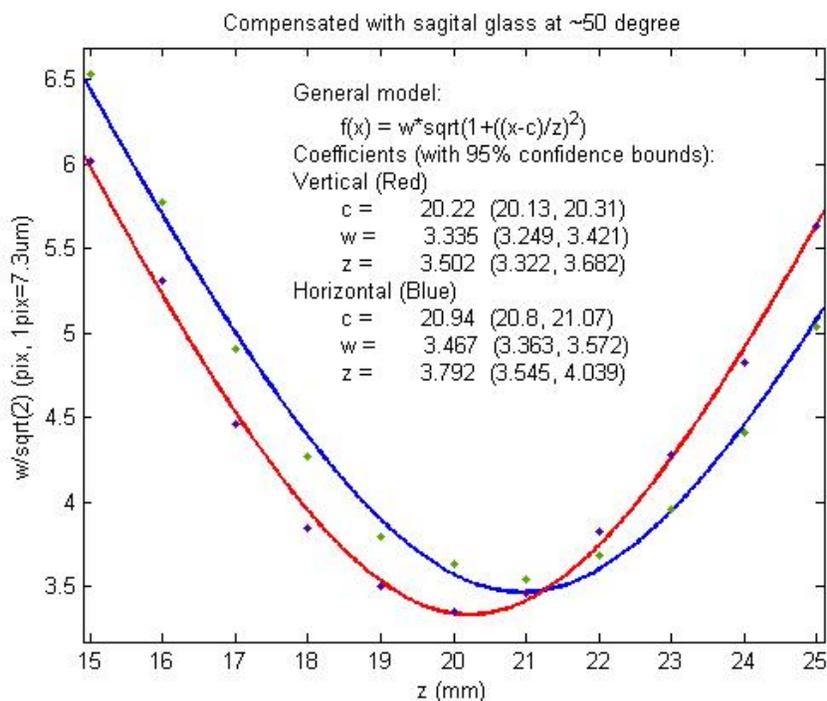
Figure 7.18: Trapping beam profile
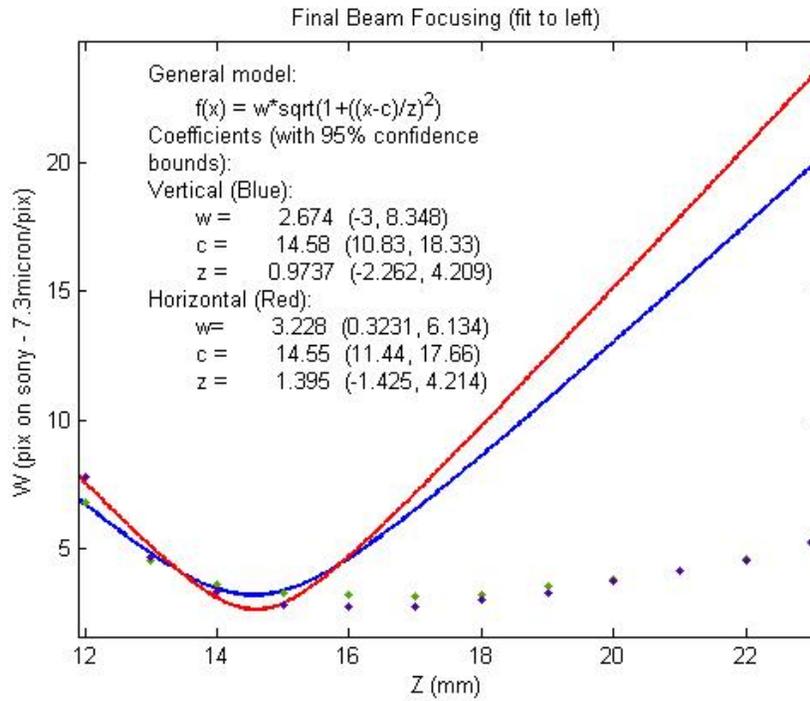
Figure 7.19: Trapping beam profile
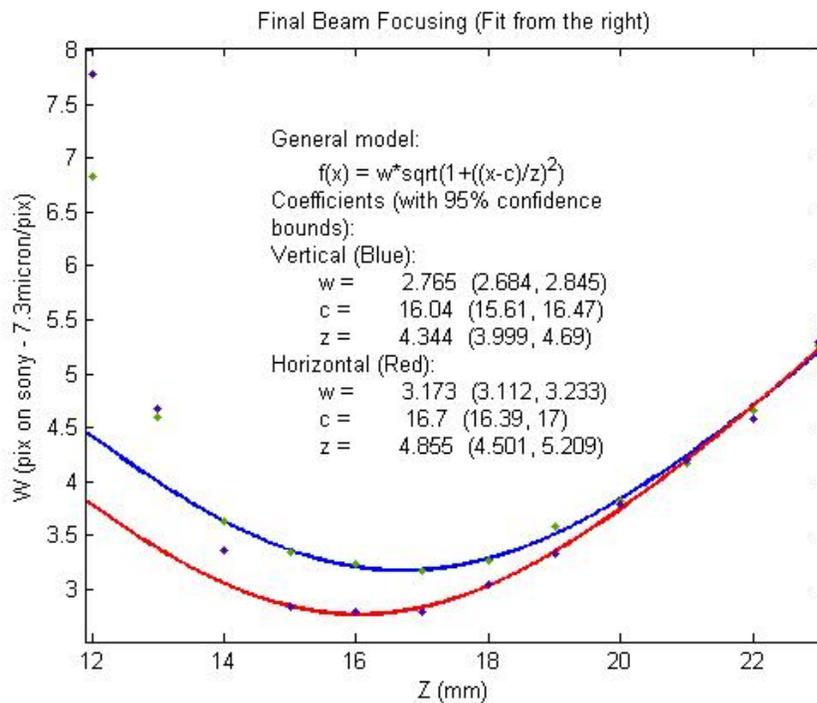
Figure 7.20: The "Fat" and "Thin" shutter combination. The "Fat" shutter is a high power water cooled shutter that can easily dissipate 20W optical power. However, its shuttering speed is slow (few ms switch time) and has a timing jitter of a few ms. The "Thin" shutter is a more reliable and faster mechanical shutter (400μs switch time). We use to the two in conjunction in our experiments. The "Thin" shutter is quickly heated by fiber laser. In our sequence, the "Thin" shutter is exposed to the light for about 10ms. Repeated usage shows burnt marks on this shutter and needs to be replaced.
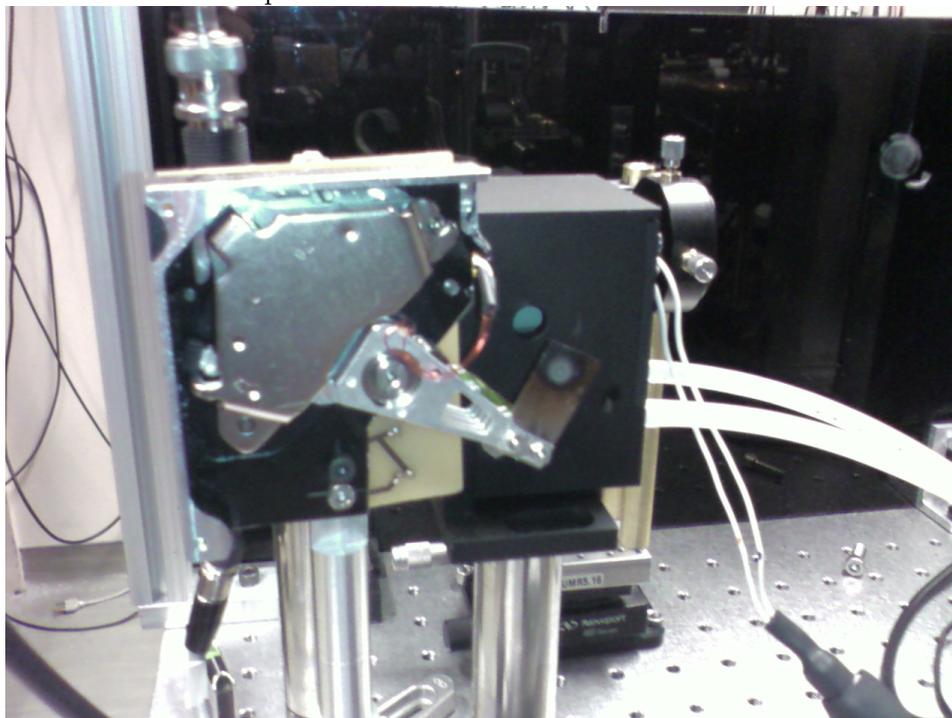
7.4 Shuttering

Since we are using the 0th order beam of the AO, this does not allow us to completely turn off the trapping beam. (We can turn it down to 30%). Thus we need high power mechanical shutters. [Figure 7.20] shows a high power water cooled shutter used in conjunction with a fast harddrive shutter to switch our trapping beams.

7.5 Assembly: How to

Chapter 8

Results

8.1 First evidence of trapping

After many months of hard work, we finally saw evidence of trapping of Rb87. We first observed this evidence using fluorescence detection with the Apogee Alta camera. We determined this in the following way. First we loaded atoms into the MOT. Then we turned on the dipole trap briefly to load atoms into the dipole trap. We then switched off all the MOT lights and residual magnetic fields. We held the atoms in the trap for a brief amount of time (500ms). Then we switched the MOT lights and fields back on and take a 20ms exposure fluorescence. [Figure 8.1] shows the result. To verify that the image indeed show evidence of trapping, we conducted two "false-positive" tests. We simply repeat the experiment (a) physically switching off the magnetic field so no MOT can form (b) physically switching off the dipole trap. Case (a) checks to ensures that the images of the trapped atoms were indeed from the trap and not mistakenly from the MOT. Case (b) ensures that no trap light was contributing to the images.

Our initial trapping evidence showed up in a 32x32 fluorescence picture (similar to [Figure 8.1]). The total sum of the pixel counts could not determine trapping because the sum of the background noise in the 32x32 picture shadowed the small number of atoms loaded in the optical trap. Thus initially it was visual evidence that gave us a hint of trapping. We then narrowed in the ROI to a 16x16 region at where we thought the atoms were. This was counter-intuitive because one would think that the MOT would always load in the same place. Curiously, we figured out that the MOT began to recapture from a different location (few hundred microns away) than its equilibrium position. This could be due to the slow ramp up time of the magnetic fields.

After some optimization, as described below, we were able to trap around $2*10^6$ rb87 atoms in our single pass trap with a lifetime of approximately 60s and rb85 with a lifetime of 40s. Lithium is work in progress.

8.2 Improving signal

After we verified evidence of trapping, we immediately toyed with some easily reversible parameters to optimize trapping and record the trap characteristics.

8.2.1 adjusting 300mm lens position

The 300mm lens is setup on a translation stage with 15mm of travel. This allows us to easily optimize the trap's longitudial position. [Figure 8.2] shows a plot of the trapped atom number

Figure 8.1: A set of images showing evidence of optical trapping. (a) Top left shows an average of 4 background images. (b) Bottom left shows the fluorescence image of reloading the MOT with atoms previously held in the trap. (c) Top right shows the same fluorescence image but without atoms contributing from the optical trap. (d) Bottom right shows the difference of (c) and (d); all axis are in pixels.
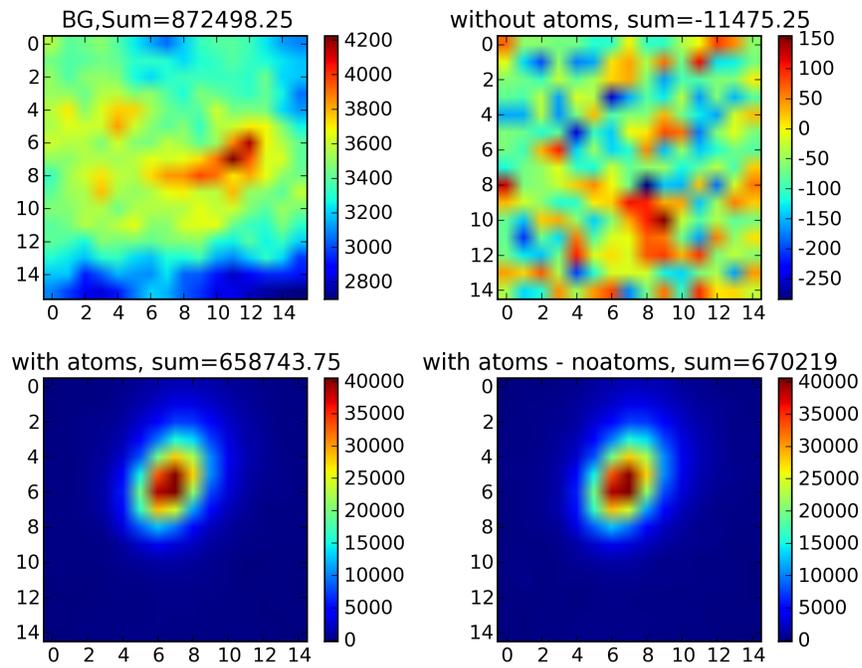
Figure 8.2: Trapped number vs 300lens micrometer position.
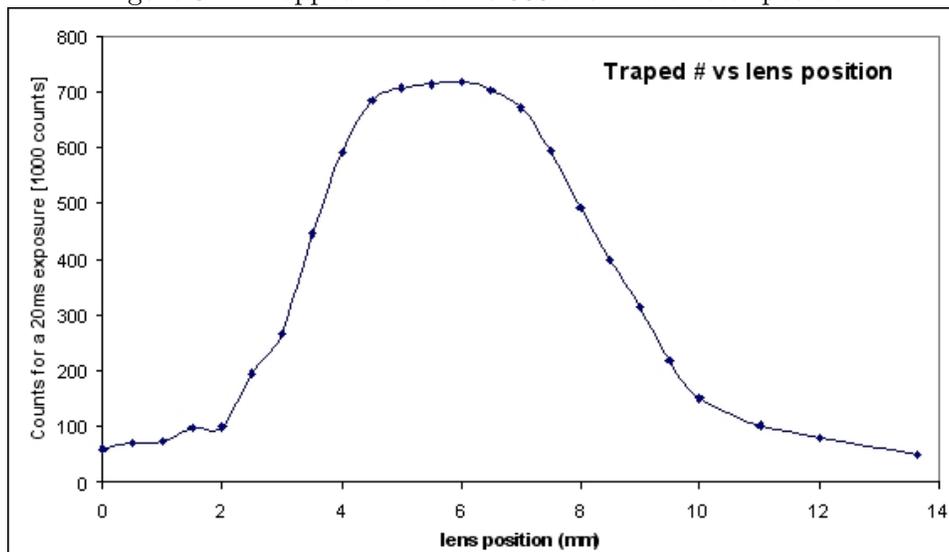
vs micrometer position. Note this plot agrees with the trap geometry. Firstly, notice the atom number is the greatest the center of the trap and decreases along both sides. Secondly, the atom number is nearly constant within the rayleigh range of the trap of 3-5mm. Thirdly, the asymmetry of the trap is shown as the atom number drops off faster on one side than the other. [Figures 8.3,8.4] show the same plot but with the trapping power reduced by half.

8.2.2   Adjusting MOT load times

[Figure 8.5] shows the plot MOT load time vs number of atoms trapped. The beginning of the curve has a rapid slope suggesting that the atoms from the MOT are filling the trap volume. In this region the MOT density is also increasing. The dropoff comes in probably when the MOT density has stopped increasing and also has overfilled the trap volume.

8.2.3   Adjusting the Trap Power

[Figure 8.6,8.7] shows a plot of the number atoms trapped vs trap beam power measured after the cell. There is some threshold at around 4-6 Watts where the potential of the trap is below the temperature of the MOT. Then the increase in trapped atom number is nearly exponential. These plots were measured using two methods: adjusting the power of the AOM and adjusting the power setting on fiber laser. The coincidence of these two plots confirm that these curves do not contain any artifacts of measurement.

8.2.4   Depumping, compression, and cooling

In general, the number of atoms trapped depend on the ratio between the temperature of the MOT and the potential of the trap. So one can obtain more atoms in the trap by either cooling the sample or increasing the trap power. For rubidium, we have not found it necessary to use advanced cooling techniques because we already load sufficient number of atoms. The only

Figure 8.3: Same measurement as [Figure 8.2] except including a scan where total trapping power is cut in half
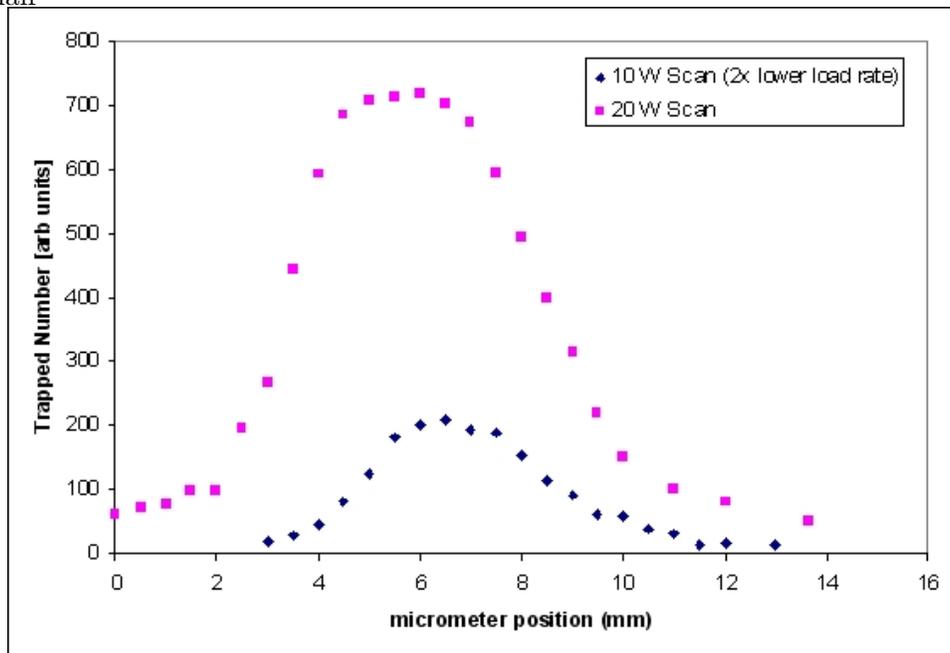
Figure 8.4: Same as [Figure 8.3] but normalized.
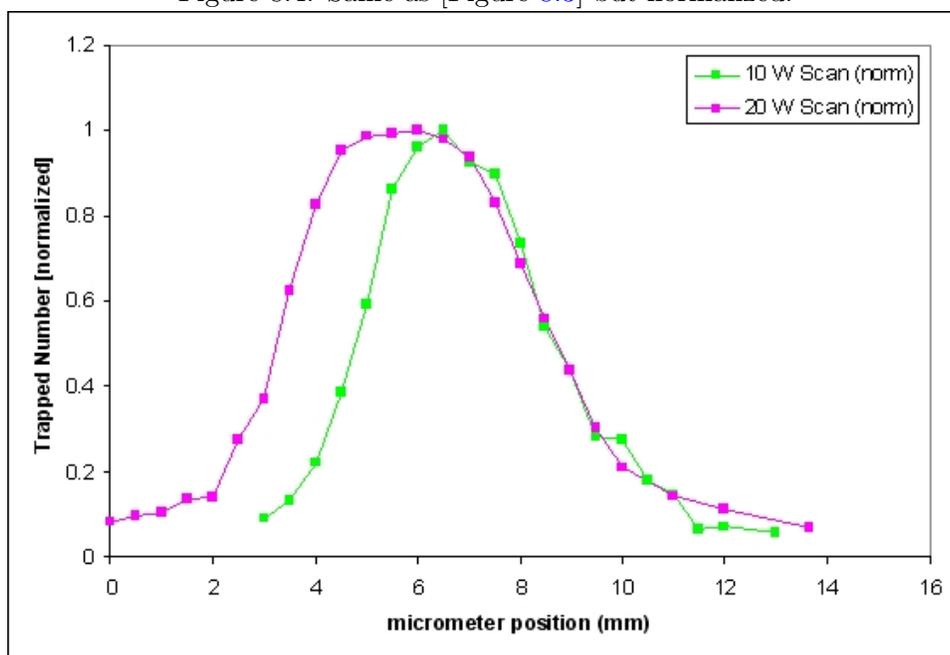
Figure 8.5: Number of atoms trapped vs MOT load time
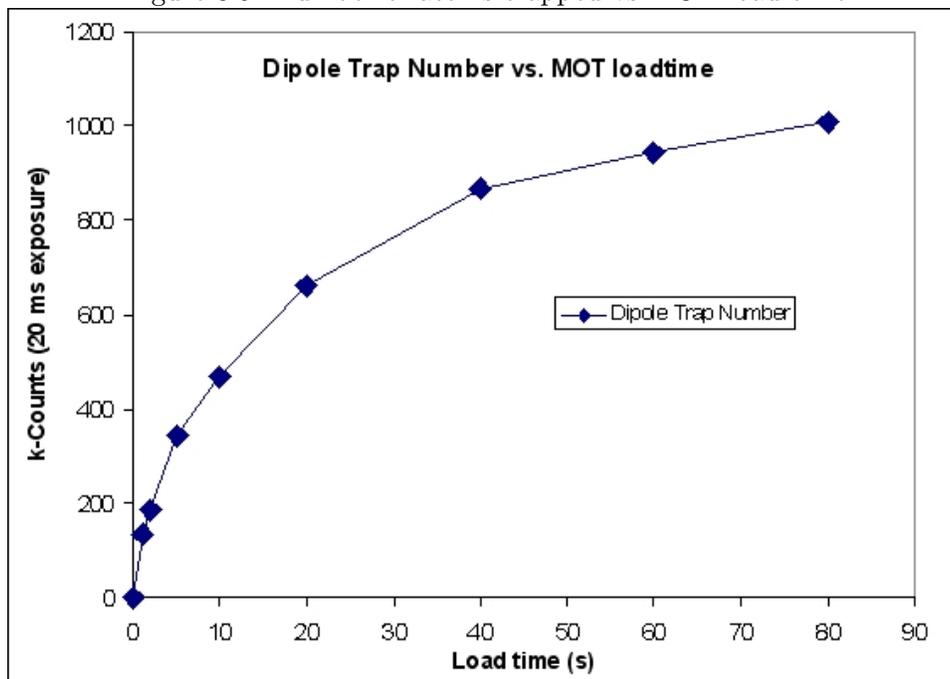
Figure 8.6: Number of atoms trapped vs Trap Power
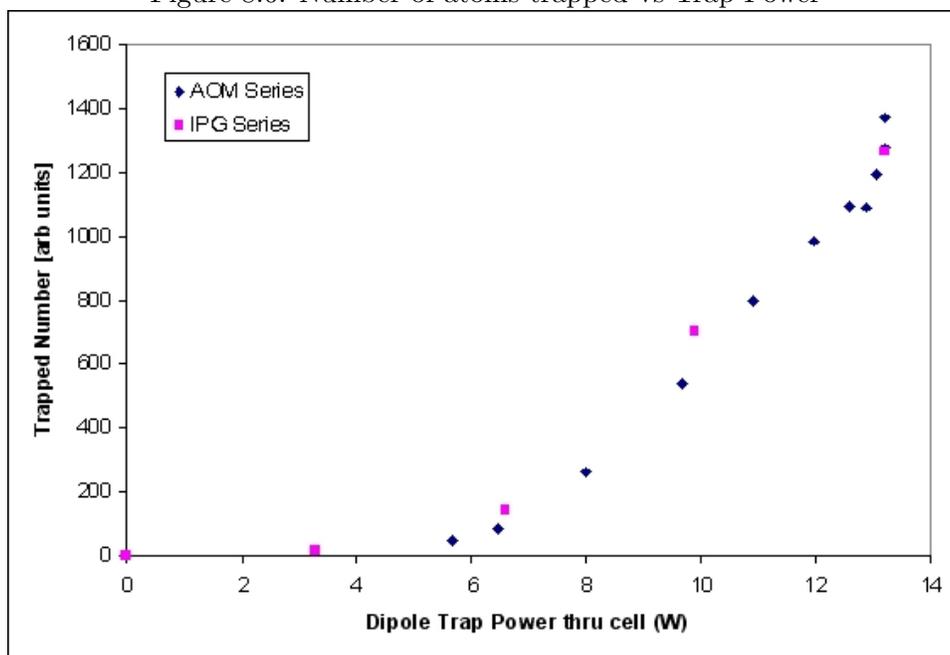
Figure 8.7: Number of atoms trapped vs Trap Power in log scale
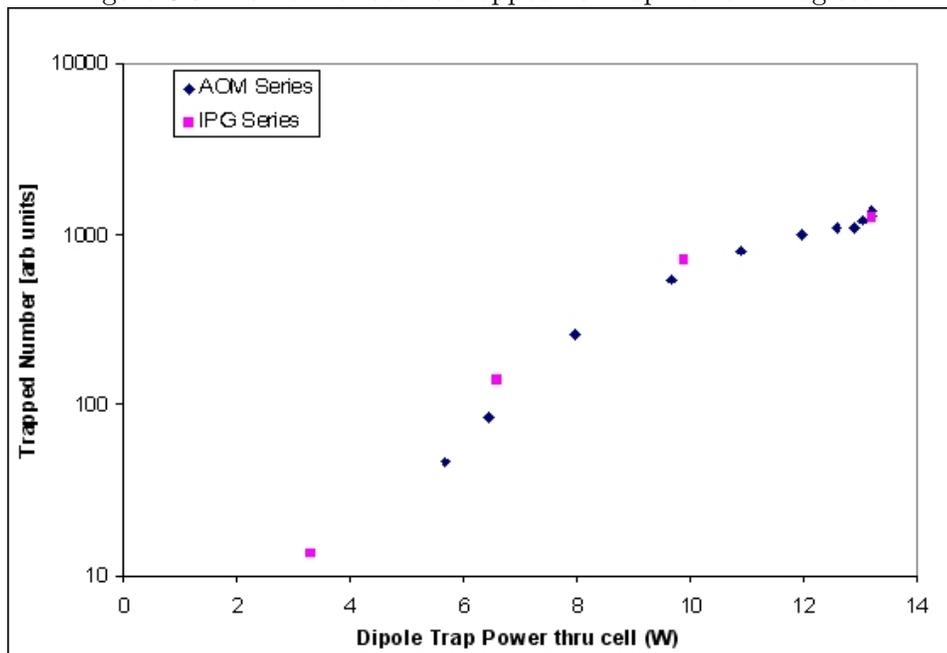
technique simple enough that we find useful is to reduce the repump intensity before loading into the trap. This gained us a factor of 2 in number of atoms. However, it is expected that our Lithium MOT is much hotter and less dense, thus compressing and cooling[11] of Li MOT is important for loading into the optical trap.

8.3 Standing Wave Trap

In an attempt to improve loading and longitudial confinement, we added in the 250mm spherical mirror after the cell to reflect the trapping beam back onto itself. We tried both the lin-lin configuration and the lin-perp-lin configurations. In the lin-lin configuration, we get an optical lattice which may or may not prevent us from effectly evaporating the sample to low temperatures. We have seen evidence of increased confinement in absorption imaging [section 8.5]. However, we also have seen dramatic decreases in trap lifetimes due to reason unknown at this time [section 8.4.3]. We speculate this could be due to multimode operation of the trapping laser. We can also switch to the lin-per-lin configuration but adding a quater waveplate between the retroreflection mirror and the cell. In this case, we lose a significant amount of power in pass through the glass walls due to incidence of S-polarized light at brewster angle (almost 10% per surface). We also noticed that the reflected power is enough to ablate surface atoms deposited on the cell walls. Thus we were unable to see improved trapping in lin-perp-lin because of the high loss in power and also the effects are immeasureable consistently due to the constant ablation of atoms.

Figure 8.8: Picomotor drivers used to remotely control the 250mm retroreflection spherical mirror
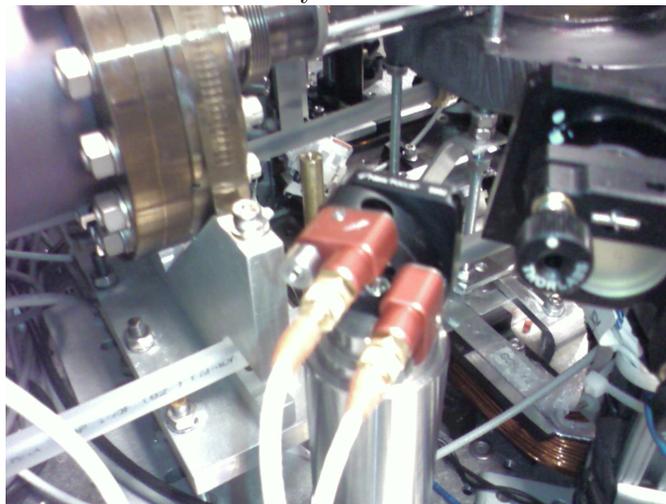
8.4 Trap Lifetimes

8.4.1 Rb87 lifetimes

[Figure 8.9]

8.4.2 Rb85 lifetimes

[Figure 8.10]

8.4.3 Standing wave trap lifetimes

The lifetimes of the trap in the standing wave is unforunately a mystery. [Figures 8.11,8.12] show a drastic decrease in the lifetimes for both states. One would expect more loss for the upper ground state due to higher density in the standing wave trap. This increases the number of inelastic collisions (such as hyperfine changing and light assisted collisions). However, such loss mechanisms do not exist for the lower ground state. The only type of loss that would affect both states are elastic background collisions. However, this is unlikely because the density increase required for such drastic changes in the lifetime would be enormous. Thus the expected plot looks like Figure 2. in [1]. One possible cause is that the fiber laser is running multimode and causing lattice heating. This is yet to be confirmed.

8.5 Absorption Imaging

Absorption imaging allows us to see the spatial structure of the trap. The key to getting good absorption images is to decrease the time between the image and the reference by as much as possible. [Figures 8.13,8.14] had the image and reference taken 5 ms apart, limited by the digitization speed of the camera. It is possible to reduce this time even futher zooming and reducing the ROI more so that there are less pixels to digitize.

Figure 8.9: Rb87 Trap lifetimes in single pass trap in both the upper and lower ground states. (a) The blue shows the decay in the lower (f=1) ground state with time constant τ of 43s. (b) The red shows the decay of the upper state (f=2). There is more than 1 time constant involved. The first is a fast decay possibly associated with 2 body loss and hyperfine changing collisions. Then followed by a long decay. The exponential fit is to the latter data points. Naively, we might expect the decay rate of the upper state to converge with that of the lower state when there are not enough atoms into the appropriate states remaining to allow hyperfine changing collisions.
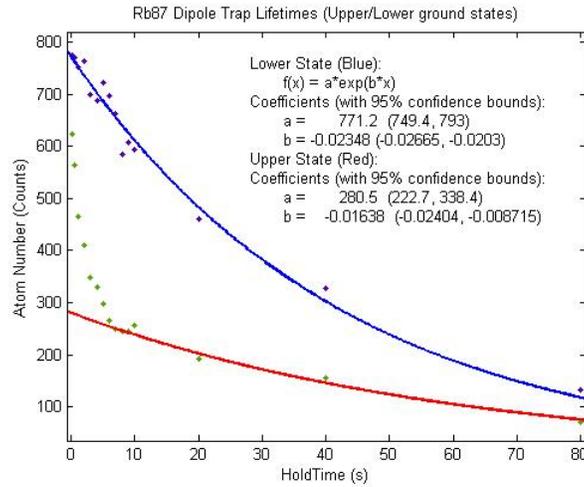
Figure 8.10: Rb85 traplife times are similiar to the Rb87 lifetimes but shorter. This is consistent with that fact that Rb85 has much higher abundance and therefore higher vapour pressure and background collisions.
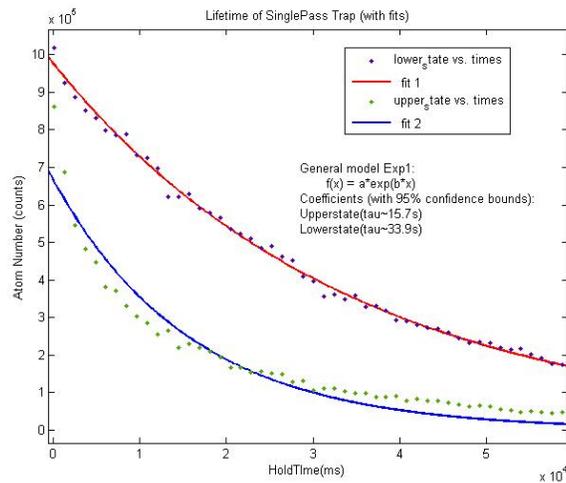
Figure 8.11: Rb87 lifetimes in standing wave trap
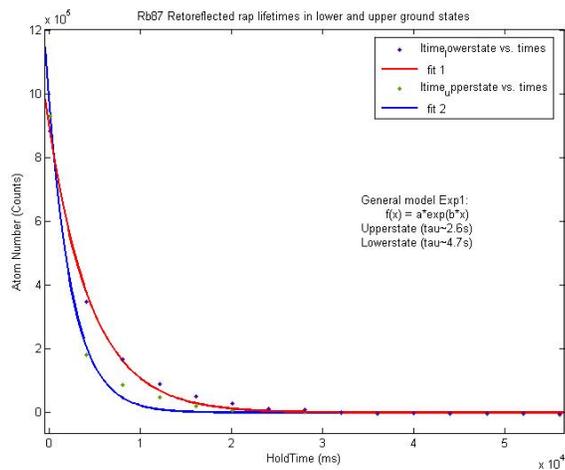
Figure 8.12: Rb85 lifetimes in standing wave trap
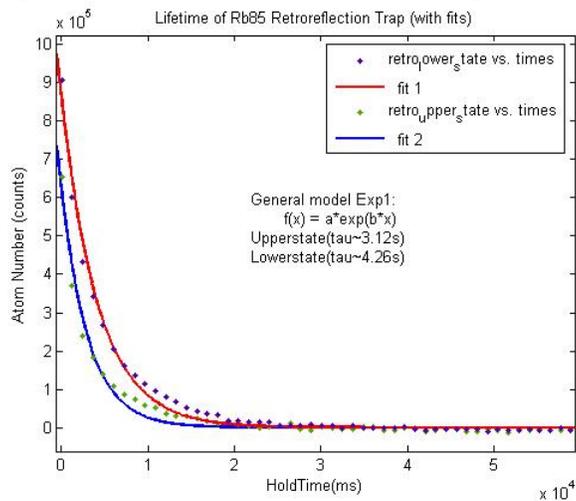
Figure 8.13: A sample absorption image of the Rb87 dipole trap. (a) Top left shows a vertical cross section. (b) Top right shows the absorption image in false colour (c) Bottom right shows a horizontal cross section (d) Bottom left shows a histogram of all the pixel values in the image
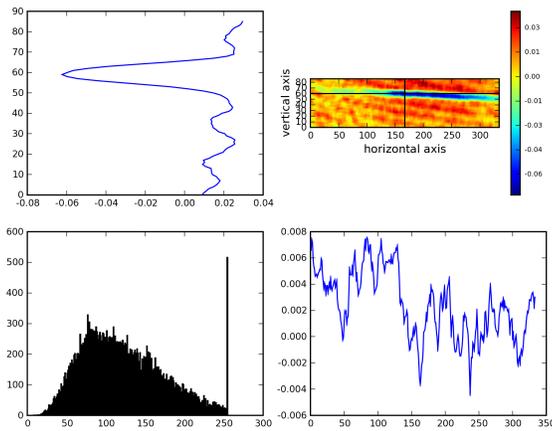
Figure 8.14: Comparing the single pass and standing wave trap of Rb87 in absorption image
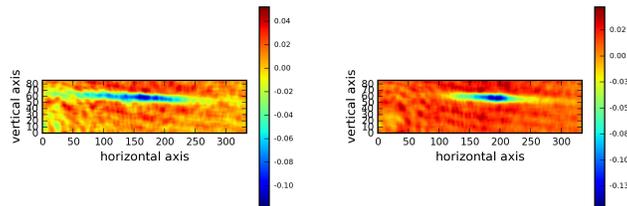
8.6 Trapping Lithium

Bibliography

[1] H. Moritz Th. Elssser A. Mosk, S. Jochim and M. Weidemller. Resonator-enhanced optical dipole trap for fermionic lithium atoms. *Optic Letters*, 26(23), 2001.

[2] Keith Ladouceur B. Experimental advances towards a compact dual-species laser cooling apparatus. Master's thesis, UBC.

[3] Butcher and Cotter. *Elements of Nonlinear Optics*. Cambridge University Press, 1990.

[4] Wieland Schllkopf Bretislav Friedrich Dima Egorov, Thierry Lahaye and John M. Doyle. Buffer-gas cooling of atomic and molecular beams. *Phys. Rev. A*, 66, 2002.

[5] Jason Remington Ensher. *The First Experiments with Bose-Einstein Condensation of 87Rb*. PhD thesis, University of Colorado at Boulder, 1998.

[6] Christopher J. Foot. *Atomic Physcs*. Oxford University Press, New York, 2005.

[7] Michael E. Gehm. Properties of lithium. Technical report, Duke University, 2003.

[8] D.J. Griffiths. *Introduction to Quantum Mechanics*. Prentice Hall, 2005.

[9] R.F.O'Connell G.W.Ford. Energy shifts for a multilevel atom in an intense squeezed radiation field. *OJ.Opt.Soc.Am.B*, 4, 1987.

[10] http://www.ccd.com/alta.html. Apogee alta technical documents.

[11] Selim Jochim. *Bose-Einstein Condensation of Molecules*. PhD thesis, Leopold-Franzens-Universitat Innsbruck, 2004.

[12] M. E. Gehm T. A. Savard S. Bali C. Freed * K. M. OHara, S. R. Granade and J. E. Thomas. Ultrastable co2 laser trapping of lithium fermions. *PHYSICAL REVIEW LETTERS*, 82(21), 1999.

[13] Paul D. Lett Kevin M. Jones, Eite Tiesinga and Paul S. Julienne. Ultracold photoassociation spectroscopy: Long-range molecules and atomic scattering. *REVIEWS OF MODERN PHYSICS*, 78, 2006.

[14] K.M.O'Hara. *Optical Trapping and Evaporation of Fermionic Atoms*. PhD thesis, Duke University, 2000.

[15] Harold J. Metcalf and Peter van der Straten. *Laser Cooling and Trapping*. Springer-Verlag, New York, 1999.

[16] Peter W. Milonni and Joseph H. Eberly. *Lasers*. John Wiley and Sons Inc., New York, 1988.

[17] Yurii B. Ovchinnikov Rudolf Grimm, Matthias Weidemuller. Optical dipole traps for neutral atoms. *arXiv:Physics/9902072 v1*, 1999.

[18] K. W. Miller T. E. Chupp * S. J. M. Kuppens, K. L. Corwin and C. E. Wieman. Loading an optical dipole trap. *PHYSICAL REVIEW A*, 62, 2000.

[19] Florian SCHRECK. *PHYSICS DEPARTMENT OF THE ECOLE NORMALE SU-PERIEURE.* PhD thesis, PHYSICS DEPARTMENT OF THE ECOLE NORMALE SU-PERIEURE (ENS), 2002.

[20] Daniel A. Steck. *Classical and Modern Optics.* Oregon Center for Optics and Department of Physics, Eugene OR, 2006.

[21] Florian Schreck Todd Meyrath. A laboratory control system for cold atom experiments. http://george.ph.utexas.edu/ control/.

[22] R.J. Knize T.Takekoshi, J.R. Yeh. Quasi-electrostatic trap for neutral atoms. *Optic Communications*, 114:421–424, 1995.

[23] www.mellesgriot.com. Melles-griot catalog.

Appendix A

AC Stark Shift in RWA

Given the time-depedent Schrödinger equations for a 2-level atom in [chapter 2.4.1]:

$$i\dot{a}_1 = -\frac{1}{2}(\chi_{12}e^{-i\omega t} + \chi_{21}^* e^{-i\omega t})a_2 \tag{A.1a}$$

$$i\dot{a}_2 = \omega_{21}a_2 - \frac{1}{2}(\chi_{21}e^{-i\omega t} + \chi_{12}^* e^{-i\omega t})a_1 \tag{A.1b}$$

To simplify we can transform to a rotating frame of reference.

$$a_1(t) = c_1(t) \tag{A.2a}$$

$$a_2(t) = c_2(t)e^{-i\Delta t} \tag{A.2b}$$

where $\Delta = \omega_{21} - \omega$

Then we can make the *Rotating Wave Approximation* by dropping the "fast" rotating terms $\omega_0 + \omega$. This approximation requires us to be "close enough" to resonance such that the following holds:

$$\omega_0 - \omega \ll \omega_0 + \omega \tag{A.3}$$

finnally we obtain

$$i\dot{c}_1 = -\frac{1}{2}\chi_{21}^* c_2 \tag{A.4a}$$

$$i\dot{c}_2 = \Delta c_2 - \frac{1}{2}\chi_{21}c_2 \tag{A.4b}$$

These equations are satisfy the Schrödinger equation with Hamiltonian given by

$$H = \frac{\hbar}{2}\begin{bmatrix} 2\Delta & -\chi^* \\ -\chi & 0 \end{bmatrix} \tag{A.5}$$

The hamiltonian has eigenenergies

$$E_{2,1} = \frac{\hbar}{2}(\Delta \mp \Omega) \tag{A.6}$$

$$\Omega^2 = \chi^2 + \delta^2 \tag{A.7}$$

where Ω is called the Generalized Rabi Frequency.

Figure A.1: The AC Stark shift of a 2 level atom in RWA
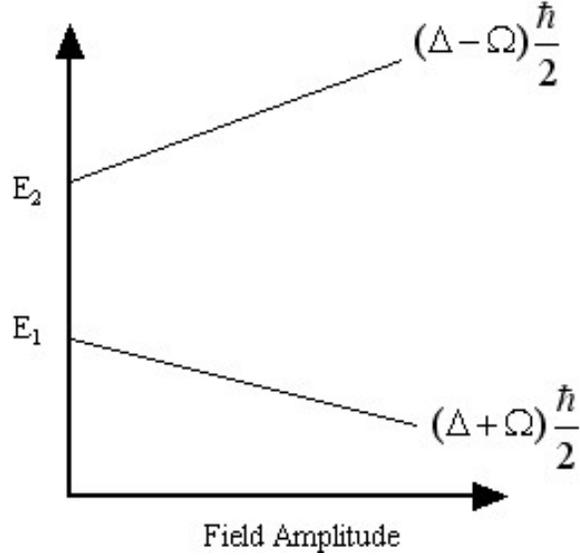
The resulting eigenenergies are shifted away from non-perturbed values by an amount that is proportial to the field amplitudes [Figure A.1]. Now if the light intensity has a spatial gradient, then there exists a force on the atom.

$$F = -\nabla U = -\nabla \left(\frac{\hbar \Omega^2}{4\Delta} \right) \tag{A.8}$$

In the case of a gaussian shaped laser beam, if $\Delta < 0$, and there is a net force on the atoms towards the center of the gaussian. On the other hand, if $\Delta > 0$, then the atoms are repelled away from the center. If the beam is made so that it comes to focus at the atoms, then there will be a force in the longitudinal direction as well. The magnitude of this force will obviously depend on the width of the focus.

Appendix B

Beam Dump Thermal Measurement

This was an attempt to study the efficiency of the beam dumps by measuring their heating rates due to the absorption of the laser. Here we assumed that most of the contribution to the heating of the beam dumps is absorption and that the beam dump is uniformly heated. It turns out that first assumption is good while the latter is bad. Nonetheless, we can estimate the power dissipated into the beam dump by looking at heating rate in the regime where the beam dump's temperature is increasing linearly with time. The experiment was done with one of the "copper elbow" beam dump designs.

A thermister was attached to the beam dump as 10W from the fiber laser was sent into the beam dump. Measurements were recorded every 10 seconds until the heating is no longer linear. In the first trial[Fig B.1], the thermister was attached to the elbow of the beam dump where most of the heating occured. In the second trail [Fig B.2], the thermister was attached to the tail of the beam dump where very little heating occurred. Taking into account the mass of the beam dump (140g) and the specific heat of copper, the upperbound for the beam dump was deduced to be 97% while the lower bound 50%. This is probably not the most accurate characterization of the beam dumps.
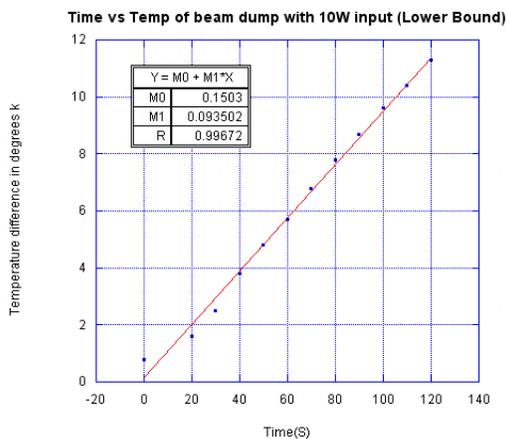
Figure B.1: Lower estimate of the elbow beam dump efficiency
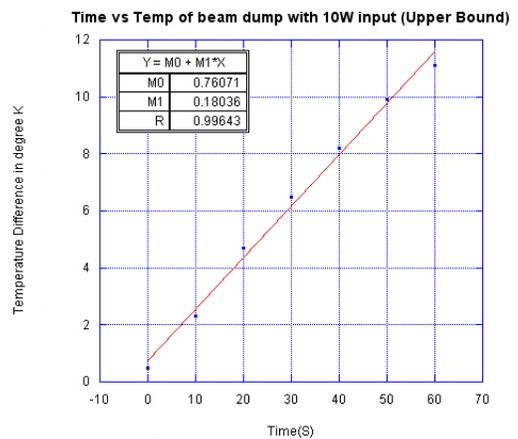
Figure B.2: Upper estimate of the elbow beam dump efficiency

Appendix C

Fiber Laser Mount Assembly

The following pages are CAD drawings produced from a solid works model of the fiber laser mount assembly. It was built by the UBC Machine Shop.

These corners can
be rounded

10.000

3.000

These corners can be rounded

1/4-20 Tapped Hole

0.500

C

C

0.250

1.000

0.250

0.500

0.500

0.250

0.250

0.250

0.250

Ø0.250

0.750

0.125

SECTION C-C

0.125

		UNLESS OTHERWISE SPECIFIED:		NAME	DATE				
		DIMENSIONS ARE IN INCHES	DRAWN						
		TOLERANCES: FRACTIONAL ±	CHECKED			TITLE:			
		ANGULAR: MACH ± BEND ± TWO PLACE DECIMAL ± THREE PLACE DECIMAL ±	ENG APPR.						
			MFG APPR.						
		INTERPRET GEOMETRIC TOLERANCING PER:	Q.A.						
		MATERIAL	COMMENTS:						
						SIZE	DWG. NO.		REV
NEXT ASSY	USED ON	FINISH				B	FiberLaserMount1_SPLIT_A		
APPLICATION		DO NOT SCALE DRAWING				SCALE: 1:2	WEIGHT:	SHEET 1 OF 1	

SECTION L-L

1.665

L   L

1/4-20 Counterbore (TYP.)

0.500

Ø0.563

0.500

3.000

0.500

0.500

$\begin{bmatrix} +0.127 \\ 30.500 & -0.127 \end{bmatrix}$
$Ø1.201 \begin{matrix} +0.005 \\ -0.005 \end{matrix}$

6.000

1.500

3.000

2.000

3.000

$\begin{bmatrix} +0.127 \\ 19 & -0.127 \end{bmatrix}$
$0.748 \begin{matrix} +0.005 \\ -0.005 \end{matrix}$

$\begin{bmatrix} +0.127 \\ 22.850 & -0.127 \end{bmatrix}$
$0.900 \begin{matrix} +0.005 \\ -0.005 \end{matrix}$

$\begin{bmatrix} +0.076 \\ 30 & 0 \end{bmatrix}$
$Ø1.181 \begin{matrix} +0.003 \\ 0.000 \end{matrix}$

TRUE R0.133

UNLESS OTHERWISE SPECIFIED:		NAME	DATE
DIMENSIONS ARE IN INCHES	DRAWN		
TOLERANCES:	CHECKED		
FRACTIONAL ±			
ANGULAR: MACH ± BEND ±	ENG APPR.		
TWO PLACE DECIMAL ±			
THREE PLACE DECIMAL ±	MFG APPR.		
	Q.A.		
INTERPRET GEOMETRIC TOLERANCING PER:	COMMENTS:		
MATERIAL			
FINISH			

NEXT ASSY   USED ON

APPLICATION   DO NOT SCALE DRAWING

TITLE:

SIZE   DWG. NO.   REV
B   FiberLaserMount1_SPLIT_C

SCALE: 1:2   WEIGHT: SHEET 1 OF 1

8   7   6   5   4   3   2   1

D   C   B   A

0.125

1.500

$\begin{bmatrix} 30 & +0.051 \\ & -0.102 \end{bmatrix}$
$\varnothing 1.181 \begin{array}{c} +0.002 \\ -0.004 \end{array}$

$\begin{bmatrix} 30.500 & +0.076 \\ & 0 \end{bmatrix}$
$\varnothing 1.201 \begin{array}{c} +0.003 \\ 0.000 \end{array}$

$\varnothing 0.250$

1/4-20 Tapped Hole

0.250

		UNLESS OTHERWISE SPECIFIED:		NAME	DATE			
		DIMENSIONS ARE IN INCHES	DRAWN			TITLE:		
		TOLERANCES: FRACTIONAL±	CHECKED					
		ANGULAR: MACH± BEND ± TWO PLACE DECIMAL ±	ENG APPR.					
		THREE PLACE DECIMAL ±	MFG APPR.					
		INTERPRET GEOMETRIC TOLERANCING PER:	Q.A.					
		MATERIAL	COMMENTS:					
NEXT ASSY	USED ON	FINISH				SIZE B	DWG. NO. FiberLaserMountPart2	REV
APPLICATION		DO NOT SCALE DRAWING				SCALE: 2:1	WEIGHT:	SHEET 1 OF 1

0.415

1/4-20 CounterBore

Ø0.563

SECTION A-A

1.500

A   A

0.125

$30 \begin{array}{c}+0.051\\-0.102\end{array}$ $1.181 \begin{array}{c}+0.002\\-0.004\end{array}$

Ø0.266

$30.500 \begin{array}{c}+0.076\\0\end{array}$
$Ø1.201 \begin{array}{c}+0.003\\0.000\end{array}$

0.250

		UNLESS OTHERWISE SPECIFIED:		NAME	DATE			
		DIMENSIONS ARE IN INCHES	DRAWN			TITLE:		
		TOLERANCES:	CHECKED					
		FRACTIONAL ±						
		ANGULAR: MACH ± BEND ±	ENG APPR.					
		TWO PLACE DECIMAL ±						
		THREE PLACE DECIMAL ±	MFG APPR.					
			Q.A.					
		INTERPRET GEOMETRIC	COMMENTS:					
		TOLERANCING PER:						
		MATERIAL				SIZE	DWG. NO.	REV
						B	FiberLaserMountPart3	
NEXT ASSY	USED ON	FINISH						
APPLICATION		DO NOT SCALE DRAWING				SCALE: 2:1	WEIGHT:	SHEET 1 OF 1

Appendix D

Calculations for Lithium-6

The following pages are mathematica notebooks calculations for Li6 trap depth, scattering rate, and trap numbers.

```
<< Statistics`NonlinearFit`
```

■ Physical Constants

```
h = 6.626068 * 10 ^ -34;
hbar = h / (2 π);
c = 3 * 10 ^ 8;
k = 1.3806503 * 10 ^ -23;
m_Li = 6.015121 / (6 * 10^23) / 1000;
ε_0 = 8.85418782 * 10 ^ -12;
```

■ Beam and MOT Parameters

```
P_0 = 10;
λ_1 = 1064 * 10 ^ -9;
w_0 = 50 * 10 ^ -6;
```

$$z[\text{w\_}] = \frac{\pi * w^2}{\lambda_1};$$

```
z_0 = z[w_0];
ω_1 = 2 π * c / λ_1;
n_MOT = 1 * 10 ^ 16;
T_MOT = 600 * 10 ^ -6;
```

$$\text{TrapVol}[\text{w\_}] = \pi^{3/2} * w^2 * \left(\frac{\pi * w^2}{\lambda_1}\right);$$

$$\text{Intensity}[\text{w\_}] = \frac{2\,P_0}{\pi * w^2};$$

■ Li6 Data

$$\mathbf{DPM_{D1}} = \begin{pmatrix} 3/2 \to 3/2 & 3/2 \to 1/2 \\ 1/2 \to 3/2 & 1/2 \to 1/2 \end{pmatrix}$$

$$\mathbf{DPM_{D2}} = \begin{pmatrix} 3/2 \to 5/2 & 3/2 \to 3/2 & 3/2 \to 1/2 \\ 1/2 \to 5/2 & 1/2 \to 3/2 & 1/2 \to 1/2 \end{pmatrix}$$

```
D_1Li = 670.992421 * 10 ^ -9;
D_2Li = 670.977338 * 10 ^ -9;
ω_D1Li = 2 π * c / D_1Li;
ω_D2Li = 2 π * c / D_2Li;
```

$$\text{DPM}_{D1} = \begin{pmatrix} -5.4117 * 10^{\wedge}-30 & -1.53066 * 10^{\wedge}-29 \\ -1.53066 * 10^{\wedge}-29 & 5.4117 * 10^{\wedge}-30 \end{pmatrix};$$

$$\text{DPM}_{D2} = \begin{pmatrix} -2.17829 * 10^{\wedge}-29 & 4.84065 * 10^{\wedge}-30 & 5.41201 * 10^{\wedge}-30 \\ 0 & -1.71143 * 10^{\wedge}-29 & 1.53075 * 10^{\wedge}-29 \end{pmatrix};$$

$$\text{g1} = \frac{\omega_{D1Li}{}^3}{3\,\pi * \epsilon_0 * \text{hbar} * c^3}\ \text{DPM}_{D1}{}^2$$

$$\text{g2} = \frac{\omega_{D2Li}{}^3}{3\,\pi * \epsilon_0 * \text{hbar} * c^3}\ \text{DPM}_{D2}{}^2$$

$\{\{2.73249 \times 10^6, 2.18599 \times 10^7\}, \{2.18599 \times 10^7, 2.73249 \times 10^6\}\}$

$\{\{4.42743 \times 10^7, 2.18639 \times 10^6, 2.73299 \times 10^6\}, \{0, 2.73299 \times 10^7, 2.1864 \times 10^7\}\}$

■ **The Trap Depth and Frequencies**
Multiply by 4 for standing waves
f_r and f_z are the radial and axial trapping frequencies

$$U_{03/2}[w\_] = \frac{3\,\pi * c^2}{2} * \text{Intensity}[w] * \left(\frac{1}{\omega_{D1Li}^3}\left(\frac{1}{\omega_{D1Li} - \omega_1} + \frac{1}{\omega_{D1Li} + \omega_1}\right)(g1[[1,1]] + g1[[1,2]]) + \right.$$
$$\left. \frac{1}{\omega_{D2Li}^3}\left(\frac{1}{\omega_{D2Li} - \omega_1} + \frac{1}{\omega_{D2Li} + \omega_1}\right)(g2[[1,1]] + g2[[1,2]] + g2[[1,3]])\right);$$

$$U_{03/2}[w_0] * 4 / k$$

$$U_{03/2\,sw} = U_{03/2}[w_0] * 4$$

$$f_r = \sqrt{\frac{4\,U_{03/2\,sw}}{m_{Li} * w_0^2}}$$

$$f_z = \sqrt{\frac{4\,U_{03/2\,sw}}{m_{Li} * z_0^2}}$$

$$\Gamma_{3/2} = \frac{3\,\pi * c^2 * \omega_1^3}{2\,hbar} * \text{Intensity}[w_0] *$$
$$\left(\frac{1}{\omega_{D1Li}^6}\left(\left(\frac{g1[[1,1]]}{\omega_{D1Li} - \omega_1} + \frac{g1[[1,1]]}{\omega_{D1Li} + \omega_1}\right)^2 + \left(\frac{g1[[1,2]]}{\omega_{D1Li} - \omega_1} + \frac{g1[[1,2]]}{\omega_{D1Li} + \omega_1}\right)^2\right) + \frac{1}{\omega_{D2Li}^6}\right.$$
$$\left.\left(\left(\frac{g2[[1,1]]}{\omega_{D1Li} - \omega_1} + \frac{g2[[1,1]]}{\omega_{D1Li} + \omega_1}\right)^2 + \left(\frac{g2[[1,2]]}{\omega_{D1Li} - \omega_1} + \frac{g2[[1,2]]}{\omega_{D1Li} + \omega_1}\right)^2 + \left(\frac{g2[[1,3]]}{\omega_{D1Li} - \omega_1} + \frac{g2[[1,3]]}{\omega_{D1Li} + \omega_1}\right)^2\right)\right)$$

```
0.00123089
```

```
1.69943×10⁻²⁶
```

1.69943×10^{-26}

```
52079.3
```

```
352.766
```

```
0.397818
```

■ **Trap Numbers-Numerically Compute the Trap Factor on a sparsetable then interpolate the points**

```
Clear[g];
Clear[β];
Clear[F];
β[x_] = -Log[1 - x];
```
$$\left(*g[x\_] = \frac{\beta[x]^{3/2}\,(1-x)^{1/2}}{x^2}\,\frac{16}{\pi}\int_0^1 u^2\,\sqrt{e^{-Log[1-x]\,(1-u^2)} - 1}\;du;*\right)$$
```
g[x_] :=
```
$$\frac{(\beta[x])^{3/2}\,(1-x)^{1/2}}{x^2}\,\frac{16}{\pi} * \text{NIntegrate}\left[u^2\,\sqrt{e^{\beta[x]*(1-u^2)} - 1}, \{u, 0.00000000001, 0.99999999999999\}\right];$$
$$F[q\_] := \frac{q^{3/2}}{2} * \text{NIntegrate}[x^2\,g[x]\,e^{q\,(1-x)}, \{x, 0.00000000001, 0.99999999999999\}];$$
```
Timing[F[5]]
```

NIntegrate::inum : Integrand $u^2\sqrt{e^{\beta[x]\,(1-u^2)} - 1}$ is not numerical at {u} = {0.5}. More…

NIntegrate::inum : Integrand $u^2\sqrt{e^{\beta[x]\,(1-u^2)} - 1}$ is not numerical at {u} = {0.5}. More…

```
{0.703 Second, 19.4269}
```

```
SparseData = Table[{z, F[z]}, {z, 0, 10, 0.1}];
Clear[A];
(*FactorFit[x_]=NonlinearFit[SparseData,a*e^(b*x^4),{x},{{a,1},{b,1}}];*)
TrapFactor = Interpolation[SparseData];
plot1 = Plot[TrapFactor[x], {x, 0, 10}, Frame → True,
   FrameLabel → {U_0/KT, N_T/N_0, "Plot of Trapping Factor F", ""}, RotateLabel → False]
(*plot2=Plot[FactorFit[x],{x,0,5},PlotRange→{0,20}]*)
(*Show[plot1,plot2]*)
```

NIntegrate::inum : Integrand $u^2 \sqrt{e^{\beta[x] (1-u^2)} - 1}$ is not numerical at {u} = {0.5}. More…

NIntegrate::inum : Integrand $u^2 \sqrt{e^{\beta[x] (1-u^2)} - 1}$ is not numerical at {u} = {0.5}. More…

NIntegrate::inum : Integrand $u^2 \sqrt{e^{\beta[x] (1-u^2)} - 1}$ is not numerical at {u} = {0.5}. More…

General::stop : Further output of NIntegrate::inum will be suppressed during this calculation. More…

Plot of Trapping Factor F
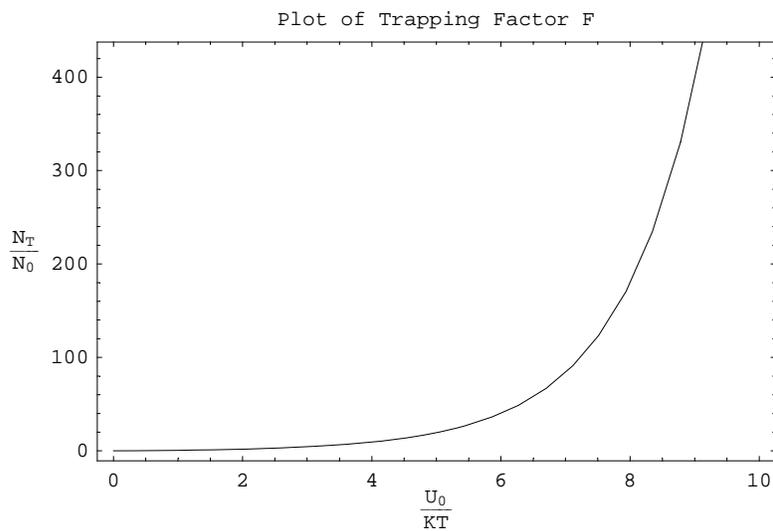
- Graphics -

■ Find the number of trapped atoms as a function of Beam Waist

$N_T[w\_] = n_{MOT} * \text{TrapVol}[w] * \text{TrapFactor}\left[\frac{U_{03/2}[w] * 4}{k * T_{MOT}}\right];$

$\text{Plot}[N_T[w], \{w, 30 * 10^{\wedge} - 6, 150 * 10^{\wedge} - 6\}, \text{Frame} \rightarrow \text{True},$
$\quad \text{FrameLabel} \rightarrow \{"w_0", "N_T", "Plot of Number of Trapped Atoms vs Beam Waist", ""\},$
$\quad \text{RotateLabel} \rightarrow \text{False}, \text{PlotRange} \rightarrow \{0, 10^{\wedge}7\}, \text{Axes} \rightarrow \text{False}]$
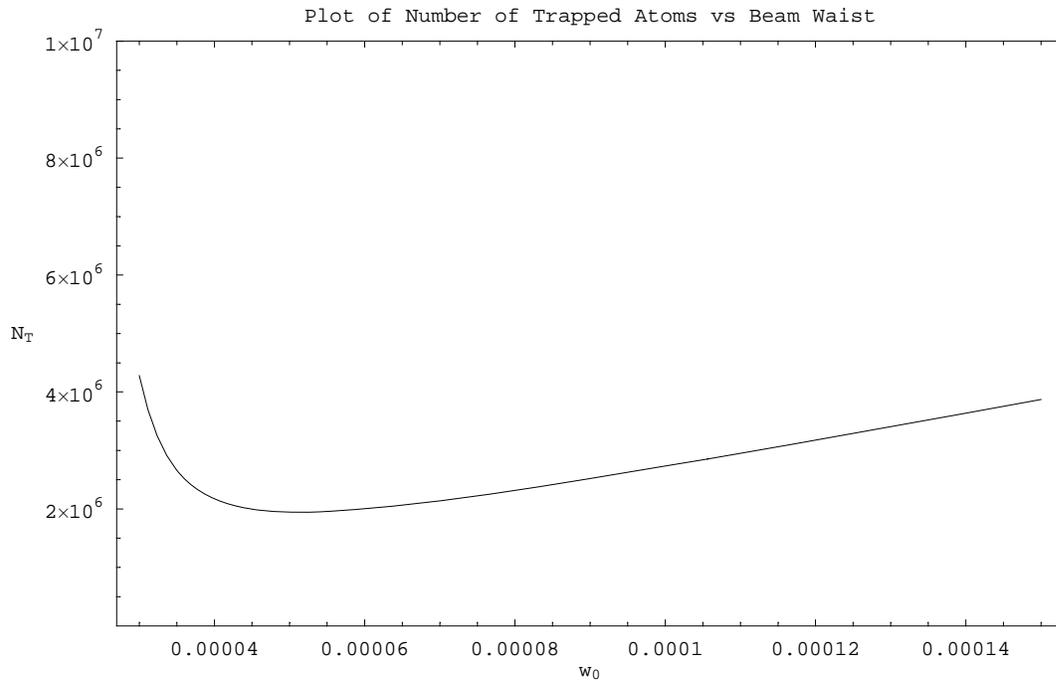
- Graphics -

Appendix E

Apogee Server Reference

The following pages are the commands used to communicate with the Apogee Server. The port for the server is typically 25000. Note all non-query commands now return a 1 byte binary string $0x01$ after completion (as Bruce requested!)

Commands

Command	Params	Function
QUIT	none	Exits the Server
Getstat	none	Get program/camera info. Returns a string containing the info.
Expose	T[Double] D[Int] N[Int]	Takes [N] image with exposure time [T] in seconds. [D] is 0 specifies dark image, otherwise light image
GetImage	none	Gets the last image taken from the server. The first 2 bytes of the packet specifies the number of pixels in the image.
Init	none	Initializes/Reinitializes all camera parameters to default values(default ROI,default mode 0, Sequencebulkdownload = false, triggermode = 0,IOPortassignment = 0x01) ;Also deletes all images stored on server.
SetROI	X[int] Y[int] DX[int] DY[int]	Sets the ROI.
GetROI	none	Gets the ROI. Returns a contiguous block of 4 integers representing x,y,dx,dy in that order
GetImageCount	none	Gets the number of images remaining on the server. Returns an integer.
SetMode	M[int]	Sets the mode [M] corresponding to the mode of the camera (0 = normal, 5 = kinetics, see AltaDevAPI for the rest)
GetMode	none	Returns an integer corresponding to the current mode of the camera (0 = normal, 5 = kinetics, see AltaDevAPI for the rest)
SetTrigMode	M[int]	Sets the Trigger Mode specified by the final 4 bits of the [M]. see below
GetTrigMode	none	Gets the current trigger mode. See below
SetKinParams	N[int] H[int] T[Double]	Sets the kinetics mode parameters with [N] sections, [H] height in pixels per section, [T] in seconds the shift interval.
GetKinParams	none	Gets the kinetics mode parameters. Returns a contiguous block of 2 integers followed by a double (8 byte) corresponding to the number of sections, height per section, shift interval in that order.
SetBulkDownload	B[int]	If [B] = 0, then images will be streamed to server

		as they arrive, otherwise images will be saved onto camera's internal memory until entire sequence is completed

To be Implemented Commands

Command	Params	Function
SetQuietExposure	Q[int]	If [Q] = 1, fans are turned off during exposure.
SetContinuousImaging	C[int]	
Expose_Continous		
SetIOPortAssignment	I[int]	Sets the I/O port mode corresponding to [I],setting it to 0x01 will enable hardware trigger and disable other I/O port functions.

More functions to come...

Trigger Modes:

An integer represented by the bits ABCD in is the parameter sent to **SetTrigMode** or received from **GetTrigMode**

bits:
A = TriggerTDIKineticsGroup
B = TriggerTDIKineticsEach
C = TriggerNormalGroup
D = TriggerNormalEach

C	D	Function
0	0	**No trig. Software control**
0	1	**If (imagecount =1) not valid;** **If(imagecount > 1) The first image of the sequence is** **begun by software control. The rest are hardware triggered**
1	0	**If (imagecount =1) requires 1 trigger to take the image, a second to download the image?** **If(imagecount > 1) The first image of the sequence is** **begun by software control. The rest are hardware triggered**
1	1	**If (imagecount =1) requires 1 trigger to take the image, a second to download the image?** **if(imagecount >1) Every image in sequence is hardware triggered.**

A	B	Function
0	0	**No trig, Software controls kinetics mode.**
0	1	**The first kinetics section is begun by software control, the rest are hardware triggered.**
1	0	**One Hardware trigger begins first section, the reset are software controlled.**
1	1	**Every kinetics section is hardware triggered.**

Example: if set mode parameter 12 (1100) and cam is in kinetics mode, then it will wait a trigger for every kinetics section.

Appendix F

Computer Program for Measuring AOM Resonance

```java
 /*
 * Main.java
 *
 * Created on September 10, 2007, 4:38 PM
 *
 * A Program to Sweep the Function Generator and Measure the Response of the RSA
 * using the GPIB-Ethernut
 */

package sweepnread;

import org.EnutCommon.*;
/**
 *
 * @author ray
 */
public class Main {

    /** Creates a new instance of Main */
    public Main() {
    }

    /**
     * @param args the command line arguments
     */
    public static void main(String[] args) {

        int FGEN_ADDR = 19;
        int RSA_ADDR = 20;
        // TODO code application logic here
        if(args.length != 2) {
            return;
        }
        EGInterface eg = new EGInterface(args[0],java.lang.Integer.parseInt(args[1]));
```

```
        if(!eg.Connect()) {
            System.out.println("FAILED TO CONNECT, ABORTING");
            return;
        }
        System.out.println(eg.getVersion());
        eg.ibConnectGPIBAddress(RSA_ADDR);
        StringBuffer buf = new StringBuffer();
        double freq = 15;
        try {

            for(freq=15;freq<150;freq+=0.1) {


                eg.ibWrite("~" + FGEN_ADDR + "~" + "FREQ:CW " + Double.toString(freq) + "MHZ"
                Thread.sleep(500);

                eg.ibWrite("~" + RSA_ADDR + "~" + ":CALC1:MARK1:MAX");
                Thread.sleep(500);

                eg.ibWrite("~" + RSA_ADDR + "~" + ":CALC1:MARK1:Y?");
                eg.ibRead(buf);
                System.out.println(Double.toString(freq) + "," + buf);
                buf.delete(0,buf.length());
            }
        } catch (InterruptedException ex) {
            ex.printStackTrace();
        }

        eg.ibCloseConnection();

    }

}
```

Appendix G

Camera Calibration

The following pages contain data for the responsivity calibration of the Sony camera used for beam profile measurements. It was found that the electronic response was not linear to the input intensity and this made the beam sizes appear wider or narrower (depending on intensity) than they actually are.

Var. Attenuator

CCD
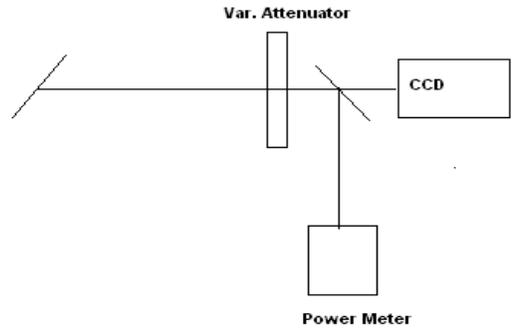
Power Meter

We measured the **Peak intensities** vs **WidthX** vs **WidthY** vs **Measured power** on the power meter.

Peak I (cnts)	Width X (px)	Width Y (px)	Power(mW)
236	24	12	6.6
218	24	11.5	5.8
206	23.7	11.7	5.4
193	23.8	11	5
183	23.2	11.1	4.6
170	22.5	11	4.2
151	22.5	10.5	3.7
139	22.6	10.1	3.4
126	21.8	9.9	3
109	20.6	9.6	2.6
90	20.2	8.6	2.2
71	18.2	7.8	1.9

Next: Fit the responsivity curve: note the behavior below 80 counts is unknown and was not measured.

Responsivity Curve of Sony Camera

Fit Model: $R(I) = a (1 - b * \exp(-c * I))$

PKI vs. Power

fit 1

Peak Intensity (counts)
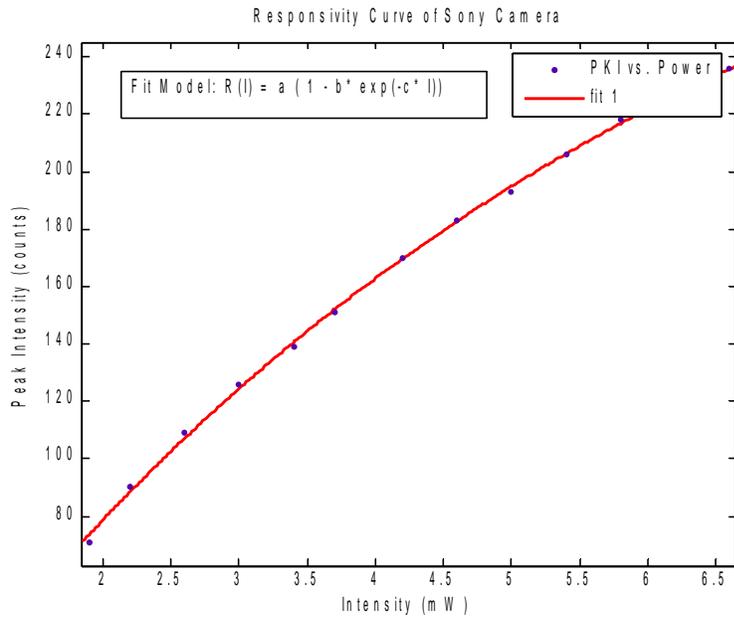
Intensity (mW)

This fit does not go through (0,0) but intersects the I axis at I = 0.6144, I tried a fit that does go through 0 but does not work as well... more data is needed at lower intensities.

Next "generate" data from measured gaussian widths and peak intensities (I didn't use the actual data because we didn't save them, but the fits on the live fitting program were "good" enough that I trust these recreations),

Then, apply the inverse response function to the data and obtain new gaussians, fit to produce:

New X Wdith	New Y Width	Peak I (cnts)	Power(mW)
20.7	10.35	236	6.6
21.1	10.11	218	5.8
21.07	10.4	206	5.4
21.4	9.89	193	5
21.03	10.06	183	4.6
20.6	10.07	170	4.2
20.88	9.74	151	3.7
21.13	9.44	139	3.4
20.55	9.33	126	3
19.61	9.14	109	2.6
19.42	8.27	90	2.2
17.66	7.57	71	1.9

- Width X
□ Width Y

"Calibrated Widths"
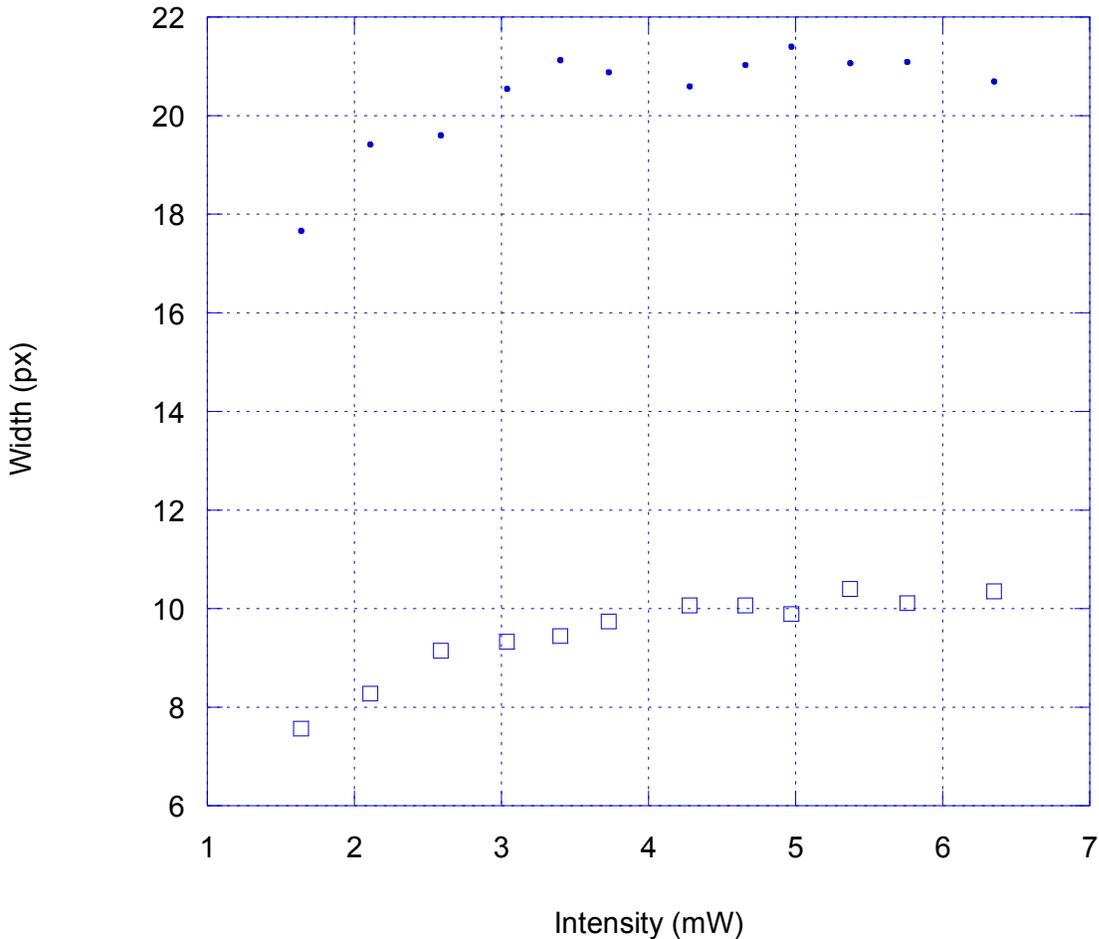
Appendix H

Optical Bistability

The following experiment was to determine the optical bistability some of our injection locked MOT lasers during a time when they were severly "misbehaving".

Bistable locking behavior in injection locking (Jan 18, 2008)

References:
Rongqing Hui et al. Optic Letters, February 15, 1993 / Vol. 18, No. 4
Vassilios Kovanis et al. Optics Communications 159 1999.177–183
Hitoshi Kawaguchi et al., IEEE JOURNAL OF QUANTUM ELECTRONICS, vol. qe-21. no. 9, september 1985
Rongqing Hui et al. , IEEE JOURNAL OF QUANTUM ELECTRONICS, vol. 21, no. 6. june 1991

Intro and Observations

Optical Bistability refers to a behavior in optical devices with feedback where 2 stable states can exist for a certain set of parameters. For diode lasers, this is defined as 2 stable values of output power for some state of the laser. This was first seen in diode lasers used as amplifiers operating near threshold, but has also been studied in injection locking. In our lasers, for a given current of an injection locked diode we have seen both a "locked" state and an unlocked state exist depending on the direction in which we tune the current. We observed the following typical "injection lock cycle":

1. Tune the slave current to a free running state
2. Tune down the current until free running oscillations of the slave begins to be suppressed **(I6)**
3. Keep tuning until all the side bands and other competing modes disappear and the main peak is "clean" **(I5)**
4. Keep tuning until the slave becomes unlocked **(I1)**
5. Tune the current in the opposite direction until lock is recovered **(I2)**

We observed that typically when we are running the slave diode in the bistable region, blocking then unblocking the injection to the slave would return it to the uninjected state.
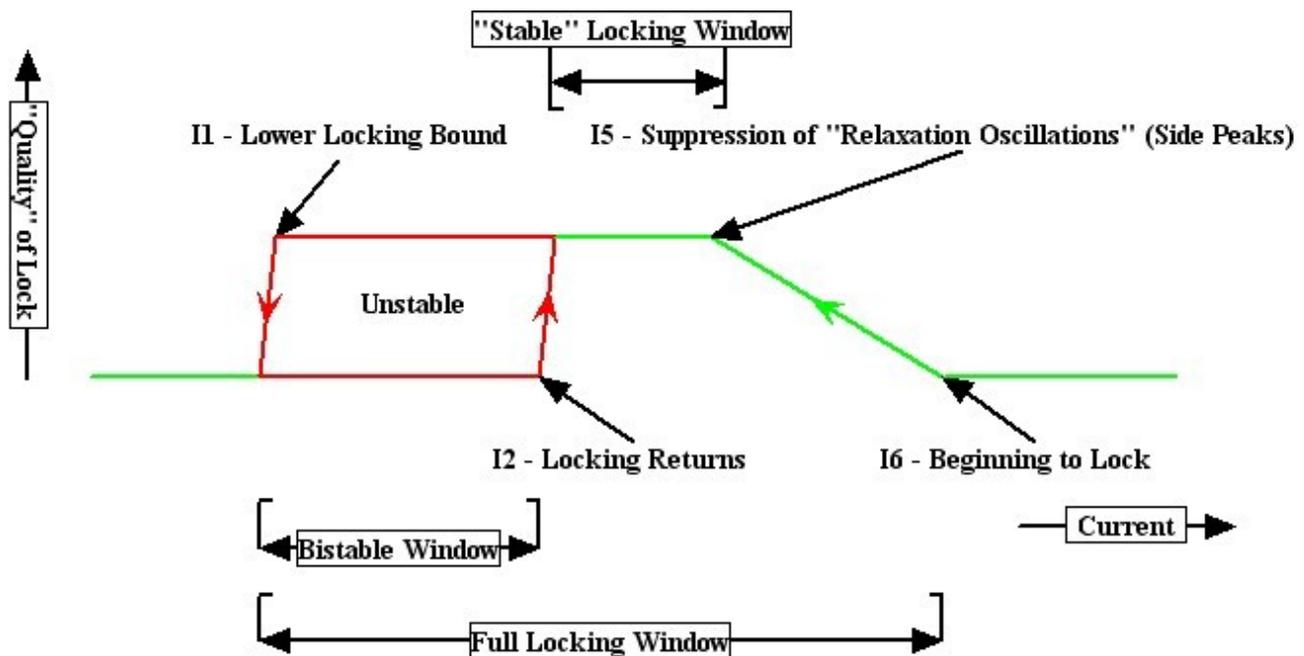
An Injection Lock Cycle

Motivation

In a study of injection locked DFBs (Distributed Feedback Lasers), Rongqing Hui discovered that the regime of bistability depends only on the ratio between the optical injection power and the output power of the slave. If this is true for fabry-perot diode lasers as well, we can decrease the injection power to reduce the size this unstable window.

Experiment

The injection power was varied by changing the alignment to fiber leading the Li light from slave 6 on the master table to slave 7 on the molecule table. For each injection power, the slave was tuned to 3 highest (below 165 mA) continguous injection windows and the properties (current, output power) at the injection states (I6,I5,I1,I2) were recorded.

Resulting Plots (Refer to previous page for description of I6,I5,I1,I2)

Bistable Window Width vs Injection Power

Locking Window Width vs Injection Power
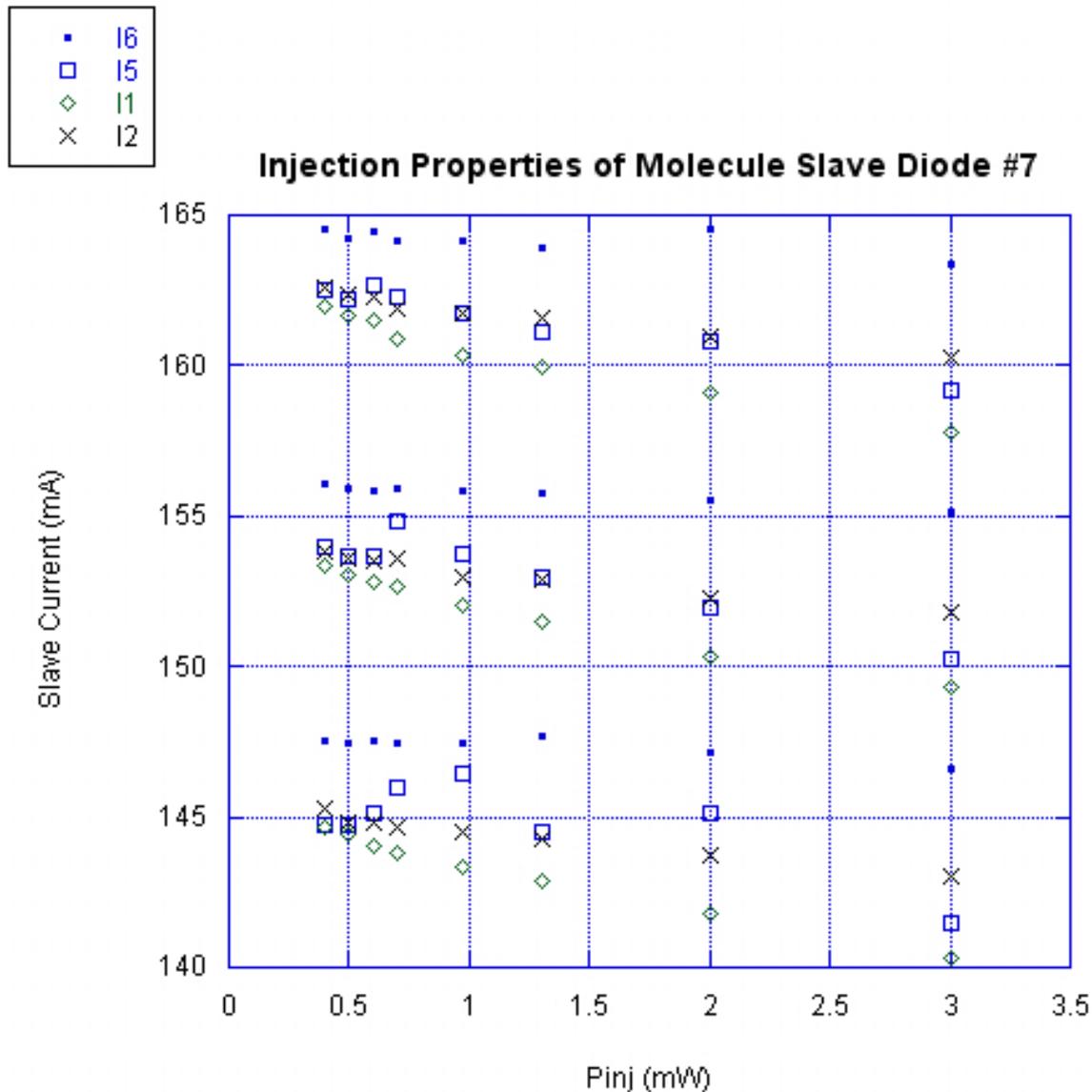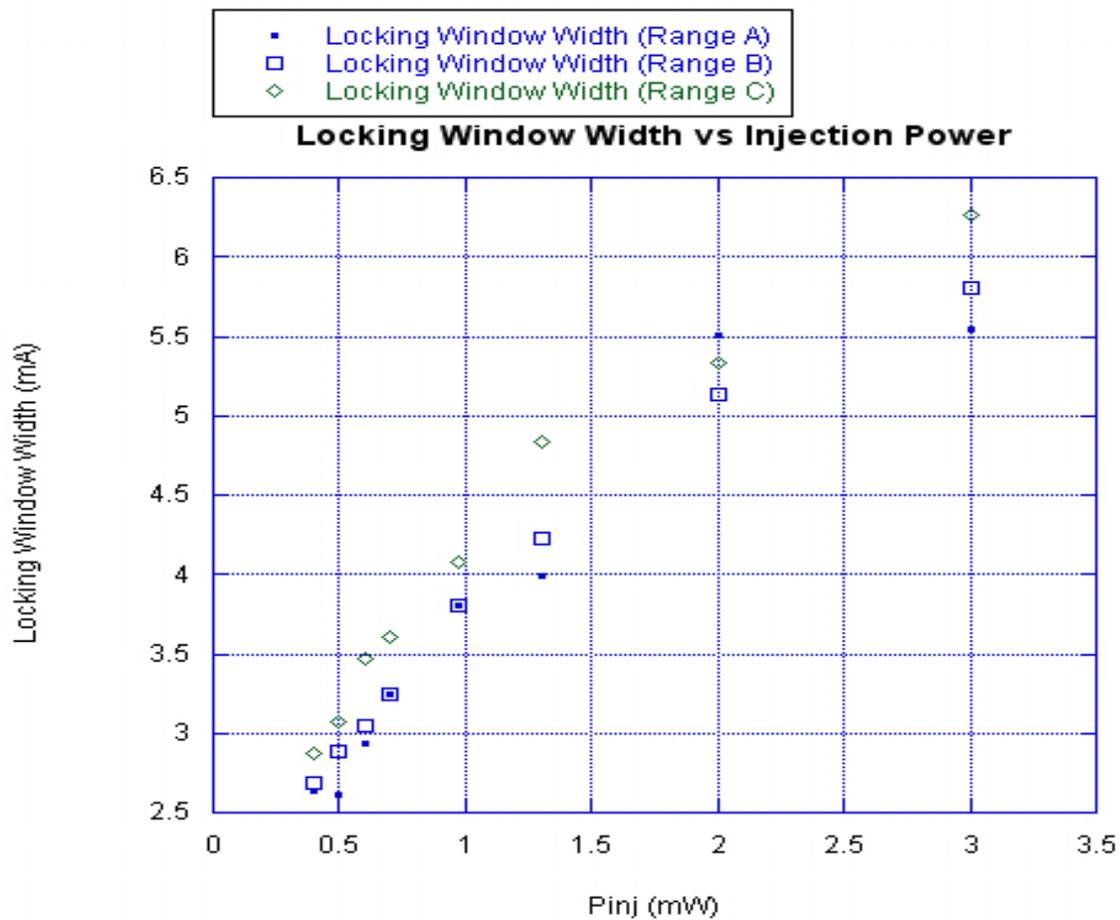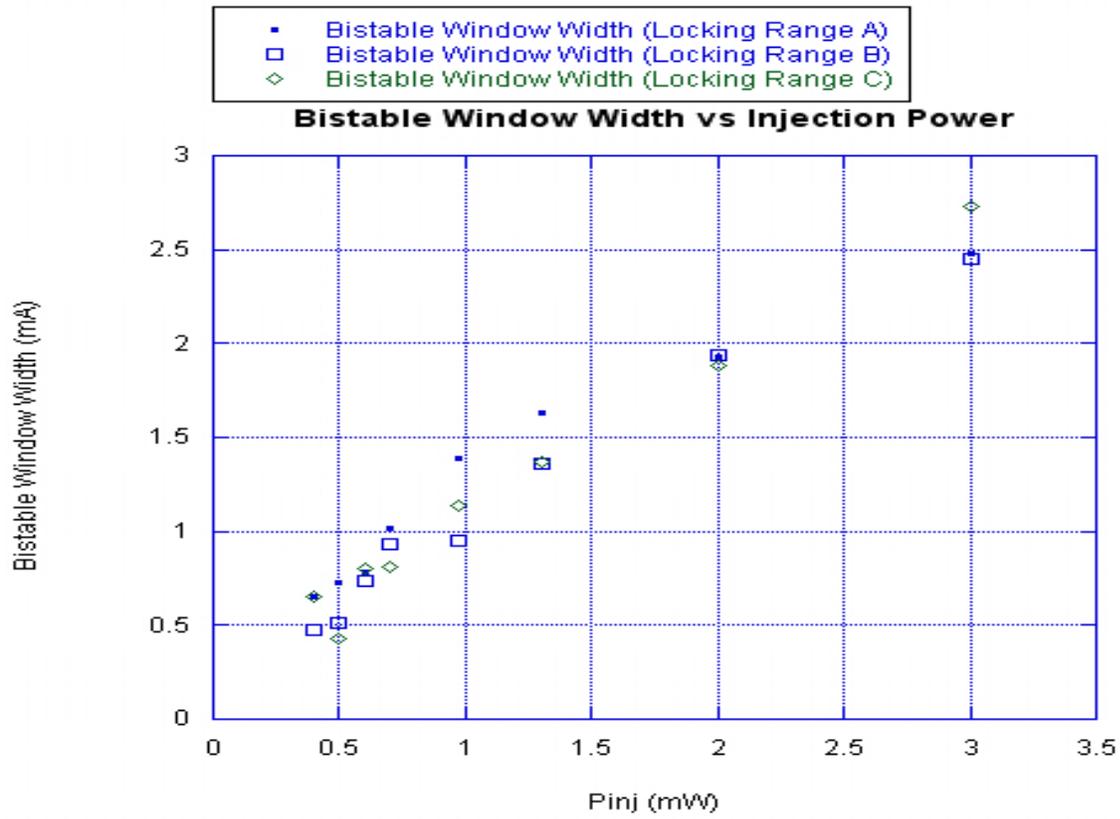
Results:

From this plot we do see that the width of the bistable window decreases with the injection power, the it looks like the width of the injection window also decreases with injection power. But the bistable window shrank faster than the injection window with decreasing injection power.

Notes:
-At 0.4 mA injection power, the free running oscillations were no longer being suppressed completely and below that injection was not seen.
-At above 3 mA, the injection windows were seen to overlap and possibly the bistable windows too but it is unclear.
-It was not clear how the bistable window changed behavior across each current window.
-I5 was a very handwavy state to record because sometimes there is no clear indications of when is the laser marginally injected and "fully" injected (ie: when all the side peaks disappear).

The last plot shows the measured widths of the "stable" locking ranges; a negative values means the bistable window was bigger than the "stable" injection window so no stable locking range exists within that window.
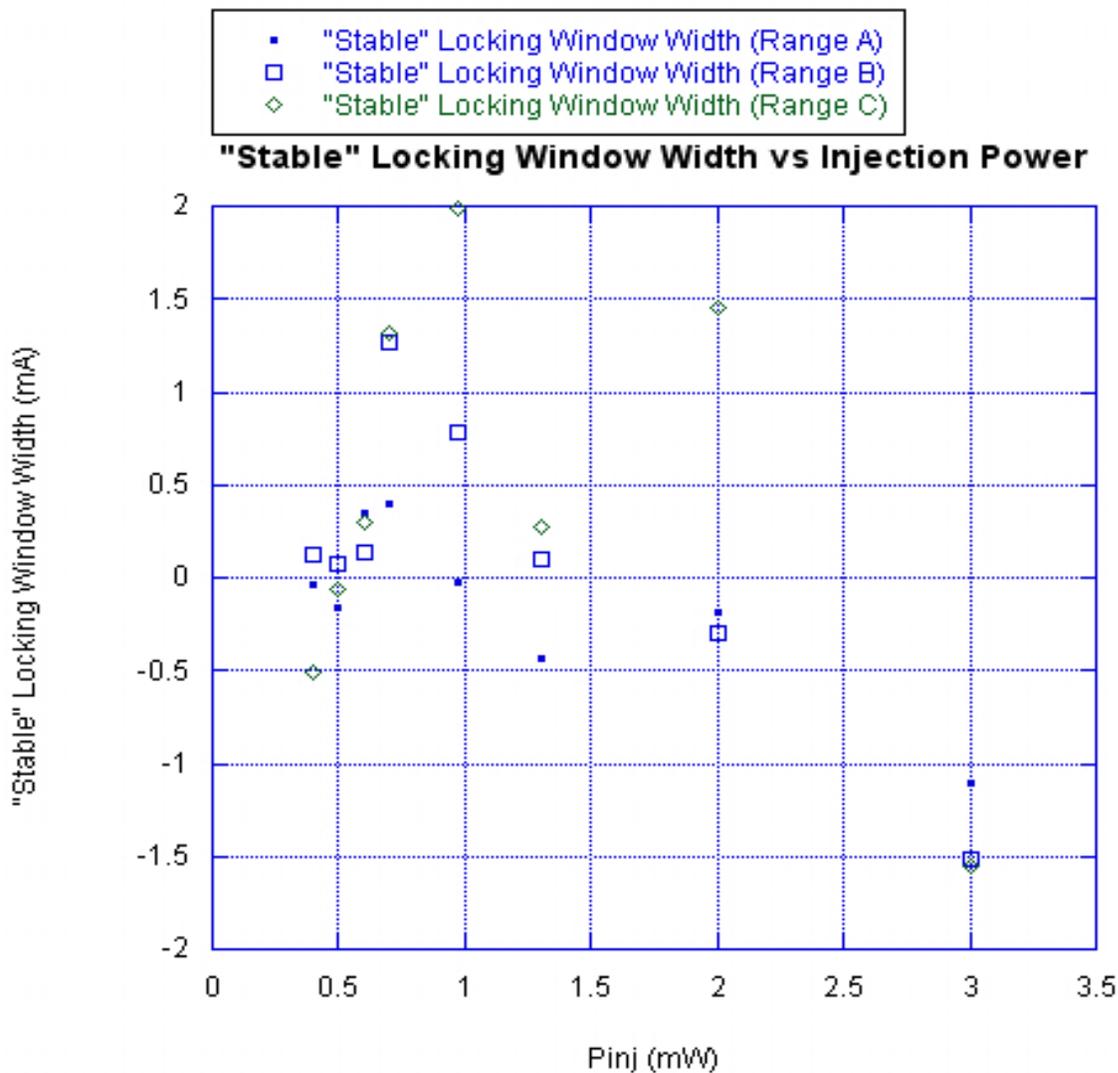
Appendix I

Sample Python Code for Magnetic Trapping

This section gives some sample code that was used to perform magnetic trapping.

```python
#...more code above ... #
X.start()
    X.Rb85_light_off()
    X.Li_mot_on(pump_dF = D['Li_pump_load_dF'],
                repump_dF = D['Li_repump_load_dF'],
                mot_coil_I = D['coil_load_I'])
    X.wait_s(D['Load_Time_s'])

    X.set_time_marker('t0') # mark time
    for i in range(5): # take 5 pictures at 25ms
        X.trigger_camera()
        X.goto_ms((i+1)*25,'t0')

    X.set_Li_pump_dF(D['Li_pump_compress_dF'])
    X.set_Li_repump_dF(D['Li_repump_compress_dF'])

    X.trigger_camera()
    X.set_mot_coil_I(D['coil_trap_I'])

    X.mot_shutter_off()
    X.wait_ms(20)

    X.set_Li_pump_dF(D['Li_pump_load_dF'])
    X.set_Li_repump_dF(D['Li_repump_load_dF'])

###################### MAGNETIC TRAPPING STAGE #################

    X.wait_ms(D['Hold_Time_ms'])
    print 'Hold Time in ms is=',D['Hold_Time_ms']

#####################################################################
    X.set_time_marker('startofrecaptureimages') # mark time
```

```python
    for i in range(110): # take 100 pictures at 20ms
        X.trigger_camera()
        X.goto_ms((i+1)*25,'startofrecaptureimages')

        if i==5: #first loading curve starts here
            T['Start_recapture_frame'] = X.nr_camera_triggers+1
            X.set_Li_pump_dF(D['Li_pump_detect_dF'])
            X.set_Li_repump_dF(D['Li_repump_detect_dF'])
            X.set_comp_coils_I(D['compx'],D['compy'],D['compz'])
            X.set_mot_coil_I(D['coil_load_I'])
            X.mot_coil_on()
            X.mot_shutter_on()

        if i==40:
            T['End_recapture_frame'] = X.nr_camera_triggers
            X.mot_coil_off()
            X.mot_shutter_off()

        if i==50:
            X.mot_shutter_on()

        if i==60: #second loading curve starts here
            X.mot_coil_on()
            T['Start_reload_frame'] = X.nr_camera_triggers+1

    T['End_reload_frame'] = X.nr_camera_triggers

    #end of recipe: now start slave and camera before starting recipe
    frames_handler = FramesHandler(data = D['Li_pump_compress_dF'])
    camera.start(X.nr_camera_triggers,frames_handler)
    time.sleep(1)

    X.set_comp_coils_I(D['compx'],D['compy'],D['compz'])
    X.mot_coil_on()

    X.end() #start
#...more code below ... #
```

Appendix J

Atomic Data for Lithium6

Table J.1: Natural Linewidth[7]

D2 Line	5.8724MHz * 2π
D1 Line	5.8724MHz * 2π

Table J.2: Saturation Intensity[7]

D2 Line	2.54mW/cm^2
D1 Line	7.59mW/cm^2

Table J.3: Dipole Matrix Elements for D1 Transition in Li6 $m_f = 1/2, m'_f = 1/2$ in C · m

$S_{1/2} \to P_{1/2}$	$F = 3/2$	$F = 1/2$
$F = 3/2$	$-5.4117 * 10^{-30}$	$-1.53066 * 10^{-29}$
$F = 1/2$	$-1.53066 * 10^{-29}$	$5.4117 * 10^{-30}$

Table J.4: Dipole Matrix Elements for D2 Transition in Li6 for $m_f = 1/2, m'_f = 1/2$ in C $\cdot$ m

$S_{1/2} \to P_{3/2}$	$F = 5/2$	$F = 3/2$	$F = 1/2$
$F = 3/2$	$-2.17829 * 10^{-29}$	$4.84065 * 10^{-30}$	$5.41201 * 10^{-30}$
$F = 1/2$	0	$-1.71143 * 10^{-29}$	$1.53075 * 10^{-29}$

Appendix K

New 30um Trap Design

The following page is a mathcad plot of the current trap setup that uses a 750mm lens and a 300mm achromat to tightly focus the fiber laser down to 30μm.

to see the value of the waist at different points you can just look at w(t) $wi \equiv 1.96 \cdot \left(10^{-3} m\right)$ $Ri \equiv 100000 \cdot mm$ $\delta := .1\,mm$

$t1 = 1\,cm$	$w(t1 - \delta) = 1.96\,mm$	$x1 \equiv 10mm$	$w0(t1 - \delta) = 1.95 \times 10^3\,\mu$
$t2 = 60\,cm$	$w(t2 - \delta) = 1.97\,mm$	$x2 \equiv 590mm$	$f0 \equiv 500mm$
$t3 = 235\,cm$	$w(t3 + \delta) = 4.89\,mm$ at acromat	$x3 \equiv 175cm$	$f1 \equiv 300mm$
$t4 = 410\,cm$	$w(t4 + \delta) = 1.68 \times 10^4\,\mu$	$x4 \equiv 175cm$	$f2 \equiv 10^8\,mm$
$t5 = 410.1\,cm$	$w(t5) = 1.682 \times 10^4\,\mu$	$x5 \equiv .1cm$	$f3 \equiv 10^8\,mm$
$t6 = 410.2\,cm$	$w(t6) = 16.832\,mm$	$x6 \equiv .1cm$	$f4 \equiv 10^8\,mm$
$tt = 410.3\,cm$	$w0(tt) = 27.3343\,\mu$	$x7 \equiv .1cm$	
$R1 = 0.3\,m$	$ws = 1.96\,mm$ $Rs = 0.3\,m$		

$ta := 50.0\,cm$ $tm1 := t2 + ta$

$w1 := \dfrac{w(tm1)}{mm}$

$tc := 39.5\,cm$ $tm2 := t3 + tc$

$w2 := \dfrac{w(tm2)}{mm}$

At Lens1 $t2 = 60\,cm$ (Arbitrary)   At AOM $tm1 = 110\,cm$ At acromat $t3 = 235\,cm$ At MOT $tm2 = 274.5\,cm$

$w(t2 + \delta) = 1.97 \times 10^3\,\mu$ $w0(t2 + \delta) = 86.33\,\mu$ $w(t3 + \delta) = 4.89\,mm$ $w0(t3 + \delta) = 27.33\,\mu$
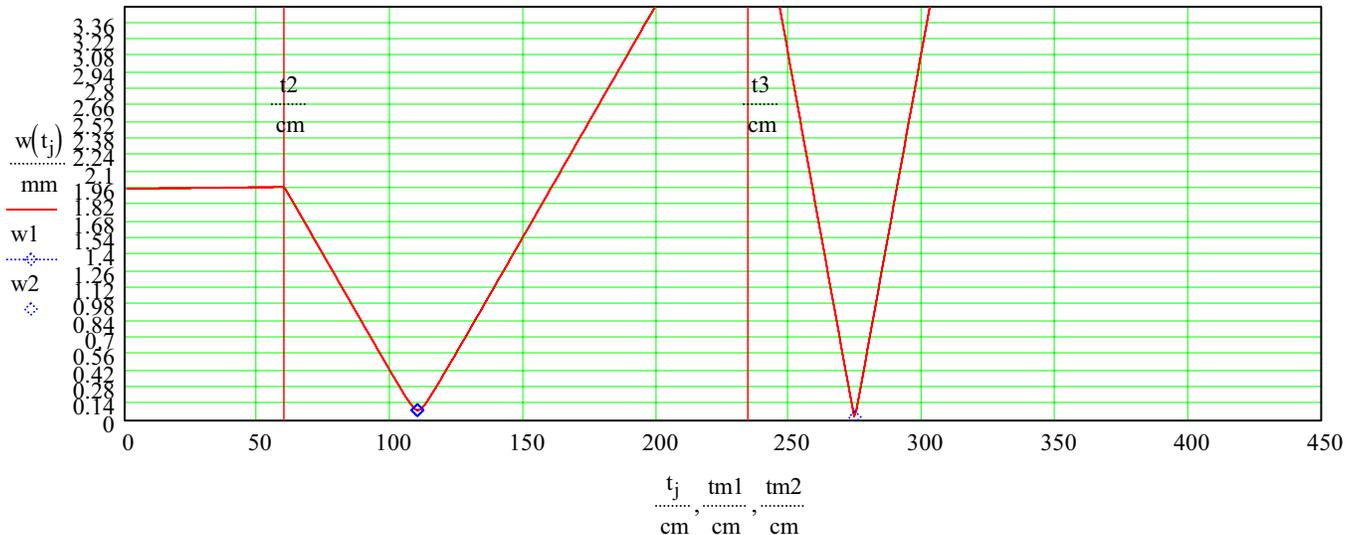
Appendix L

Apogee Trigger Protection Circuit

Originally we used a TTL line from the UTBus to directly trigger the Apogee camera. However, we discovered that noise from other circuits on the table (namely the mechanical shutters) could induce voltage spikes which would erroneously trigger the camera. Thus we built a protection circuit which optically isolates the camera from other electronics and also includes a voltage regulator to send 3.3V LVTTL signals (as specified by the camera manufacture) instead of 5V. The circuit uses the camera's 12V line to drive the regulator and an optocoupler for switching. If other lines on the Apogee I/O are needed, then a separate isolator should be used and connected in the same manner as the trigger line in [Fig L]. The connector used is a 8 pin **MINI DIN** connector available from digikey.

Figure L.1: Protection Circuit Box

Figure L.2: Protection Circuit